



Plasma Cutting with Industrial Robots in Automotive Mass Production

MASTER'S THESIS

Performed to achieve the academic degree

Diplom-Ingenieur (Dipl.-Ing.)

Master of Science (MSc.)

Master's degree programme: Mechanical Engineering and Business Economics

Submitted to

Graz University of Technology

Supervisor

Univ.-Prof. Dipl.-Ing. Dr.techn. Franz Haas

Institute of Production Engineering

by

Stefan Riepan, BSc

Graz, October 2015

In collaboration with:

MAGNA Cosma Innovative Manufacturing Solutions

Part of Formex Automotive Industries, S.A. de C.V.

Bld. Santa Maria 1700
Parque Industrial Santa Maria
Ramos Arizpe
Coahuila, C.P. 25903

+ 52 (844)411-79-04



Contact:

Harold Oliveros

Maurilio Udave

Stefan Plotz

Statutory Declaration

I declare that I have authored this thesis independently, that I have not used other than the declared sources / resources, and that I have explicitly marked all material which has been quoted either literally or by content from the used sources.

Eidesstattliche Erklärung

Ich erkläre an Eides statt, dass ich die vorliegende Arbeit selbstständig verfasst, andere als die angegebenen Quellen nicht benutzt und die den benutzten Quellen wörtlich und inhaltlich entnommenen Stellen als solche gekennzeichnet habe.

Graz, October 2015



Stefan Riepan

Preface

Mein größter Dank gilt meiner Familie die mich all die Jahre ohne zögern unterstützt und an mich geglaubt haben. Es erfüllt mich jedes Mal mit Glück wenn ich mit ihnen Zeit verbringen darf.

Stefan Riepan

Graz, 2015

Abstract

Five axis machines with laser heads are state of the art to separate parts in an automotive manufacturing line. Since technology is improving and the cost pressure on the manufacturing techniques are high the manufacturer are always looking for cheaper solutions and began to switch to robotic cutting solutions. Robotic laser cutting is spreading more and more due to its flexibility and high velocity cutting.

The next step to improve the cost per part even more is using another cutting technology. There plasma cutting which is well known for handheld cutting and mechanized xyz-cutting all over the industry could an option.

The present thesis is dealing with the question if robotic plasma solution is an alternative to robotic laser cutting. The technological borderline and implementation of the solution into the manufacturing line are elaborated in further detail.

Symbols

List of Greek Symbols

α	$Wm^{-2}K^{-1}$	Heat transfer coefficient
α_c	$^{\circ}$	Kerf cut angle
α_e	$^{\circ}$	Angle of the edge accuracy
α_{HV}	$^{\circ}$	Angle of the Vickers pyramid
$\Delta 3D$	mm	3D cut accuracy
$\Delta 3D_{diff}$	mm	3D cut geometry change due to the difference in cut length
$\Delta 3D_{lagging}$	mm	3D cut geometry change due to the lagging effect
$\Delta 3D_p$	mm	3D cut geometry change due to the plasma system
$\Delta 3D_R$	mm	3D cut geometry change due to the robot repeatability
Δc	mm	Circle cut accuracy
$\Delta c_{lagging}$	mm	Circle cut geometry change due to the lagging effect
Δc_p	mm	Circle cut geometry change due to the plasma system
Δc_R	mm	Circle cut geometry change due to the robot repeatability
Δc_T	mm	Circle cut geometry change due to the heat influence
Δc_u	mm	Circle cut accuracy of the upper kerf width
Δe	mm	Edge cut accuracy
$\Delta e_{lagging}$	mm	Edge cut geometry change due to the lagging effect
Δe_p	mm	Edge cut geometry change due to the plasma system
Δe_R	mm	Edge cut geometry change due to the robot repeatability
ΔE_{kin}	J, eV	Change of kinetic energy of an electron travelling through potential difference U ; 1 eV equals $1.602 \cdot 10^{-19}$ J
Δl	mm	Linear cut accuracy
Δl_p	mm	Linear cut geometry change due to the robot repeatability
Δl_R	mm	Linear cut geometry change due to the robot repeatability
ε	—	Emission coefficient
ε_0	Vm^{-1}	Electrical field constant
η_c	—	Efficiency of the compressor

κ, α	m^2s^{-1}	Temperature conductivity or thermal diffusivity
K, λ	$Wm^{-1}K^{-1}$	Thermal/Heat conductivity
μ	–	Outflow number
ρ	kgm^{-3}	Density of the material
ρ_a	kgm^{-3}	Density of the process gas at the required pressure
ρ_D	m	Debye length
ρ_i	kgm^{-3}	Density of the process gas at environmental pressure
σ	mm	Process spread
σ_ε	Wm^2K^4	Stefan Boltzmann-constant
φ	$^\circ$	Phase angle
Ψ	–	Outflow function
ω_0	s^{-1}	Eigenfrequency
ω_R	s^{-1}	Resonance frequency

List of Symbols

A	mm	Finished-part nominal dimension
A_d	m^2	Area of the gas nozzle
A_α	m^2	Area for the convective heat transfer
A_ε	m^2	Emitting radiation area
B	mm	Cutting-part nominal dimension
b_c	m	Thickness of the cutting plate
B_l	mm	Lower border dimension
B_u	mm	Upper border dimension
C_p	–	Process capability
C_{pk}	mm	Process capability with consideration of the position of the distribution
c	$Jkg^{-1}K^{-1}$	Specific heat capacity of the material
c_e	Nm^{-1}	Stiffness
D	Nsm^{-1}	Damping constant
d	m	Middle width of the kerf
d_m	mm	Average lower kerf diameter
d_{mu}	mm	Average upper kerf diameter
d_n	mm	Nominal diameter

d_{lmax}	mm	Biggest lower kerf diameter
d_{lmin}	mm	Smallest lower kerf diameter
d_{umax}	mm	Biggest upper kerf diameter
d_{umin}	mm	Smallest upper kerf diameter
d_{HV}	μm	Diameter of the impress
e	C	Elementary charge equals $1.602\ 176 \cdot 10^{-19} C$
E_{line}	Jm^{-1}	Energy input per millimetre, Line energy
E_i	J	Energy of the ion
g_m^a	kg	Statistical weight of the atoms with consideration of the inertia
g_m^i	kg	Statistical weight of the ions with consideration of the inertia
h	$m^2 kg s^{-1}$	Planck constant which is $6.62607004 \cdot 10^{-34}$
h_m	Jkg^{-1}	Specific melting enthalpy of the material
h_{torch}	m	Torch height (distance between the tip and the work piece)
HV	–	Hardness value according Vickers
I_{adj}	A	Adjusted current
k	JK^{-1}	Ludwig Boltzmann constant; k equals $1.380\ 6488 \cdot 10^{-23} JK^{-1}$
LSL	mm	Lower specification limit
m	kg	Mass
m_e	kg	Mass of the electron
n	–	Amount of samples
N_a	m^{-3}	Number density of atoms
N_e	m^{-3}	Number density of electrons
N_i^+	m^{-3}	Number density of ions
p	Nm^{-1}	Pressure
p_2	Nm^{-2}	Required process air pressure
p_a	Nm^{-2}	Process gas pressure before the nozzle
P_{arc}	W	Generated power over the arc
P_c	W	Cutting power
Pe	–	Peclet number
P_{el}	VA	Required electrical power to run the equipment
PF	–	Power factor
P_{HL}	W	Power of the heat loss
P_{HV}	$pond$	Force which presses on the Vickers pyramid
p_i	Nm^{-2}	Environmental air pressure

P_m	W	Power to melt and evaporate the kerf
P_r	W	Real consumed electrical energy
P_v	W	Power needed to compress air with a compressor
P_w	W	Power to warm the material up to the melting temperature
\dot{Q}_α	W	Convective heat flow
\dot{Q}_ε	W	Heat flow over radiation
\dot{Q}_λ	W	Conductive heat flow
r	m	Radius
r_{ecorr}	mm	Greater cut radius which results out of the bigger upper kerf width
r_i	m	Inner radius of the plasma
r_{lk}	mm	Lower kerf radius
RP	mm	Robot tolerance of position at repeated positioning
RT	mm	Robot tolerance of the path at repeated program execution
R_{th}	mKW^{-1}	Resistance of the material against heat conduction
r_{uk}	mm	Upper kerf radius
R_z	μm	Roughness depth
s	mm	Standard derivation
s_c	mm	Standard derivation of circular cuts
s_{cR}	mm	Standard derivation of the robot at circular cuts
s_{cp}	mm	Standard derivation of the plasma system at circular cuts
s_l	mm	Standard derivation of linear cuts
s_{lR}	mm	Standard derivation of the robot at linear movements
s_{lp}	mm	Standard derivation of the plasma system at linear cuts
T	mm	Specification spread
t	s	Time
T_∞	K	Ambient temperature
T_{air}	K	Temperature of the surrounding air
T_ε	K	Temperature of the black body surface
T_i	K	The inner or melting temperature of the material
T_m	K	Temperature distribution in the material
T_p	K	Plasma temperature
T_{pl}	K	Surface temperature of the plate
U	V	Acceleration potential
u	mm	Perpendicularity

U_{arc}	V	Generated voltage in the arc
USL	mm	Upper specification limit
\dot{V}	m^3s^{-1}	Required gas flow
v_c	ms^{-1}	Cutting speed
w_{lk}	mm	Lower kerf width
w_{uk}	mm	Upper kerf width
w_{uke}	mm	Bigger kerf width in the edge
\bar{x}	mm	Arithmetic average
x_{d-corr}	mm	Corrected x value for evaluating edge cut accuracy
x_e	mm	Measured x value for evaluating edge cut accuracy
y_{d-corr}	mm	Corrected y value for evaluating edge cut accuracy
y_e	mm	Measured y value for evaluating edge cut accuracy
z_0	mm	Zone diameter of a fly-by-point
Z_a	kg	Sum of the state of atoms
z_e	mm	Helping factor for the graphical calculations of edge cut accuracy
Z_i	kg	Sum of the state of ions

Explanation of Abbreviations

CIMS	Cosma innovative manufacturing solutions
iLC	Iterative learning control
Robotstudio	Offline programming software for robots
Kerf	Cut or incision made by a thermal cut
HAZ	Heat affected zone
BCC	Body centred cubic structure
FCC	Face centred cubic structure
CO2	Carbon dioxide
Dipl.-Ing.	Diplom-Ingenieur
MSc.	Master of Science
ns.	Not assessed
cf.	confer or compare
et al.	(et alii) and others
pp.	multiple pages
qtd.	quoted in
ref.	reference / referring to

Contents

Statutory Declaration.....	I
Eidesstattliche Erklärung.....	I
Preface.....	II
Abstract	III
Symbols.....	IV
1. Introduction of robotic plasma cutting	1
1.1. Motivation and scope of this research	2
1.2. Initial position - cutting processes in a manufacturing line.....	3
1.2.1. Requirements and driving factors on the cutting process.....	3
1.2.2. Different types of cutting.....	7
1.2.2.1. Laser Cutting	7
1.2.2.2. Plasma Cutting.....	10
2. Theory.....	12
2.1. Cutting Process.....	12
2.1.1. Theories to thermal cutting.....	13
2.1.2. Energy input and heat flow.....	14
2.1.3. Material and Heat affected zone.....	16
2.2. Plasma cutting technology.....	24
2.2.1. The plasma starting sequence.....	26
2.2.2. Materials.....	27
2.2.3. Plasma arc vortex	27
2.2.4. Different types of consumables and plasmas	28
2.2.5. Rotating of the torch.....	29
2.3. Robot technology	30
2.3.1. Edge movements – Vibrations.....	33
2.3.2. Motion control.....	34
2.3.3. Iterative learning control – iLC.....	36

2.3.4.	3D – Cutting - importance to have a good TCP	37
2.4.	Standards of cutting techniques.....	38
2.5.	Process capability	42
3.	Experiments	46
3.1.	Test configuration and Test Cell	46
3.2.	Cut accuracy and quality	48
3.2.1.	Stabilizing of the plasma vortex – run-in zone.....	48
3.2.2.	Cut shape influencers	49
3.2.2.1.	Real cut geometry at ideal settings	49
3.2.2.2.	Velocity influence (feed rate)	50
3.2.2.3.	Torch distance influence.....	52
3.2.3.	Cut shape quality	54
3.2.3.1.	Straight cuts.....	54
3.2.3.2.	Circular cuts.....	56
3.2.3.3.	Cutting of edges.....	64
3.2.3.4.	3D-Cutting.....	72
3.2.4.	Cut quality - Dross.....	75
3.2.4.1.	Dross dragging along.....	77
3.2.4.2.	Heat	78
3.2.4.3.	Dross in a tube	79
3.2.5.	Adapting of amperage on the flight – command Corner Current.....	79
3.3.	Metallurgical properties as a quality criteria	82
3.3.1.	Plasma gas	82
3.3.2.	Influencers on fatigue	83
3.4.	Implementation of robotic plasma cutting.....	91
3.4.1.	Torch height control	91
3.4.2.	Tool changer.....	93
3.4.3.	Robot position	93
3.4.4.	Plasma integration into the programming infrastructure of the robot	94

3.5.	Benchmark robotic plasma cutting against robotic laser cutting.....	95
3.5.1.	Cut shape quality	95
3.5.2.	Metallurgical properties.....	97
3.5.3.	Costs	98
3.5.3.1.	Investment costs	99
3.5.3.2.	Operative costs	100
4.	Conclusion	106
4.1.	Guideline for decision process Plasma or Laser cutting.....	107
4.2.	Prospect	108
	References	110
	Literature.....	110
	Online sources.....	112
	Appendix	114
A.1	Powermax system 3 mm thickness – AISI 1018 – kerf	114
A.2	Powermax system 3 mm thickness – AISI 1018 – Perpendicularity u	115
A.3	Powermax system 3 mm thickness – AISI 1018 – kerf	116
A.4	Powermax system 3 mm thickness – AISI 1018 – Perpendicularity u	116
B.1	High performance system 3 mm thickness – AISI 1018 – kerf.....	117
B.2	High performance system 3 mm thickness – AISI 1018 – Perpendicularity u.....	118

1. Introduction of robotic plasma cutting

Plasma cutting is a well-known process which has been introduced to the market in the 1960s. It is part of the thermal cutting processes and is widely used and well known for its fast and easy handheld- and mechanized (X-Y-tables) cutting solutions. Thermal cutting stands for cutting the material by melting it down and blowing it out at the same time. As a result there is no need of touching the part itself, no immense wear out of the tooling and it produces clean and accurate cuts compared to traditional cutting methods.

Another big advantage is the ability to mount it space-saving on a robot. Due to that fact 3D shapes are able to be cut at hard to reach positions. An example of a plasma cutting tool moved by a robot can be seen in Figure 1.

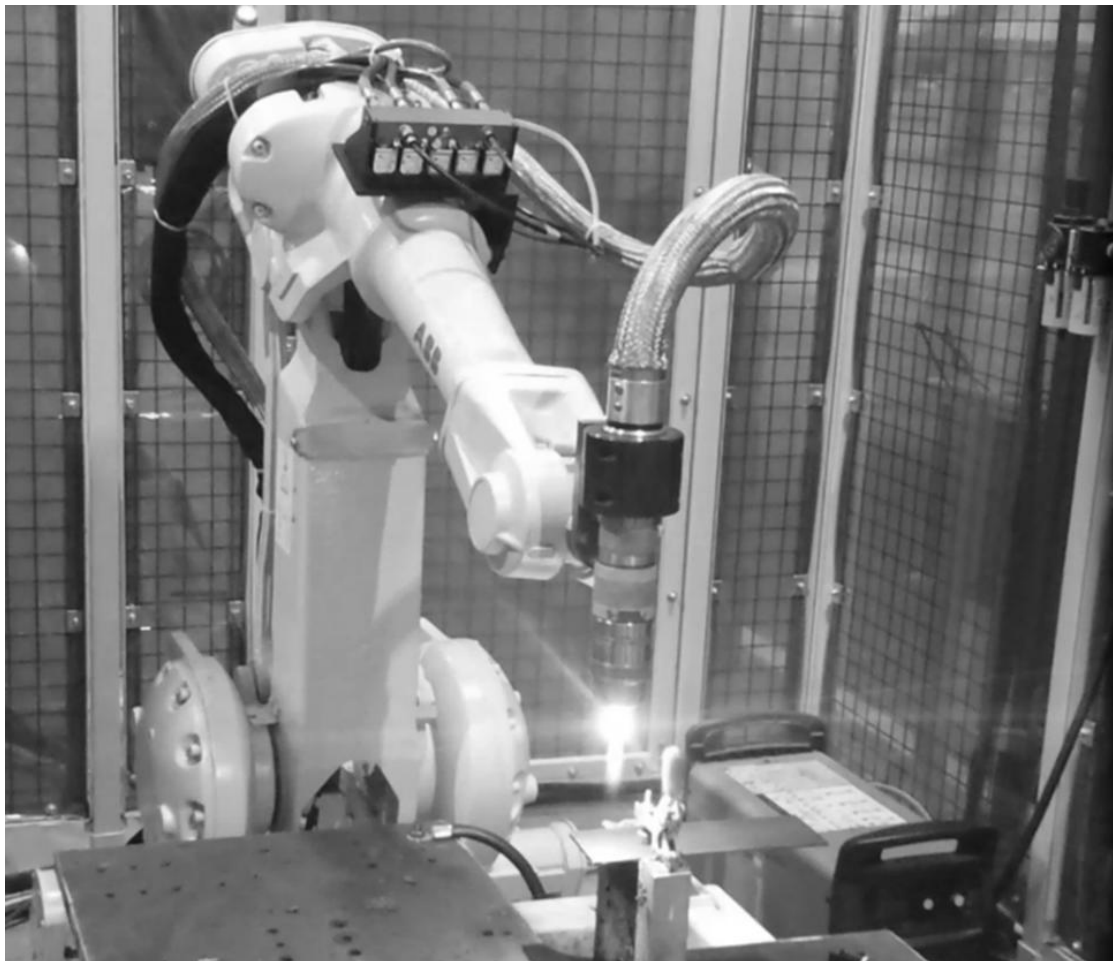


Figure 1: Robotic high performance plasma cutting, Source: own illustration

In fact ideal preconditions for cutting parts in an automotive production line. But what is hindering the market spreading of robotic plasma cutting? Technological reasons could be the cut quality and the reliability. The plasma is a hot plasma gas vortex with flow characteristics. This gas flow is only working without exception at specific environment properly. The environment is optimized for ideal

cut quality, cut velocity and dross avoidance at a specific material and thickness. There are a lot of variables but at the bottom line the main issue is the velocity. Plasma cutting has a specific working area, as seen in Figure 2. A derivation of this working area leads to different cut geometry, to dross and to inappropriate heat input to the material which is undesirable and comes down to not catching the required tolerance or even worse to scrap parts.

The maintenance of velocity at every shape with the required path accuracy is the challenge for the guidance device. The buckling arm robot should be examined and tested as a plasma cutting machine. As there is shown in Figure 2, there is a small overlapping zone.

To cut at the worst shapes in this zone or above in the ideal cut zone is the challenge of this thesis. It has to be found out which cutting parameters make plasma cutting with robots possible.

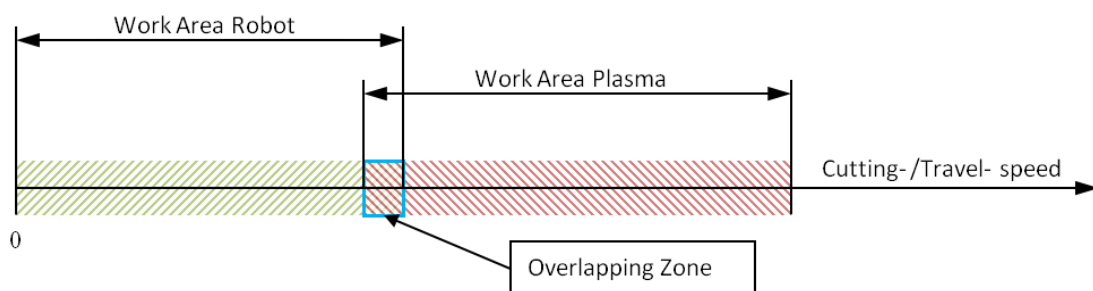


Figure 2: Problem of Robotic Plasma Cutting, Source: own illustration

Technology advances in both, the plasma cutting technology and the robot technology. Moreover there are also improvements in the controlling technology. The question is if the state of the art plasma cutting technology is capable to cut with the same quality than laser cutting. Therefore laser cutting is the benchmark technology in this thesis.

1.1. Motivation and scope of this research

The scope of this work can be divided into three main points in order to close the knowledge gap of the automotive supplier industry concerning the robotic plasma cutting technology.

- 1) Parameters and effects which influence the robotic plasma cutting process
- 2) Solutions and settings for robotic plasma cutting and
- 3) Guideline to facilitate the decision-making process if to use robotic plasma or laser cutting and to help choosing the right cutting system.

Besides the technological knowledge gap another big motivational factor is the opportunity to offer the customer an additional option. Sure laser cutting will always be the professional high quality solution but there is a market potential for the economic robotic plasma cutting. An economic solution because

the market competition is hard on the global market, the proportion of material costs in production line is immense high and not every part requires the high quality solution.

1.2. Initial position - cutting processes in a manufacturing line

This chapter serves to give at first an overview of the requirements and driving factors for cutting processes by explaining the production of two different parts. After that a brief description introduces the relevant cutting techniques.

1.2.1. Requirements and driving factors on the cutting process

In order to see all the influence of the cutting process it is helpful to zoom out to see the big picture. By doing so it is fast recognizable that the final part itself and the way of its production define the specifications. How is the part coming to the cutting station? Which tolerances have to be reached at the end of the cutting? These are the main questions here, see Figure 3 below.



Figure 3: Cutting in the process, Source: own illustration

To demonstrate this process there are two completely different parts picked which are later on in our tests also the benchmarks for the robotic plasma cutting.

In Figure 4 below there can easily be seen that these parts have completely different preprocesses and therefore different characteristics when they arrive to the cutting process.

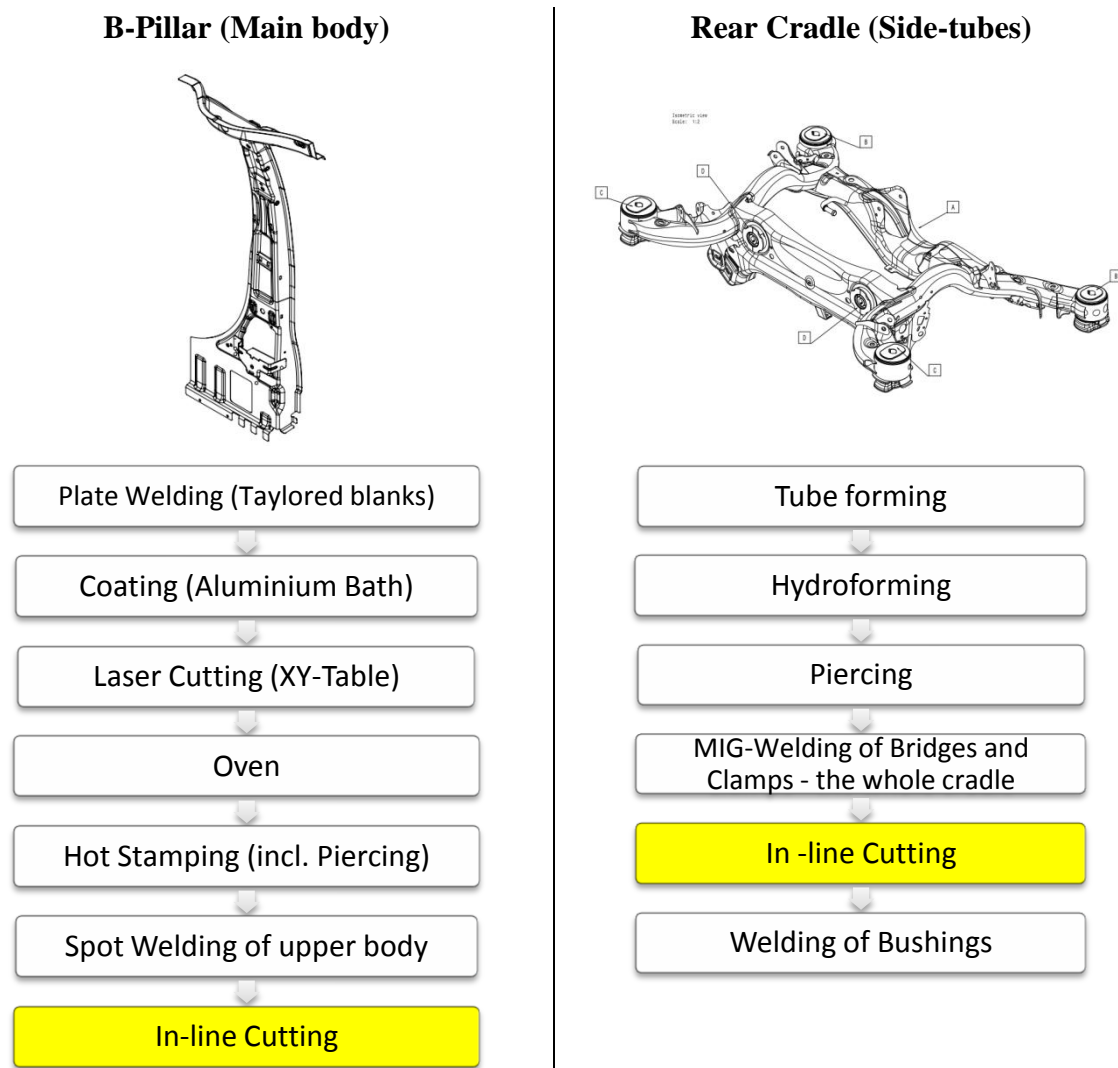


Figure 4: Comparison of the production steps of a B-Pillar and a Rear Cradle, Source: own illustration

The characteristics of each of these parts are described in Table 1 below. The B-pillar is characterized by the good form stability due to the hot stamping process. Due to the process the big twisting due the MIG-welding at the cradle does not exist. As a result this part is by far easier to clamp in a tooling than the other Cradle. The only unknown variable is the material and the coating. Tests should reveal the issues due to this matter.

On the other hand there is the rear cradle characterized by the hydro forming process and the MIG-welding of the bridges. During the whole pre-production steps, MIG-welding, forming or positioning, there is always a clearance and at the end there are parts coming to the cutting process with a lot derivation. This deviation is a lot higher at the rear cradle than at the B-pillar. Furthermore the thickness of the material of the tube is more than twice of the one from the B-pillar.

Characteristics/Consequences of pre-production steps

B-Pillar

- Good Formstability (absence of spring back due to Hot Stamping)
- No MIG-Welding (less twisting)
- Thin material (1,2 mm)
- Martensitic material

Rear Cradle production:

- Hydroforming has more variance in the process (the side-tube has variance)
- MIG-Welding (higher degree of twisting)
- Thicker Material (3 mm)
- High strength low-alloy steel

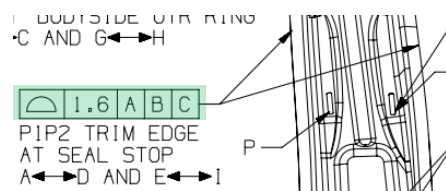
Table 1: Characteristics/Consequences of Pre-Production steps, Source: own illustration

The following Table 2 represents a short summary of the required tolerances in shapes, circles and surfaces. The tolerance which stands out here is the window of tolerance of the circles with 0.22 mm at a diameter of 6.5 mm.

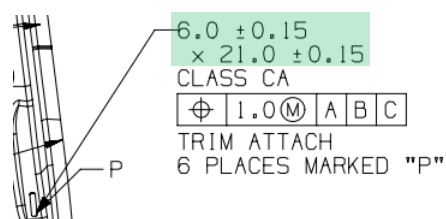
Further steps requirements:

B-Pillar Tolerances:

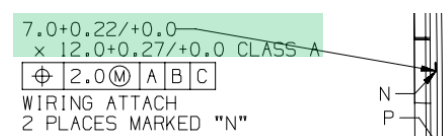
1) Outer contour – Profile of a Surface



2) Rectangulars



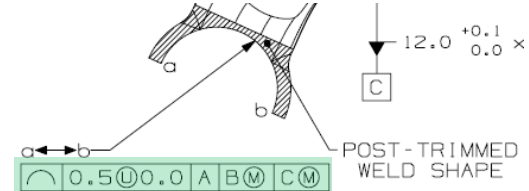
Smallest tolerance:



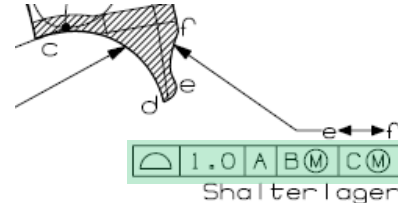
3) Hole

Rear Cradle Tolerances:

1) Profile of a line



2) Profile of a Surface



3) Hole & smallest tolerance

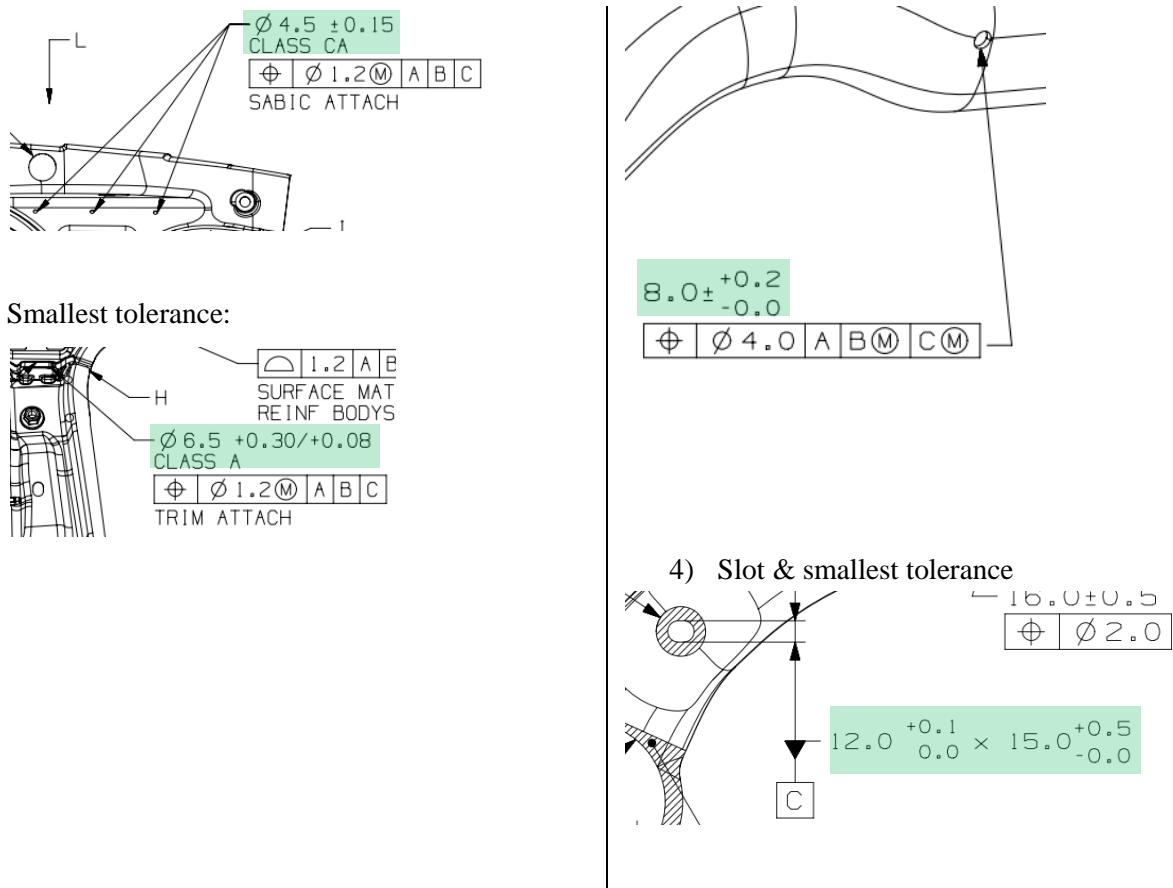


Table 2: Further steps requirements, Source: own illustration

What does this mean for the robotic cutting process itself? On the one hand there are the requirements which have to be complied with which can be seen in Table 2 above and on the other hand there are the characteristics of the parts which enter the process (Figure 4).

Figure 5 provides an overview of the technical cutting influence factors. First of all the derivation of the part itself and the influence on the position accuracy of the cut are considered in the position point. This factor can be divided into special requirements of the tooling and of the torch height control for the cutting equipment. Secondly there is the cut geometry and the accuracy which can be achieved. At third there is the cut quality in respect the dross formation. Also the thickness plays here an important role. At fourth the material properties have to be considered. What is happening in the heat affected zone (HAZ) and how is this affecting the fatigue of the part is a major question. Since in production the time is equally to costs the shortest possible cycle time and maximum cutting speed have to be considered.

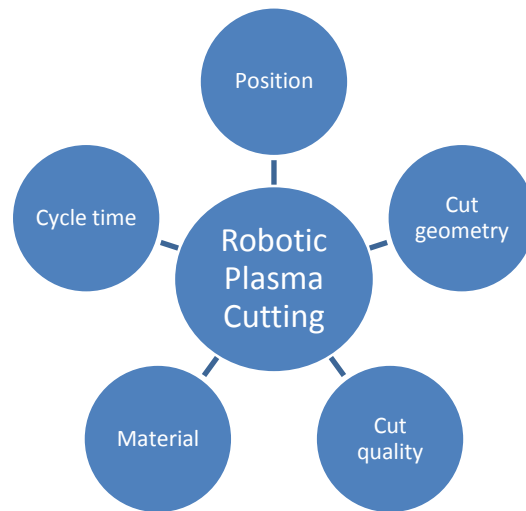


Figure 5: Overview of the cutting influence factors, Source: own illustration

1.2.2. Different types of cutting

There are two different types of cutting qualified for our purpose, Laser Cutting and Plasma Cutting. Both have their pros and cons and are mountable on a robot for automated activities.

1.2.2.1. Laser Cutting

Laser Cutting is using laser light to melt the material and needs an additional air stream to blow the liquid material out of the cut. The laser light can be created by several different power sources, but the in the industry most common used ones are the CO₂-Laser or the fibre-laser (solid state laser). The main difference in-between these two is the frequency of the laser light itself. CO₂ produces light with a wavelength of 10,6 μm and on the other hand solid state laser at 1 μm wave length. Despite the higher wavelength beneficial for the CO₂ laser are the higher beam quality and therefore the possibility of smallest focus diameter and at the same time great focus depth. These are the main reasons for the widespread use of this technology in the industry.

Accompanied by the development of the solid state laser there rises the opportunity to guide the light by fibre cable, which is ideal for the robotic application. Besides that the better absorption of the short waved laser light of the metallic surfaces is an additional advantage.¹

¹ Klocke (2007) p. 246 ff.

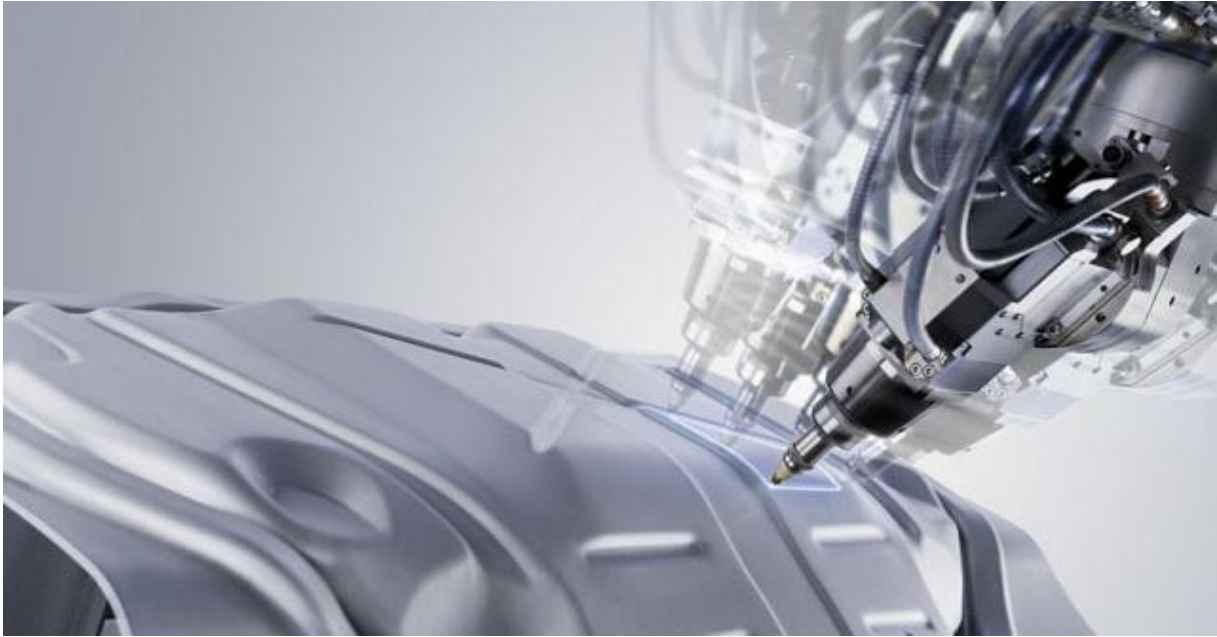


Figure 6: CO2 Laser Cutting of Body in white, Source: Trumpf GmbH + Co.KG (2015), Online Source [27.07.2015].

The laser beam can be focused to a diameter of 0.1 to 0.6 mm with the use of a power source up to 6 kW. That means that the laser beam in the Raleigh length has an immense high energy density compared to other cutting technologies. With that small kerf width the out blown material is less and therefore the possibility of dross is less.

In Figure 6 below there is a comparison of the advantages and disadvantages of the laser cutting technology. Laser cutting is from the technology side a very good solution for the separation of different parts. When we look at the reverse side of the medal we easily find that the technology has its price. As it could be seen in history of laser cutting by a wider use of this technology also in other industries the costs could probably decrease and this trend will perpetuate in the future.

Characteristics of the laser cutting technology

Advantages

- Specialized cutting technology for metal sheets with a thickness less than 6 mm
- Possibility of energy reduction (Pulsing)
- High power density
 - High cutting speed
 - Less head affected zone
 - Less warping and twisting of the part
 - Small cutting kerf

Disadvantages

- High investment costs
 - Laser Power sources
 - Chiller
 - Beam guidance
 - Handling (head – torch height control)
 - Controlling
 - Safety measures (coverage effort)
- Maintenance costs

<ul style="list-style-type: none"> - Small cut radius <p>Non-contact machining</p> <ul style="list-style-type: none"> - No tooling wear - Cutting of instable parts - Simple handling of tooling <p>Simple controlability</p> <ul style="list-style-type: none"> - Less moving masses - High degree of automation - Integration in flexible manufacturing systems - 2D/3D – shape cutting 	<ul style="list-style-type: none"> - Cleaning effort - Special educated people to implement/maintain this solution
---	--

Table 3: Characteristics of laser cutting technology, Source: cf. Klocke (2007) p. 247

One point which is to highlight here is the explanation of the more-effort at the implementation and at the usage of this process in an automotive production line. The higher effort refers to the protection of the workers because of danger of the laser light. For better understanding it is explained by an example below.

Figure 7 illustrates a production line of a B-Pillar with a robotic laser cutting cell at the very left, the very beginning. In that picture can be seen the fully integrated cell with two cutting robots, tooling, scrap conveyors and that the loading which is also done by a robot. Moreover what can be seen is that the whole cell is covered by an enclosure at all sites. If the customer requires building in a control window to supervise robot, the regulations require special coated glass, which is very expensive. Furthermore it requires a roll-up door inside the line, which can be an additional factor if it comes down to cycle time problems.

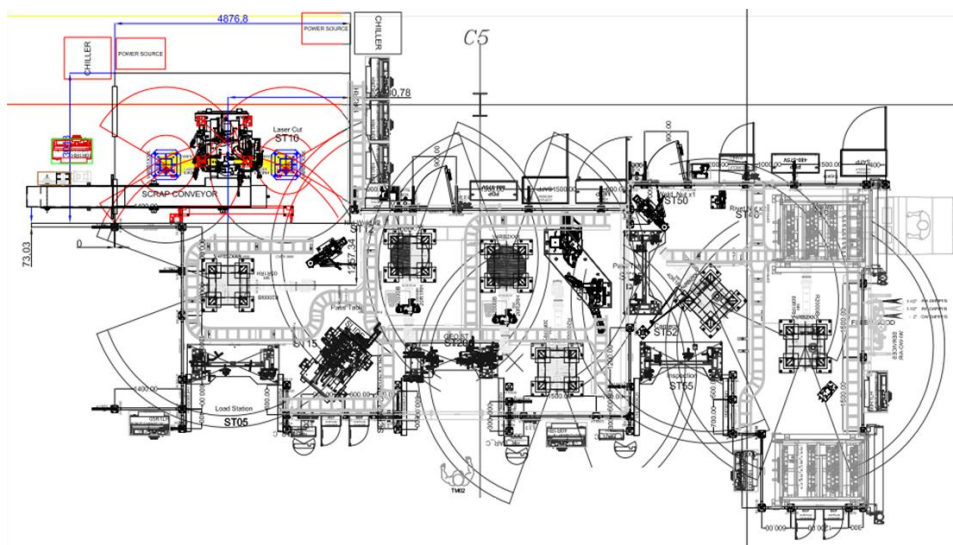


Figure 7: Production line of a B-pillar, Source: Magna CIMS (2015)

1.2.2.2. Plasma Cutting

In contrary to the laser cutting, plasma cutting is using a hot gas stream in form of a vortex to cut material. The high temperature of the gas is created by initiating plasma in the vortex in-between the electrode and the part. “In plasma cutting gas is transformed into plasma when it is heated, and comprises positive ions, neutral atoms and negative electrons, which results in extremely high temperatures being generated (i.e., up to 27,000°C).”² With that stream of extremely high temperature gas the metal is molten and at the same time blown out of the part, as seen in Figure 8.

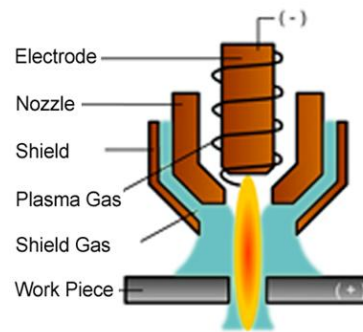


Figure 8: Illustration of Plasma Cutting, Source: Hypertherm Inc. (2015), Online Source [30.07.2015].

In the following Table 4 there is an overview of the characteristics of the plasma cutting technology compared to the laser cutting technology. There the main differences of performance of the technologies can easily be seen.

Characteristics of the plasma cutting technology

Advantages

Specialized cutting technology for metal sheets with a thickness greater than 6 mm

Non-contact machining

- Cutting of instable parts
- Simple handling of tooling

Simple controlability

- Less moving masses
- High degree of automation
- Integration in flexible manufacturing systems
- 2D/3D – shape cutting

Disadvantages

Power density in the cut is less than with laser

- Lower cut speed than with laser
- Bigger head affected zone
- Bigger kerf width
- Bigger cut radius

Consumables

- Need to change the consumables every 2 cut hours
- For full automation, need of a toolchanger

Dross probability

² Ian D. Harris (1997) p. 7

Investment costs	- Need of revision/rework station
- Cheap Power source	Cut geometry
- No need of a chiller	- Cut has an angle
- Handling (torch height control possible with the robot – indulgent behavior)	More heat affection in the material
- Controlling	
- No safety measures (same as robot welding)	
Maintenance costs	
- Cleaning effort is less	
- No need of special educated people to implement/maintain this solution	

Table 4: Characteristics of plasma cutting technology, Source: own illustration

The biggest advantage of plasma cutting is the easy handling and unbeatable price. Since there is a global competition companies have to fight for their position, plasma cutting is a very good alternative at this aspect. There is a closer view on the plasma cutting technology in chapter 2.2.

2. Theory

The present chapter provides the essential theoretical background which is necessary for performing this assessment and benchmark of the robotic plasma cutting process. First there is annotated the cutting process with the effects on the heat affect zone. Then there is a deeper view on the plasma cutting- and the robotic technology. At the end of this chapter a deeper look on the standards and norms which are needed to perform the assessment is provided.

2.1. Cutting Process

According to standards and literature thermal cutting processes can be divided into three different areas.³

a) Reactive cutting or flame cutting

In reactive cutting the kerf is created by the oxidation of the material and the created products are blown out by a stream of oxygen gas. Benefit of this type of cutting is the lower energy consumption due to the reaction enthalpy and the resulting higher cut speed. A disadvantage is the creation of the remaining oxide layer. An example is oxi-fuel cutting.

b) Melt cutting

At melt cutting the material is molten and partly vaporized by the high density plasma gas or the laser beam and blown out by a process gas similar to flame cutting above. Beneficially is the nearly oxide free cutting edge. Disadvantageous is the high gas consumption and the higher energy demand.⁴

c) Vaporization cutting

At vaporizing cutting high energy is used to evaporate the material. The created products are removed from the kerf due to the expansion or an additional gas flow. Used with laser technology.⁵

Figure 9 illustrates laser- and plasma cutting which are used for our application and considered in the category melt cutting. Laser cutting uses a focused laser beam to melt and evaporate the material and a cutting gas to push out the material from the kerf. The required acceleration for pushing the molten material out of the kerf is provided by the compression force and the shear-force transfer of the cutting gas.⁶

On the other hand plasma cutting uses a plasma gas flow to melt and evaporate the material. And at the same time this gas is used to push out the material from the kerf.

³ cf. EN ISO 9013 (2002), p. 25-26

⁴ cf. Poprawe, R. (2005) pp. 330

⁵ cf. Poprawe, R. (2005) p. 341

⁶ cf. Poprawe, R. (2005) p. 336

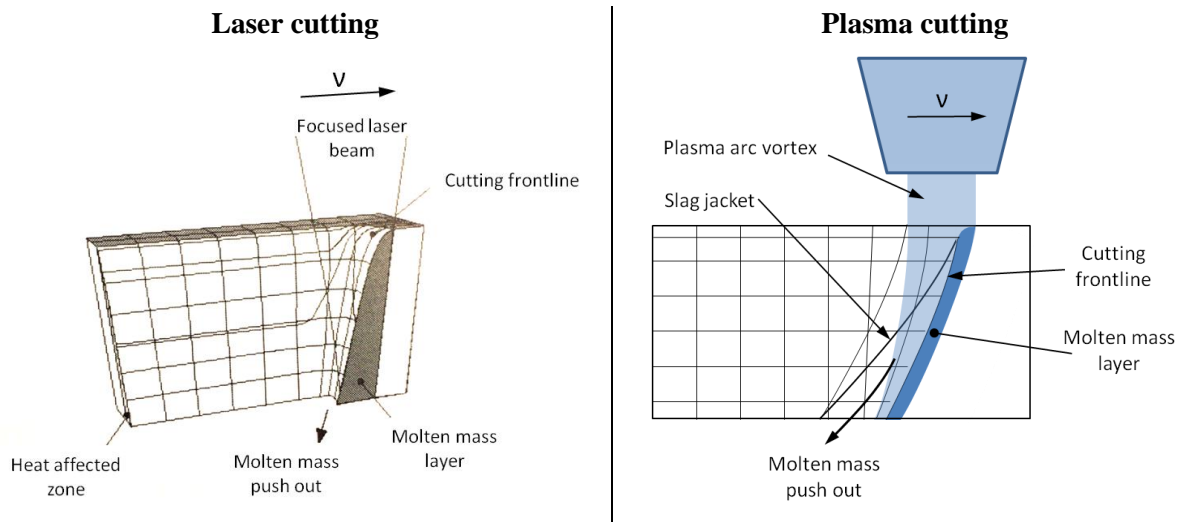


Figure 9: Laser- and Plasma Cutting, Source: left Popraque (2005) p. 337 (slightly modified), right own illustration

2.1.1. Theories to thermal cutting

The necessary power for cutting P_c is composed of the power of warming up P_w , the power to melt and evaporate the material P_m and the power of heat loss P_{HL} which consists mainly of the heat conduction into the surrounded material and the out blown energy. The energy which is used to push out the material of the kerf is not considered in the formula below.⁷

$$P_c = P_w + P_m + P_{HL} \quad [J/s] \quad (1)$$

The power of warming up P_w is the power which is needed to heat the material in the kerf up to the process temperature T_p which is lying between the melting- and vaporizing temperature. To melt and vaporize the complete material the following formula describes how to calculate P_w and P_m :

$$P_w + P_m = b_c d v_c \rho \cdot \left(c \cdot (T_p - T_\infty) + h_m \right) \quad (2)$$

b_c stands for the thickness of the cutting plate, d is the middle width of the kerf, v_c is the cutting speed, ρ is the density of the material, c the specific heat capacity of the plate, T_p is the process temperature, T_∞ is the ambient temperature and h_m the specific melting enthalpy of the material. Involving the Peclet-Number $Pe = b_c v_c / 2\kappa$ results in:

$$P_w + P_m = 2Kd \cdot \left(T_p - T_\infty + \frac{h_m}{c} \right) \cdot Pe \quad (3)$$

⁷ cf. Poprawe, R. (2005) pp. 321

Pe is a dimensionless number and defines the ratio of the convective and conductive heat transfer. κ specifies the temperature conductivity and K the heat conductivity and it is considered as:⁸

$$\kappa = \frac{K}{c \cdot \rho} \quad (4)$$

At plasma cutting the cutting current I_{adj} can be adjusted and the resulting voltage in the arc U_{arc} can be measured. The arc power P_{arc} represents the supplied energy to the process and can be calculated as follows.

$$P_{arc} = U_{arc} \cdot I_{adj} \quad (5)$$

As a consequence the power of heat loss P_{HL} can also be calculated by the difference between the added energy P_{added} and the energy which is used to heat up and melt the material $P_{removed}$. This can be seen in the following formula:

$$P_{HL} = P_{added} - P_{removed} = P_{arc} - P_w - P_m \quad (6)$$

2.1.2. Energy input and heat flow

By taking P_{arc} and dividing it by the cut speed v_c the energy input per millimetre material is calculated what can be seen in the following formula. This energy is called line energy and a common term in the welding and cutting industry.

$$E_{line}(v) = \frac{U_{arc}(v_c, h_{torch}) \cdot I_{adj}}{v_c} \quad [J/mm] \quad (7)$$

A plasma cut has specific measurements (example see in 3.2.2.1 Real cut geometry at ideal settings) and a specific amount of material which is melted down and blown out. This specific amount correlates to the energy which is injected at this specific location. That means by changing the cut speed v_c there has to be an adjustment on the site of the energy input which can be seen in Figure 10. The green line is the line of equal energy input per millimetre.

⁸ cf. Poprawe, R. (2005) pp. 321

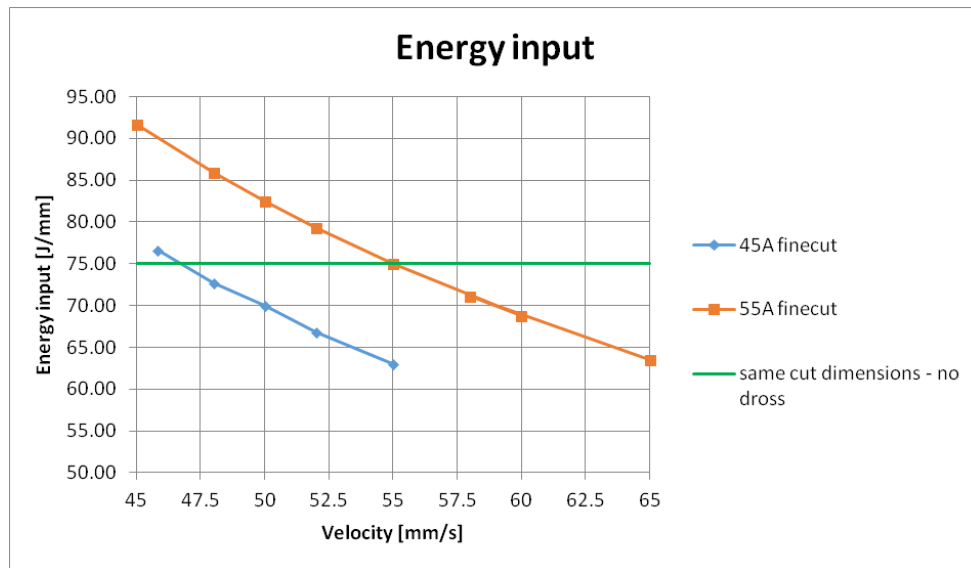


Figure 10: Energy input in the material, Source: own illustration

According to Radaj “The more unevenly the temperature is distributed at a particular time, the more rapidly the temperature changes”⁹ which describes that the driving force of heat flow is the temperature difference.

The heat can flow through the three main heat flow processes. First it flows through the material as conduction. The connection between the heat flow density q_λ and the local temperature gradient $\frac{\partial T}{\partial n}$ through the coefficient of thermal conductivity λ can be described with the Fourier’s law.

$$q_\lambda = -\lambda \frac{\partial T}{\partial n} \quad (8)$$

With the field equation for heat conduction the in-stationary temperature distribution in the material can be calculated.

$$\frac{\partial T}{\partial t} = \frac{\lambda}{c\rho} \left(\frac{\partial^2 T}{\partial x^2} + \frac{\partial^2 T}{\partial y^2} + \frac{\partial^2 T}{\partial z^2} \right) \quad (9)$$

The term $\lambda/c\rho$ is abbreviated to the coefficient for thermal diffusivity a .

$$a = \frac{\lambda}{c\rho} \quad (10)$$

Secondly it flows over convection into the surrounding air, as described in the following formula. This formula describes the heat transfer with a basic proportional factor which does not imply consideration as laminar or turbulent, or free or forced flow. This approach is based on the Newton-cooling law.¹⁰ α represents the heat transfer coefficient, A_α the area for the convective heat transfer, T_p the surface temperature of the plate and

⁹ Radaj, D., (1992) p. 25

¹⁰ cf. Herwig, H., et al. (2006) p. 88

$$\dot{Q}_\alpha = \alpha A_\alpha (T_{pl} - T_{air}) \quad (11)$$

The third heat transfer mode is the radiation of the energy to other objects in the environment as described in the formula below which arises out of the Stefan-Boltzmann law.¹¹ \dot{Q}_ε represents the amount of energy which is transferred, σ the Stefan Boltzmann constant, A_ε the emitting area and

$$\dot{Q}_\varepsilon = \sigma \cdot \varepsilon \cdot A_\varepsilon \cdot T_\varepsilon^4 \quad (12)$$

According to these three heat flow processes it becomes clear that the main driving factor for the heat transfer is the temperature difference between two locations within a material, two phases or between two objects. The higher the difference, the higher is the heat flow.

2.1.3. Material and Heat affected zone

For the present investigation there are two different materials in use. First there is the mild steel S460MC which is used for the side tubes of a rear cradle. These tubes are hydro-formed and possess the initial material characteristics. The other material is high strength steel Usibor 1500 or 22MnB5 which is used for the B-Pillar of cars because of their great strength to weight ratio. Since this part is formed by a hot-stamping process where the material is cooled down rapidly the initial structure gets changed completely.

Table 5 shows the chemical composition of the two tested materials. The main difference here is the carbon, the silicon content and the boron content.

Table 5: Nominal chemical composition of the tested materials (% by weight), Source: Rautaruukki Corporation (2015), Online Source [06.09.2015].

	Carbon	Mangan	Phosphorus	Sulfur	Si	Alu	Nb	V	Ti	B
S460MC	0.1	1.5	0.025	0.01	0.03	0.015	0.09	0.2	0.15	
Usibor 1500	0.22	1.1	0.015	0.015	0.4	0.03			0.04	0.005

Figure 11 shows the equilibrium diagram for the meta-stable $Fe - Fe_3C$ phase diagram, better known as the iron carbon phase diagram. It describes the cooling down of liquid iron with carbon and its changes in structure and phases in equilibrium with the environment. In other words the cooling is performed in infinite time. This diagram can be divided into two main areas, on the left pure iron

¹¹ cf. Herwig, H., et al. (2006) p. 153

combined with carbon up to 2% of carbon, resulting in steel alloys and on the right side with higher carbon content than 2% cast iron.

The left side of steel alloy can be divided into the hypo-eutectoid, the eutectoid and the hyper-eutectoid areas.

The borderline of the hypo- and the hyper-eutectoid areas is the eutectoid area which is at exactly 0.8% carbon content and the cooling structure ends up at room temperature in pure pearlite. This phases independent transformation is called eutectoid transformation.

The in this thesis relevant zone is the hypo-eutectoid steel area and consists of pearlite and proeutectoid ferrite. The hyper-eutectoid zone is a mixture of pearlite and proeutectoid cementite.¹²

This paragraph develops a brief summary of the relevant phases and micro-constituents which is needed to perform a founded assessment in the experimental part of this paper.¹³

- α -Ferrite is phase of pure iron at room temperature with a concentration of lower 0.01% of carbon. Its cubic structure is body-centered which leads to a soft and ductile characteristic of this zone.
- Cementite is also known as iron carbide or Fe_3C . It is an intermetallic compound, melts at 1837°C and is characterized by its hardness and brittleness. Pure cementite can be seen in the phase diagram on the right corner at 6.67% of carbon. When cementite occurs in steel it increases the hardness and decreases the ductility and toughness.
- Pearlite cannot be declared as a phase. It is rather a constituent or a mixture of the phases α -ferrite and Fe_3C (cementite). This structure is formed of alternated layers of each of them. Their characteristic is the combination of the hardness of the cementite and the ductility of the ferrite.
- Austenite is known as the γ -iron. Its main characteristic is its face-centered cubic structure. It is not present at room temperatures but it has a big influence in the processing of steel. Often the forming of steel performed in that phase because it is softer than ferrite and has therefore a high formability.

¹² cf. Bramfitt, B. L., et al. (2002) pp. 26

¹³ cf. Bramfitt, B. L., et al. (2002) pp. 25

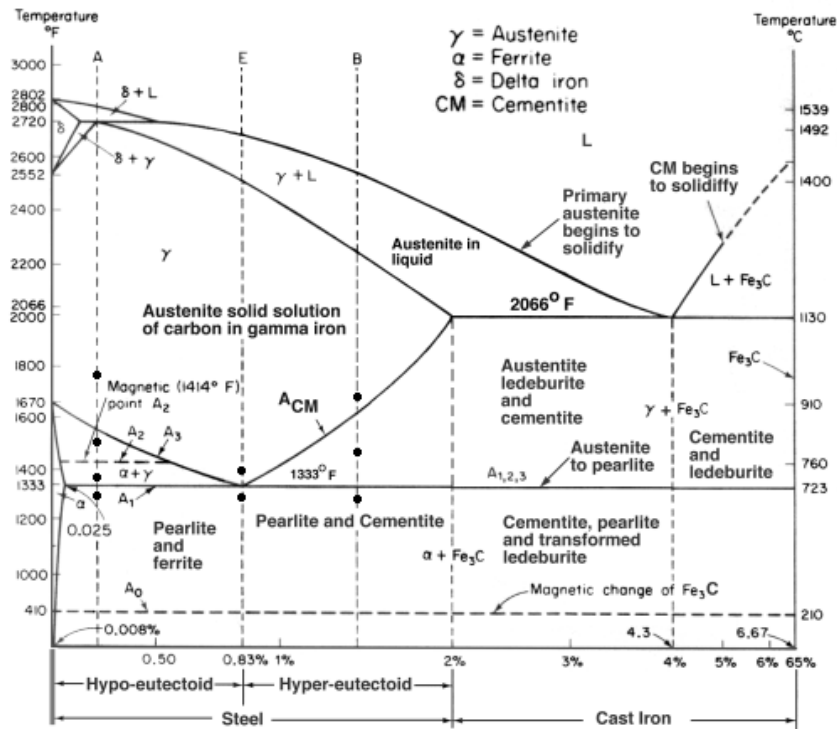


Figure 11: Iron carbon phase diagram, Source: Laboratory for scientific visual analysis (2015), Online Source [05.09.2015], qtd. in Pollack (1988)

With a carbon content higher 0.025% and below 0.8% both of these material have in their initial state a pearlitic and ferritic base structure as can be seen in the iron carbon phase diagram Figure 11 at the cooling line A and in the following Figure 12.

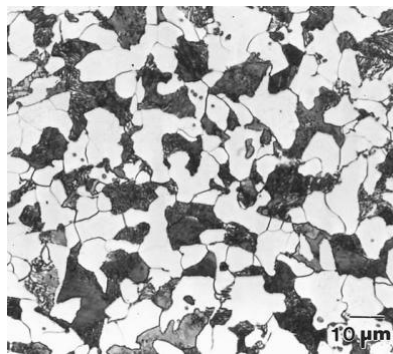


Figure 12: Ferritic and pearlitic initial structure, Source: Bramfitt, B. L. (2002) p. 28

Figure 12 shows a hypo-eutectoid structure consisting of ferrite (white constituent) and pearlite (dark constituent).

Since the iron carbon phase diagram and the initial structure of our materials are cooled down with infinite time, the considerations of the effects on the structure of rapid cooling, quenching is made in the following paragraphs.

Heat affected zone

At common thermal cutting techniques the heat source is travelling with the cutting speed v_c . When looking at on a straight path the heat propagation around the moving high power source can be seen as quasi-stationary.

Figure 13 helps to understand the temperature distribution on a specific location in the material perpendicular to the cutting direction even though it illustrates the temperature field around a momentary point source at welding. The left-hand figure shows the temperature distribution from the centre of the power source. In case of thermal cutting a vertical line at 3 mm can be drawn in order to illustrate the cutting face. The encasing line of all the temperature distributions is the curve of the maximum temperature T_{max} which is important for estimating the HAZ width later on. The right-hand figure represents the temperature distribution of specific locations over time and is important to evaluate the hardness.

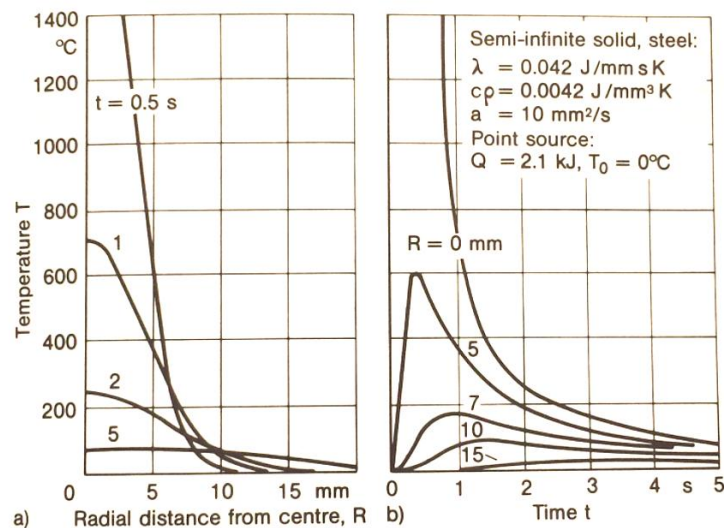


Figure 13: Temperature field around momentary point source on semi-infinite solid, temperature T over radial distance from centre R (left) and over time t (right), Source: Radaj (1992) p. 39.

In chapter 2.1.1 and 2.1.2 the heat input into the material has been calculated and the heat flow methods have been explained. Based on equation (7) the energy input (Line energy) E_{line} and the formula below the maximum temperature distribution for a rapidly moving high-power source in the infinite plate¹⁴ can be calculated. Based only on heat conduction.

T_0 stands for the working temperature, b_c for the thickness of the plate, λ the thermal conductivity, c the specific heat capacity of the material, t the time, r the distance from the power source and a the coefficient of thermal diffusivity.

¹⁴ Radaj, D., (1992) p. 50

$$T - T_0 = \left(\frac{E_{line}}{b_c \sqrt{4\pi\lambda\rho ct}} \right) e^{-\frac{r^2}{4at}} \quad (13)$$

With the help of the formula above the distribution of the maximum temperature in the material can be calculated. Figure 14 shows qualitatively the distribution of T_{max} and a part of the iron carbon phase diagram. The importance here is that the material which is heated above the A_{c1} temperature is part of the heat affected zone because it is full or partly austenitized and in combination with a high cooling rate this leads to changes in the microstructure.

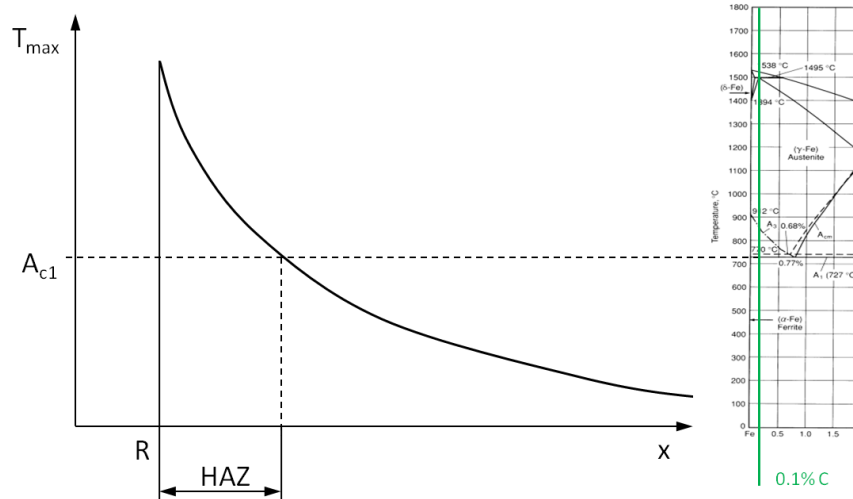


Figure 14: Cooling of the border zone of the cut, Source: own illustration

To analyze the cooling of the material in the HAZ the cooling time from 800 to 500 degrees $t_{8/5}$ is used. The cooling time only applies for a certain location as already seen in Figure 13 (right). Rykalin analyzed the cooling time $t_{8/5}$ of the heat affected zones for welding purposes by the formula below. This formula does not exactly apply for thermal cutting methods, but it is a valid approximation.

$$t_{8/5} = \frac{1}{2\pi\lambda} \frac{q}{v_c} \left(\frac{1}{500 - T_0} - \frac{1}{800 - T_0} \right) \quad (14)$$

Noticeable in Figure 13 (left) is the high temperature difference at the kerf. The high difference is the driving force for the heat flow. As a result the material cools down faster close to the cut as can be seen in Figure 13 (right) than with higher distance from the cut. The arrows highlight the temperature gradient $\frac{\partial T_m}{\partial t}$. Furthermore it is noticeable that the temperature with distance from the cut surface is reaching its peak later with a time delay.

These different cooling rates affect the structure of the material. The following Figure 15 illustrates the TTT-Diagram of an AISI 1010 material which has a carbon concentration of 0.10%. In this diagram the transformation into the different phases and constituents depending on different cooling rates can be seen. The zone A stands for Austenite, zone F for Ferrite, zone P for Pearlite, zone B for Bianite and zone M for Martensite. The curved lines which start at the top left corner are the lines of constant cooling rates. The more left the line the higher is the cooling rate and the higher is the percentage of martensitic structure in the material.

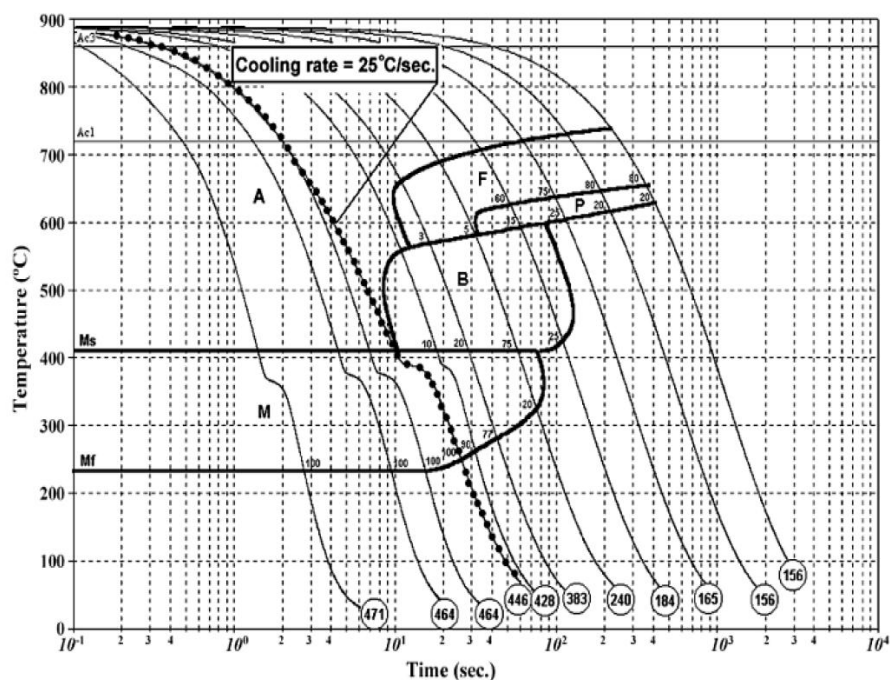


Figure 15: CCT-Diagram of 22MnB5, Source: Naderi M. et al. (2007) p. 446.

The interesting phase transformation is the transformation into the martensite constituent which occurs by high cooling rate (higher than 25 degrees per seconds as highlighted in the diagram) and high undercooling from the gamma-area (Austenite) down to room temperature. The transformation from cubic face-centered to cubic body-centered structure happens without diffusion of the carbon. As a result there is an extreme oversaturated alpha-solid solution created which tetragonal-distorted. Bramfitt results martensite as “The interstitial carbon atoms in solid solution in the parent austenite before transformation are “trapped” in the martensite lattice. Carbon steels with a fully martensitic structure are generally hard and have very little ductility in the as-quenched condition.”¹⁵

Bainite constituent is formed when cooling with intermediate speed, for example between water quenching and air cooling. Bhadeshia states “Bainite and martensite are generated from austenite without diffusion by a displacive mechanism. Not only does this lead to solute-trapping but also a

¹⁵ Bramfitt, B. L., et. al. (2002) p. 35

huge strain energy term, both of which reduce the heat of transformation. The growth of individual plates in both of these transformations is fast, but unlike martensite, the overall rate of reaction is much smaller for bainite.¹⁶ Bainitic steels are well-known for their high strength and good toughness balance.

Figure 16 is an intersection of the iron-phase diagram and the cooling speeds in the border are of the cut. Depending on the gradient $\frac{\partial T_m}{\partial t}$, the TTT-Diagram and the zone in the iron-phase diagram it is tried based on theory to divide the HAZ in different zones. Below is a description of the zones and the transformation.

- (0) Initial structure is a ferrite and pearlite constituent. This remains the same because of the low gradient $\frac{\partial T_m}{\partial t}$.
- (1) The initial structure is changed because the material is heated above the A_{c1} temperature and due to the higher cooling rate more pearlite is generated in the structure.
- (2) Due to faster cooling also bainite is created besides ferrite and pearlite. This area has already a greater hardness, but still a good toughness. The size of the ferrite grain increases with increasing temperature in the austenitic phase.
- (3) The high cooling rate in this zone leads to martensitic structure. This zone can have a great hardness and a low ductility.

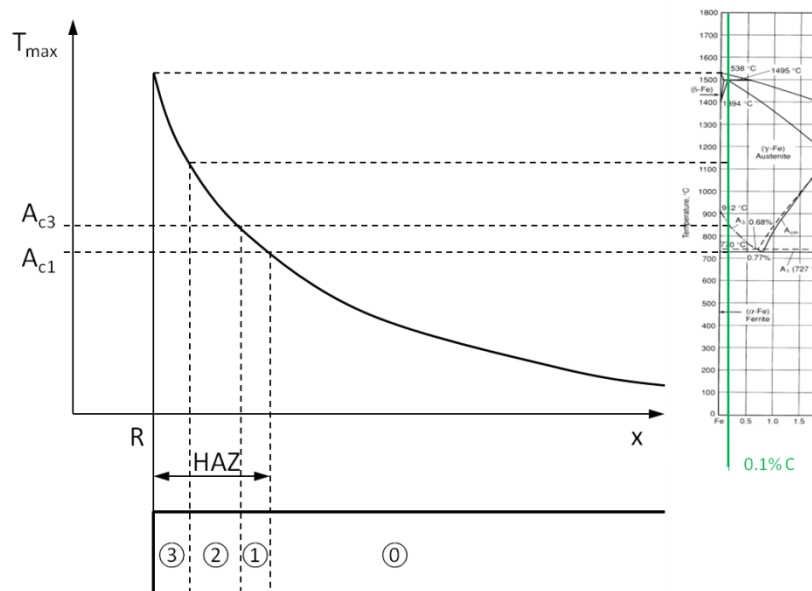


Figure 16: Zones in the HAZ of the cut, Source: own illustration.

Depending on the heat flow and material there is the creation of martensitic structure in the border zone of the cut and this can causes beneficial or unbeneficial effects.

¹⁶ Bhadeshia, H. K. D. H., (2007) p. 23

In case there is martensitic formation and the part requires hardness at the border zone then with martensite is a nice side-effect included in thermal cutting.

In the opposite case there also is martensite formation but additionally the final part has to perform at high dynamic and alternating forces with high hardness at border zones including low ductility and low plastic formability. Formability is defined by Meyers by “the combination of a low yield stress, high tensile stress, and a good total elongation in dual-phase steels leads to good formability.”¹⁷ Exactly that elongation is missing at the martensitic constituent and leads at locations with high alternating tensions and eventually to micro-cracks, as can be seen in Figure 17 below. These micro-cracks can result in an unexpected break down of the part earlier than it was built for. This effect is known as fatigue break downs. Therefore border zone hardness can be an important factor to foresee fatigue issues in the future. This hardness has been tested in the present paper to compare the plasma to the laser cutting technologies.

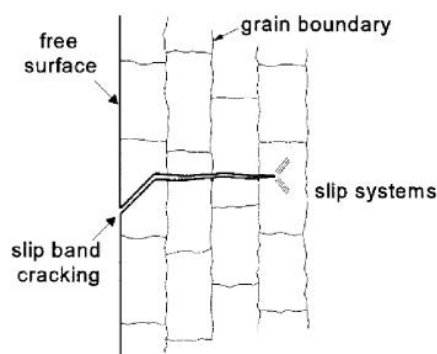


Fig. 2.4 Cross section of microcrack.

Figure 17: Cross section of a microcrack, Source: Schijve, J. (2009), p. 19.

The resistance against fatigue break downs can be compared to the resistance of the material as a bulk property against the crack growth. If there is a crack it is no longer a surface phenomenon.¹⁸

Tests and analyses regarding the fatigue need to know the case of application and the resulting state of the stress. If there are high alternating stress risers at the border zone of the material a separate fatigue tests have to be performed. At these tests the fatigue strength as the infinite life fatigue are simulated and illustrated in the Woehler-diagram which is shown in Figure 18 below.

¹⁷ Meyers, M. A., et al. (1984) p. 527

¹⁸ cf. Schijve, J. (2009), p. 21

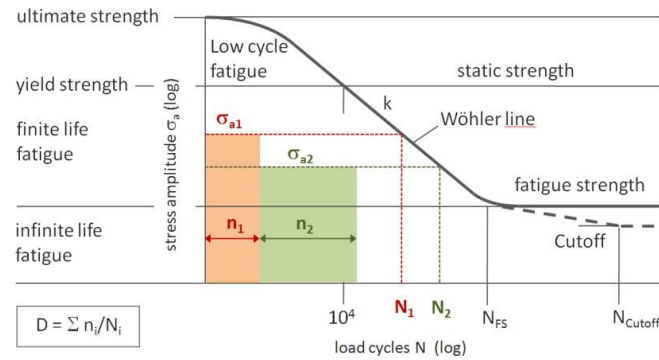


Figure 18: Wohler diagram, Source: CAE Simulation & Solutions (2015), Online Source [20.09.2015].

2.2. Plasma cutting technology

Different materials with different states of matter are surrounding us in the daily life. There is the solid, liquid and the gaseous phase and the presence of a state depends on characteristics of the material, the temperature and the environmental pressure. The main difference of the common three phases is the density.

When looking at the particle model the movement of the particles is an indicator for the temperature of the material. The type of movement of the three states is very different. For example in a gas the movement is straight as billiard balls, in a liquid state the particles have to squeeze through their neighbours and at solid materials the movement of the particle is much lower and just around a specific location.

By adding sufficient power to a gas the movements are getting even stronger and this leads to violent shocks of the particles to each other and molecules are getting dissociate, electrons separating from neutral atoms and the matter is ionized above 1 eV. In that state physical characteristics change again and that state is called plasma as the fourth state. Plasma can be seen in nature as lightning, the famous aurora lights or almost every star which can be seen in the universe is in the plasma state. In plasma state the gas is electrically conductive, the heat conduction is increasing and the density is also changing.

The addition of power or the excitation of molecules can be realized through different methods. In the case of cutting plasma it is the excitation through an electrostatic field. In physics electronvolt is a unit of energy at the atom level and can be calculated by the formula below. It demonstrates the change of the kinetic energy of a particle with the charge e by travelling through a potential difference U .

$$\Delta E_{kin} = e \cdot U \quad (15)$$

To describe the plasma state physicians developed a range of equations. In the following it is showed how to calculate the ionization grade. This grade defines the thermal energy which is created by transforming neutral atoms to simply ionized atoms A^+ and electrons e . The more ions are created, the more thermal energy is created and the higher is the ionization rate.¹⁹



Plasma per definition is a mixture of neutral atoms, ions and free, as can be seen in the Dalton-law below. This law describes furthermore that the total pressure is the calculated sum of the partial pressures. p stands for the total pressure, N_a , N_i^+ and N_e for the number density, k for the Ludwig Boltzmann constant and T for the temperature in the mixture.

$$p = (N_a + N_i^+ + N_e)kT_p \quad (17)$$

The plasma moreover can be declared as quasi-neutral as can be seen in the formula below where the number density of the electrons N_e equals the number density of the ions N_i^+ .

$$N_e = N_i^+ \quad (18)$$

The saha-equation defines the ionization rate and is a correlation to the prevailing temperature in the plasma and can be seen below. m_e stands for the electron mass, k for the Boltzmann constant, h for the Planck constant as the action quantum in quantum mechanics. N_a equals the number density of the atom, E_i the energy of the ion and $Z_a(T_p)$ and $Z_i(T_p)$ the sum of the state of the atom and the ion.

$$\frac{N_e N_i^+}{N_a} = 2 \frac{Z_i(T_p)}{Z_a(T_p)} \frac{(2\pi m_e k)^{3/2}}{h^3} T_p^{3/2} \exp\left(-\frac{E_i - \Delta E_i}{kT_p}\right) \quad (19)$$

The calculation of the sum of the states of the atom and the ion is calculated by the formulas where E_m^a , E_m^i stands for the term energy of the atom and the ion, g_m^a and g_m^i the statistical weights of atom and ion.

$$Z_a(T_p) = \sum_m g_m^a \exp\left(-\frac{E_m^a}{kT_p}\right) \quad (20)$$

$$Z_i(T_p) = \sum_m g_m^i \exp\left(-\frac{E_m^i}{kT_p}\right) \quad (21)$$

The lowering of the ionization energy can be calculated as by the formula below and is also considered in the Saha equation. ρ_D stands for the Debye length, ϵ_0 for the electrical field constant and e for the elementary charge.

¹⁹ cf. Neger, T. (2013) p. 24.

$$\Delta E_i = \frac{1}{4\pi\epsilon_0} \frac{e^2}{\rho_D} \quad (22)$$

For further information regarding the mathematical description of the plasma the author refers to specific literature.

Transportation process

According to the second law of thermodynamics heat energy is always flows as long as there is a difference in temperature. Furthermore it states that heat flows from hotter to colder bodies.

Heat energy can flow by the following three methods as already described in chapter 2.1.2 Energy input and heat flow:

- 1) Heat conduction
- 2) Convection
- 3) Radiation

The way how the plasma arc melts the metal is a product of all these three methods.

2.2.1. The plasma starting sequence

The starting of the plasma arc is described by the following steps.

- 1) The start input signal is sent to the power supply. The power supply simultaneously opens the circuit voltage and the plasma gas flow to the torch. No arc is created in the torch.
- 2) When the gas flow is stabilized, the high frequency circuit is activated as can be seen in Figure 19 below. This high frequency creates a bridge over the gas flow and between the electrode and the nozzle, which is connected to the plus pole. This bridge is created by ionizing the gas, the plasma pilot arc.

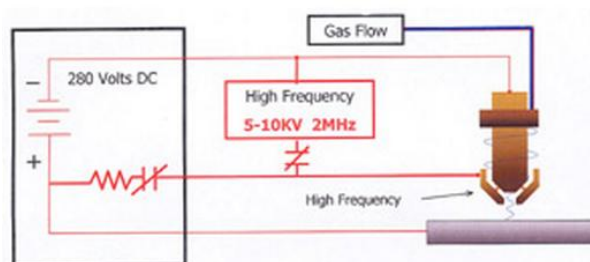


Figure 19: Cutting circuit while starting, Source: Hypertherm Inc. (2015), Online Source [21.09.2015]

- 3) Due to the strong gas flow the plasma pilot arc is pressed out of the nozzle and then attaches to the work piece which is also connected to the plus pole. When current flow over the work piece is sensed the high frequency is deactivated as can be seen in Figure 20. The current takes the way over the work piece because the resistance is less.

- 4) The energy of the plasma arc melts the material down and removes the molten material out of the kerf as can be seen in Figure 20 below – steady state.

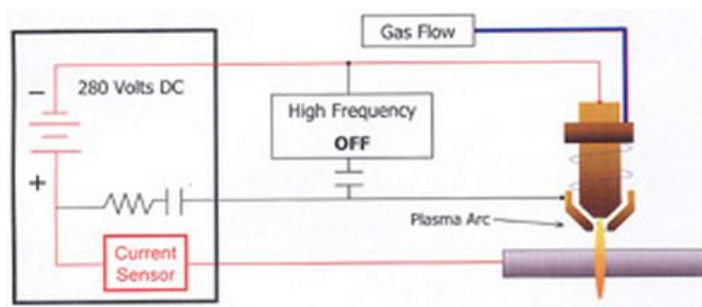


Figure 20: Cutting circuit while cutting, Source: Hypertherm Inc. (2015), Online Source [21.09.2015]

2.2.2. Materials

Since plasma cutting systems are based on ionizing the gas by an electrostatic field the work piece has to be electrical conductive. Therefore all metals and non-ferrous metals like aluminium, copper and brass can be cut.

2.2.3. Plasma arc vortex

The plasma gas flow is carrier of the energy. It contains the energy to melt the material down and to push it out of the kerf. Furthermore it is responsible for a lot of other factors like the formation of dross, the cut quality and perpendicularity.

When flow passes the negative charged electrode it gets ionized to a certain degree within in the potential field of the negative charged electrode and the positive charged part. Electrons are moving to the plus pole and ions are moving to the minus pole. And as can be seen in Figure 21 the ionized gas is centred in the middle of the vortex. It shows similarities to DC current in a conductor which is also self-centred. In the middle it has the highest temperature and energy density.

This influence can be attributed to the swirl gas flow. Due to the swirl the non-ionized atoms of the gas which are heavier and cooler are distributed to the outer layer of the swirling gas column which can be seen in Figure 21 on the left. That effect helps to protect the consumables because the temperature is lower at the outer column. Furthermore the swirl improves the cut quality. Without the swirling gas the kerf would be bevelled on both sides as can be seen in Figure 21 on the right picture A. The swirling effect leads to the better cut distribution and more perpendicularity as can be seen in Figure 21 right B. Nowadays every plasma system uses a swirl gas flow.

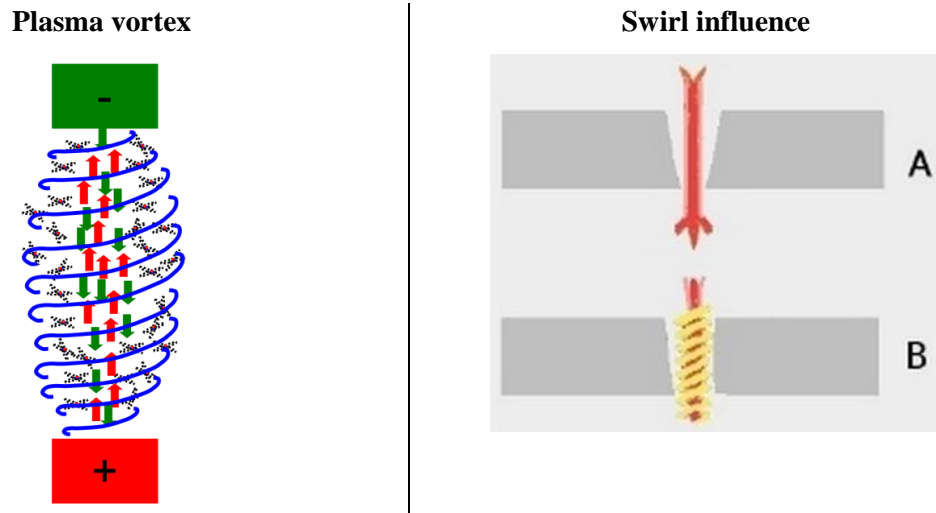


Figure 21: Plasma vortex, Source left picture: Hypertherm Inc. (2015), Online Source [21.09.2015], Source right picture: IDA Control (2015), Online Source [22.09.2015].

2.2.4. Different types of consumables and plasmas

Plasma systems can be divided according to different factors. In the present chapter plasma systems are divided according to two different characteristics.

The first one is the division into plasma systems with a shield gas and the systems without a shield gas. Unshielded gas stands for the use of only the plasma gas without any protection to the environment. The powermax finecut which is used in the following benchmark is an example for single gas systems. The benefit is that the design of the torch is very lean and the accessibility therefore is very high. The shielded version is the version displayed in Figure 22 below. That means that there is a second gas used for protecting the inner plasma gas from the environment which leads to less hardness and weld ready cuts as described in chapter 3.3.1 Plasma gas. Moreover it constricts and supports the plasma vortex which leads to a thinner kerf and a more stiff vortex. Furthermore it cools the nozzle, protects the nozzle from radiation and helps to remove molten material.

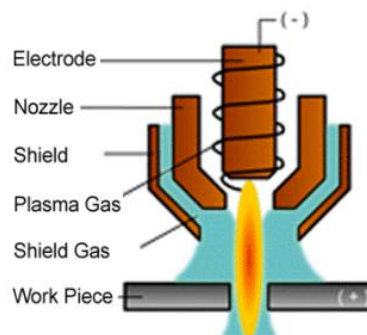


Figure 22: Conventional plasma, Source: Hypertherm Inc. (2015), Online Source [21.09.2015]

Some manufacturers also differ into the single gas and dual gas version. At the single gas version the plasma gas and shield gas are the same whereas those differ at the dual gas version.

The more common division is the division between the conventional plasma and the high performance plasma systems. The basic difference is that the plasma arc at the high performance system is more constricted and has a higher energy density. An illustration is shown in Figure 23 below.

This higher energy density is achieved by high-velocity flow vortex due to higher gas pressure, better mixing chambers and magnetic fields. Figure 23 illustrates that solution whereas the left picture illustrate the shielded version and the right one the unshielded one. Furthermore can be seen the flows of the process mediums. A and B stands for the flow of the cooling medium, C for the plasma process gas and D for the secondary shield gas.

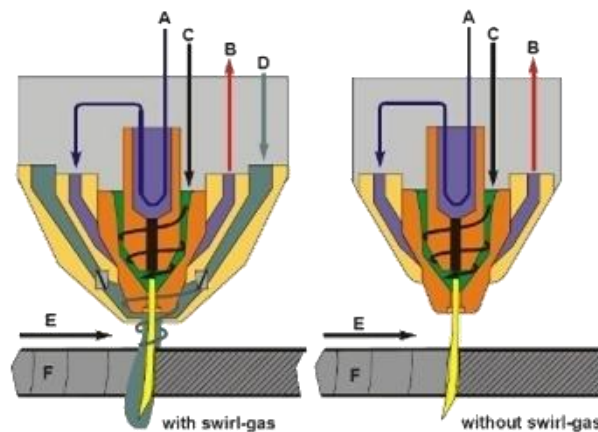


Figure 23: High performance plasma system, Source: IDA Control Automation Robotics, Online Source [22.09.2015]

2.2.5. Rotating of the torch

As described above the injected plasma swirl produces a good-side and a bad-side of the cut. By looking from above on the plasma vortex, as shown in Figure 24, the sides can be differed easily. The behaviour is similar to milling, climb-milling and up-milling.

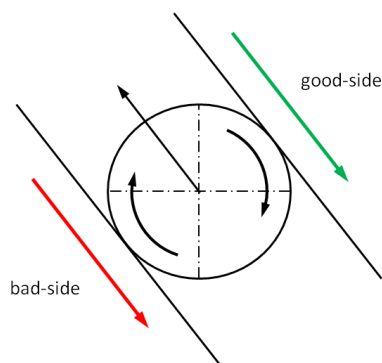


Figure 24: Good- and bad-side of the cut, Source: own illustration

When cutting a radius it comes to a relative movement. The red coordinate system in Figure 25 illustrates a turning movement of the torch and the black one illustrates a not turning one. At the red system the torch rotates with the radius and at the black not. This initiates an additional relative

movement. Comparing to the initiated swirl rotation this difference in speed is infinite and can be neglected as can be seen in Figure 25 on the right.

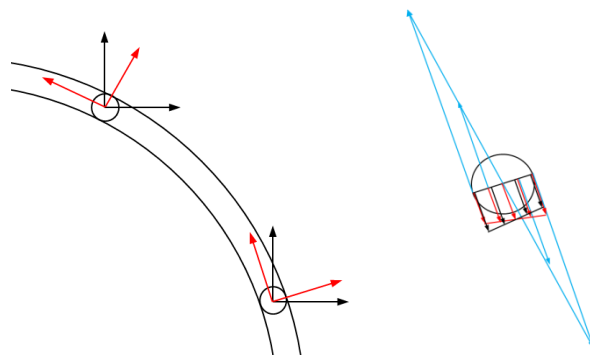


Figure 25: Robot movement in radius cuts, Source: own illustration

2.3. Robot technology

Ever since humans are dreaming of automate things and have more time for social activities. Automate because humans are not made for repeating and hard work which is not challenging at all. Since the industrial revolution at the beginning of the last century almost every industrial sector has been facing automation in order to work more precisely and with more productivity. Hesse, S. et al. specify automation as a social process where continuously human operations are replaced by functions of artificial systems (machines, robots, computer).²⁰ From 1970 on robots become an important member of the automation. Nowadays robots are getting more and more integrated into the complex structure of whole systems. In other words robots, automation and peripheral devices are merging together and become at the same time more flexible. With the use of artificial intelligence in the future these interplay with peripheral devices will become even easier. This applies for the industry and also for the private sector where robots will enter our own household.²¹

This paper only focuses on industry robotics and in more detail on the buckling arm robot. The buckling arm robot is usually built with six controlled axes connected in series. These axes are usually pivot joints where every pivot has its axis drive servomotor as can be seen in Figure 26.

²⁰ Hesse S. et al (2010) p. 19

²¹ cf. Hesse S. et al (2010) p. 26

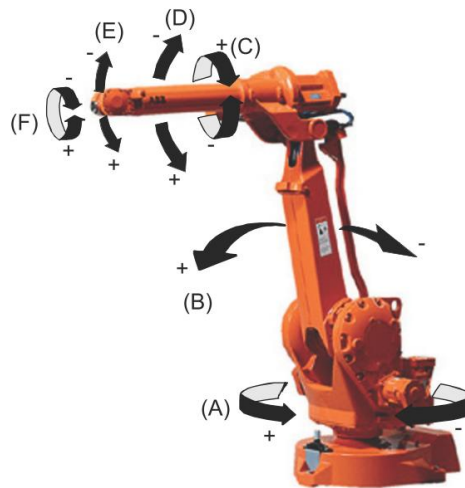


Figure 26: Buckling arm robot with six axes, Source: ABB product specification IRB 2400, p. 10

Due to their wide range, space saving size and flexibility they are widely used the industry. This joint of pivot axis has also some disadvantages. Since every axis is basically mounted on the other the inaccuracies are summed together. The inaccuracies occur due to the pivot axis but to a greater degree due to the clearance and the stiffness of the transmissions in the axes. As an effect the robot has less repeatability and problems with vibrations compared to a joint of five linear axes which is often used at laser machines. These machines are due to its design stiff, accurate and very fast.

Transmissions are basically used to transform the speed of the motor to the required speed. For the robot application special transmissions with a high gear ratio are used. As mentioned above clearance and stiffness are the main issues with these transmissions. Figure 27 illustrate gearings in use. Clearance is the distance between gear 4 and the gears 1 and 2 and stiffness is defined as the elastic deformation of the gears to each other.

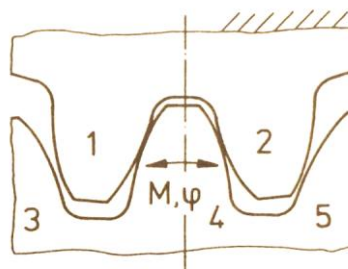


Figure 27: Gears in use, Source: Gerstmann U. (1991) p. 52

Clearance can be reduced by preload, geometric adaptation and precision production. Another method is to use few gearing levels and a high gear ratio at the last level or to use two engines to drive the axle.

Gerstmann (1991) assesses transmission by the static resilience curve as shown in Figure 28 below. This curve is created by adding the force F on the tip of the robot. For performing this test the breaks in the axes have to be released. When F becomes bigger than the weight of the lifted part the clearance appears in the diagram as a jump in the path. Since there are two axes in this force direction there are also two clearances. The stiffness or the static resilience can be described as the gradient of this curve.

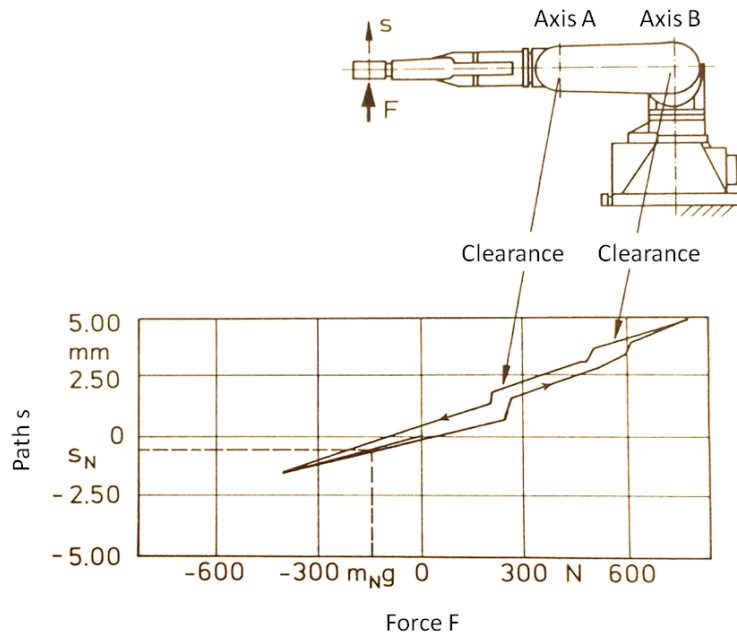


Figure 28: Static resilience line, Source: Gerstmann U. p. 75 (slightly adapted)

Nowadays almost in every robot transmission harmonic-drive transmissions are used which can be seen in Figure 29 below. The motor is connected to the elliptic wave connector in the middle and drives the flex spine. As the flex spine with the gears is flexible it maintains the elliptic shape and is pressed by the wave generator to the circular spline. Due to the high relative speed of the wave generator and the flex spine the gear ratio is created. This transmission has higher stiffness than the other transmissions and almost no clearance. Moreover its design is space saving and therefore it is commonly used in the industry.

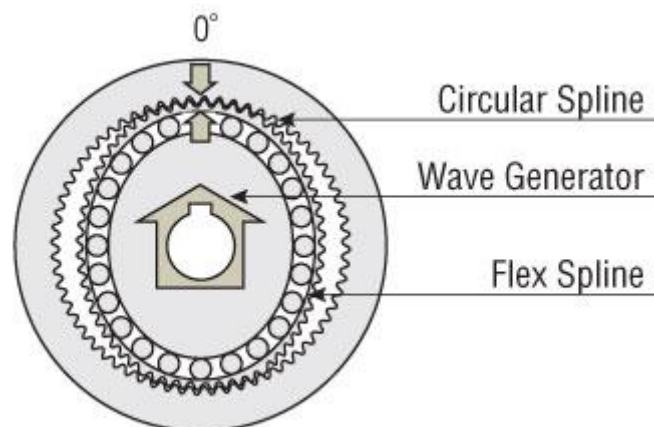


Figure 29: Harmonic-drive transmission, Source: Oriental motor U.S.A Corp (2015), Online Source [15.09.2015]

These explanations should help to understand why the transmissions are the softest parts in a robot. As a comparison at linear axes the transmission can be designed more rigid and therefore the stiffness of the whole machine is higher. Since the industry desires a cheaper solution than the five axes machines the trend is to cut also with a buckling arm robot. Therefore this robot is part of the benchmark in the present paper.

2.3.1. Edge movements – Vibrations

Moving through edges is one of the hardest challenges for the robot and the motion control. To maintain the required speed is not possible because of the inertia of the robot arm and the elasticity of the transmissions. If the robot has to reach a specific point and then goes in a completely new direction it has to decelerate to zero and then accelerate again. If the robot does not stop the remaining inertia in the moment when the robot tries to change the direction is used to deform the softest part in the transmission – the gears. This results in the vibrations of the TCP as shown in Figure 30 below.

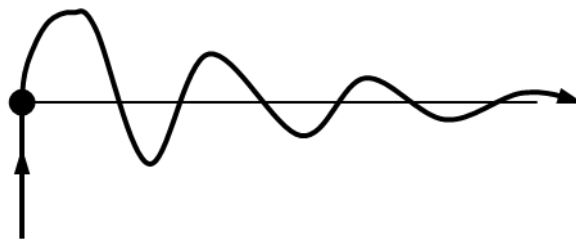


Figure 30: Vibrations after the corner without decelerating, Source: own illustration

The frequency with which the robot is vibrating is the eigenfrequency ω_0 and can be calculated with the following formula. c_e is the stiffness of the complete arm and m is the mass of the part which is vibrating. As a conclusion it can be said that the stiffer and lighter the arm is the higher is the eigenfrequency.

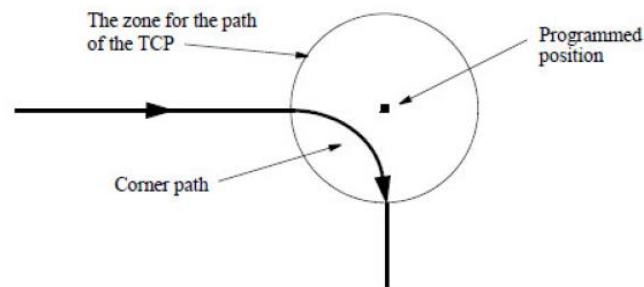
$$\omega_0 = \sqrt{\frac{c_e}{m}} \quad (23)$$

Formula (24) is showing how the resonance frequency is calculated when considering a damping ratio.

$$\omega_R = \omega_0 \sqrt{(1 - 2D^2)} \quad (24)$$

To prevent these vibrations robot manufacturer invented the corner zones where the robot not exactly reaches the programmed point but rather flies-by. These points are often called fly-by points. When

programming one can define the zone-diameter and the motion controller interpolates the best path and fastest path for the robot.



xx1100000643

Figure 26: A fly-by point generates a corner path to pass the programmed position.

Figure 31: Fly-by point, Source: ABB technical reference manual RAPID overview, p. 118

Depending on the diameter of the zone the motion control calculates the proper speed for travelling around the corner.

2.3.2. Motion control

The movement of a robot requires different steps as can be seen in Figure 32. Starting point is the planning of the path which is dependent on path parameter and the control for restrictions. The path parameters are specified by the robot programmer off- or online. The outcome of the first process is path parameters in Cartesian coordinates which are the input for the interpolation of the path. After this step the path is divided into path segments – one segment consists of various single points - which are transformed back to different coordinate systems in pivot angles in order to control the different pivot gears. These signals q_d are input for the axle gear control loop.

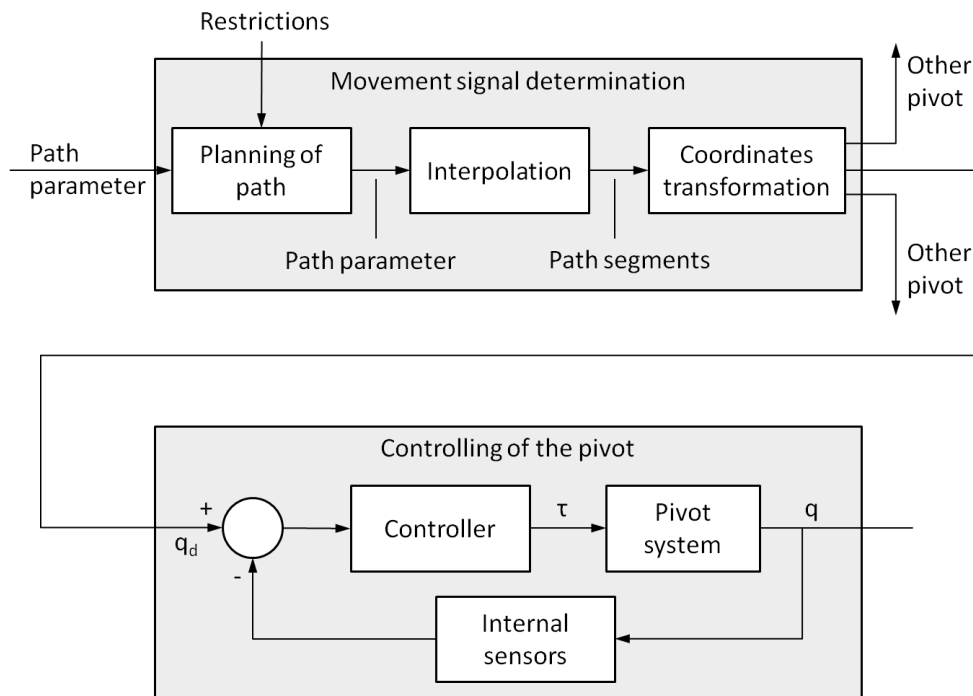


Figure 32: General structure of a robot control, Source: Hesse S. et al. (2010) p. 160 (slightly adapted)

The control of the robot movement can be divided into three different types:

1) Point-to-point control

At this type of control the path between the support points is not defined by the programmer. The motion control is calculating that the axes which are needed to perform the movement.

2) Multi-point control

At this type of control the programmer defines the path manually and the motion control is recording the movement and the orientation of the axes. The path cannot be described by lines or curves. Disadvantageous is the necessary high amount of storage.

3) Continuous-path control

This type of robot movement control is used when the TCP has to follow a specific path at every moment. The path is defined by the support points and extended by information regarding the shape of the path, the velocity and accelerations. Based on this information the speeds for the axes are calculated. All processing steps like cutting should be programmed in that way. ²²

For the movement of a robot alongside a path the motion control needs an interpolator. This interpolator is a central processing unit which divides the required path into points in order to guide the different joints. To do so there is the position- and the orientation interpolator which can be seen in Figure 33 below.

²² cf. Hesse S. et al (2010) p. 162 pp

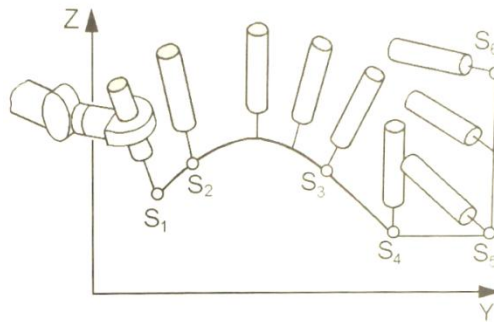


Figure 33: Orientation interpolation, Source: HesseS. et al. (2010) p. 191

Programming a robot

A programmer has two interests when programming a robot. The robot must follow a desired path at a required speed or in other words the programmer tells the robot where he must go and how. By doing so the motion control calculates the requested path first at Cartesian coordinates and transforms it back to different coordinate systems of the pivots. Besides that the control interplays between the different axes and calculates the possible speed to go through the path according to the axes' capabilities and restrictions. In other words the robot sets the speed at the end.

The motion control always will adapt the requested speed due to the following factors:

- Requested path
- Location of the part
- Axes position
- Restrictions due to maximum speeds of the pivots, singularities

Since at cutting processes maintaining the requested speed is important, the motion control tries to get close to it. By doing so the motion control often lets single axes move faster but what happens is that the path accuracy is decreasing by fast moving axes. Therefore uniformity in movement of the axes is desired. With some manufacturers it is possible to adapt the restrictions of orientation speed to increase the accuracy of the path.

2.3.3. Iterative learning control – iLC

Many robot manufacturers developed special software functions to improve the path accuracy. ABB developed for laser cutting a function called iterative learning control – iLC to improve the path accuracy at shapes, like circles or slots because laser faces the same problem at low speed and too much energy input.

iLC measures due to the sensors in the axes the path shape. After recording it compares the real shape with the desired one and creates offsets. In that way with every iteration the shape is getting more and more accurate as can be seen in Figure 34.

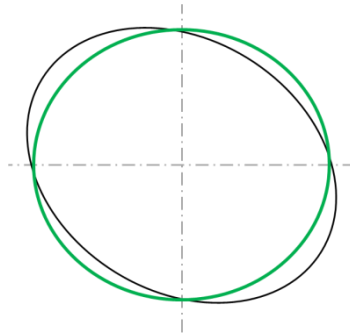


Figure 34: iLC optimized hole, Source: own illustration

The only disadvantage of iLC is that the method has to be done over and over again when changing the position of the shape. Furthermore when the robot also apply the torch-sensing this function is not working.

2.3.4. 3D – Cutting - importance to have a good TCP

The tool center point – TCP is the working point or tool reference point at the end of a robot arm. This point follows the path and has to be calibrated properly in order to get good results. Figure 35 illustrates the effect of a proper calibrated TCP and the one from a improper TCP. It clearly can be seen that the upper cut varies from the original one which leads to inaccurate cuts.

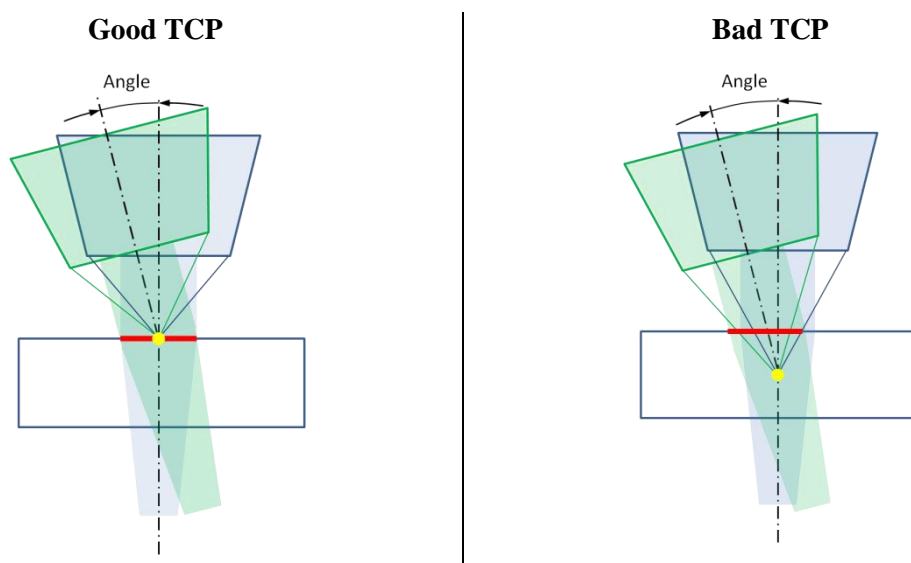


Figure 35: TCP effects when cutting, Source: oen illustration

2.4. Standards of cutting techniques

The present paper makes reference to the EN ISO 9013:2002 and the DIN 2310 (correlated ÖNORM 7857) which are the standards for the thermal cutting processes.

These standards refer to two different qualities and tolerances the cut surface quality and the size tolerance.

The main characteristics of the surface quality are the perpendicularity u or the tilting of the surface u , which can be seen in Figure 36, and the roughness depth R_z . With these characteristics it is tried to quantify the quality of the surface as can be seen in Figure 37 and Figure 38 which illustrate the perpendicularity u over the thickness of the material with plasma cutting and laser cutting. Noticeable is that the plasma working area is far bigger than the one from laser cutting. That illustrates one more time the strength of plasma cutting in the broad range of thickness that can be cut. Furthermore can be seen that the plasma is not as accurate as the laser solution. The validation of this statement in the range from 1 to 3 mm is part of the investigation here.

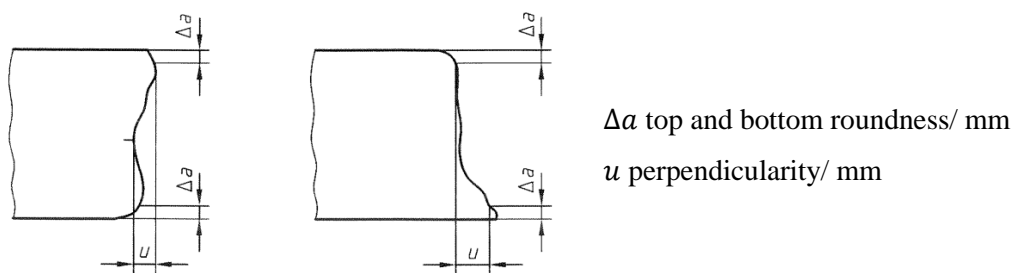


Figure 36: Perpendicularity/Tilting of the surface u , Source: cf. EN ISO 9013:2002

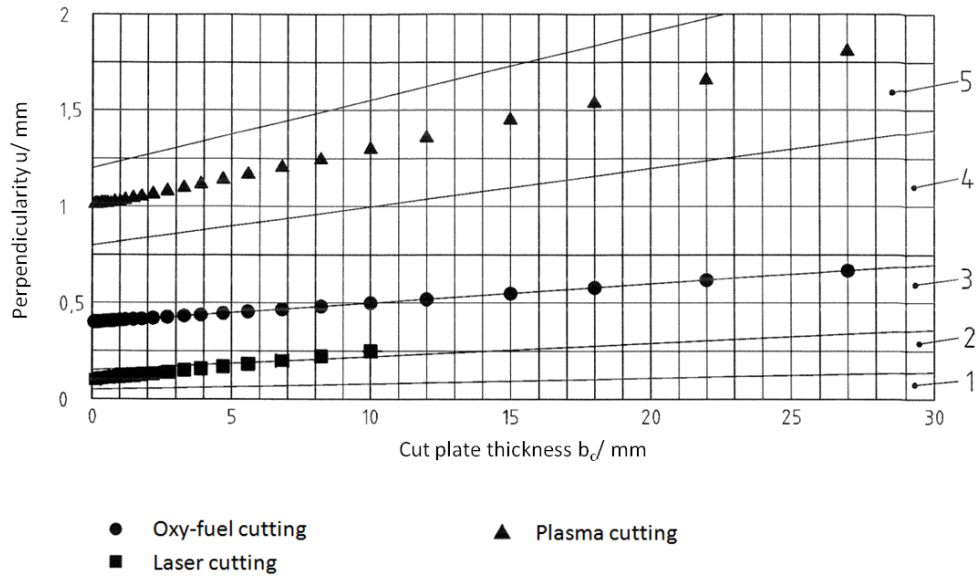


Figure 37: Perpendicularity/Tilting with Oxy-fuel-, Plasma- and Lasercutting, Source: cf. EN ISO 9013:2002 (slightly modified)

Figure 38 below shows the roughness depth R_z from plasma- and laser cutting. According to this standard the roughness of laser cutting at 3 mm thickness is $40 \mu m$ and the one from plasma cutting is $70 \mu m$.

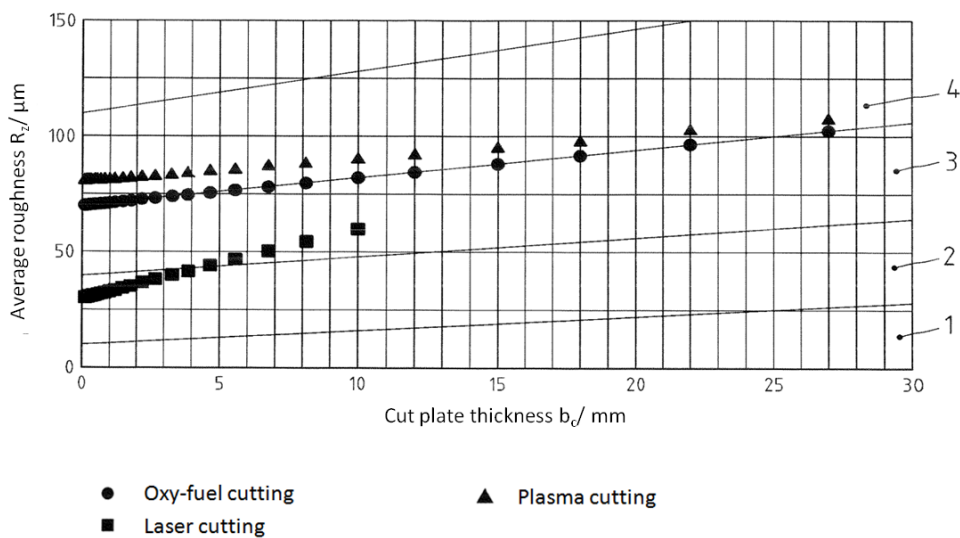


Figure 38: Surface roughness tolerance with Oxy-fuel-, Plasma- and Lasercutting, Source: cf. EN ISO 9013:2002 (slightly modified)

Size tolerance is the second major quality parameter. The part has to fit into an assembly and therefore the cutting-part nominal dimension B arises from the finished-part nominal dimension A minus the upper border dimension B_u , can be seen in Figure 39. The actual dimension of a part that is produced

by a thermal cutting process is always equal to the maximum value in the case of external dimensions and the minimum value in the case of internal dimensions.²³

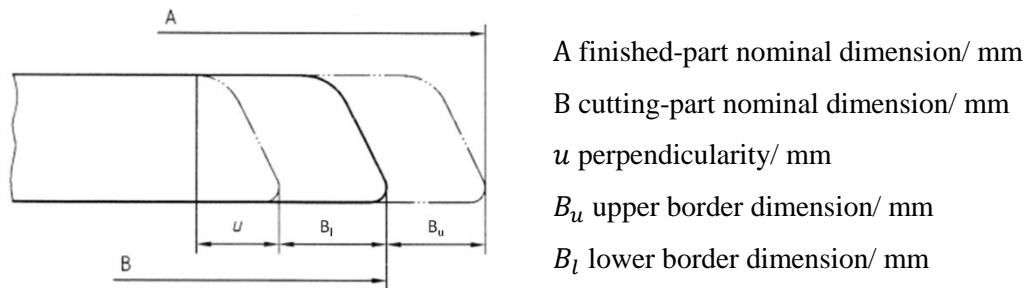


Figure 39: Size tolerance definition, Source: cf. EN ISO 9013:2002

To caption Figure 39 A is the finished-part nominal dimension, B is cutting-part nominal dimension, B_l is the lower border dimension and B_u id the upper border dimension.

The size tolerance quantifies the reachable tolerances on basic sizes in-between two lines or locations. Table 6 and Table 7 below show the reachable tolerances depending on the tolerance class and the size of the tolerance depending on the boundary dimension.

The size of the tolerance field for plasma cutting starts at 3 mm material thickness and it therefore cannot be proper used for plasma cutting solutions for automotive applications. Also the size of the boundary dimension does not help by fundamental questions for the plasma or the laser solution.

This is an additional knowledge gap which we try to close with this investigation.

Table 6: Size Tolerances for plasma cutting, Source: cf. DIN 2310

Toleranz- klasse	Werkstückdicke	Grenzabmaße für Nennmaße			
		35 bis unter 315	315 bis unter 1000	1000 bis unter 2000	2000 bis unter 4000
mm					
C	3 bis 50	± 1,0	± 1,0	± 1,5	± 2,0
	über 50 bis 100	± 1,5	± 2,0	± 2,5	± 3,0
D	3 bis 50	± 2,0	± 2,5	± 3,0	± 3,5
	über 50 bis 100	± 2,5	± 3,5	± 4,0	± 4,5

Table 7: Size Tolerances for laser cutting, Source: cf. DIN 2310

²³ cf. EN ISO 9013 (2002), p. 25-26

Toleranz- klasse	Werk- stück- dicke	Grenzabmaße für Nennmaße					
		bis 3	über 3 bis 10	über 10 bis 30	über 30 bis 120	über 120 bis 315	über 315 bis 1000
mm							
K	bis 1	± 0,03	± 0,04	± 0,05	± 0,06	± 0,08	± 0,1
	über 1 bis 3	± 0,08	± 0,1	± 0,12	± 0,15	± 0,2	± 0,25
	über 3 bis 6	± 0,16	± 0,2	± 0,25	± 0,3	± 0,35	± 0,45
	über 6 bis 10	± 0,3	± 0,35	± 0,4	± 0,5	± 0,6	± 0,7
L	bis 1	± 0,1	± 0,15	± 0,2	± 0,3	± 0,4	± 0,5
	über 1 bis 3	± 0,2	± 0,3	± 0,4	± 0,5	± 0,6	± 0,8
	über 3 bis 6	± 0,4	± 0,5	± 0,6	± 0,8	± 1,0	± 1,2
	über 6 bis 10	± 0,6	± 0,7	± 0,8	± 1,0	± 1,2	± 1,6

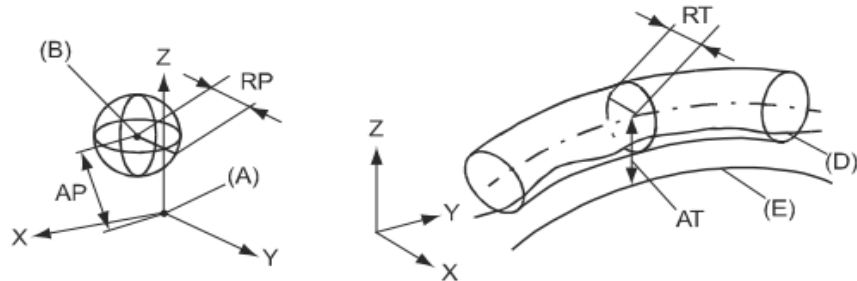
Additional to the cutting system there is the robot as an influence in the achievable accuracy. Figure 40 illustrates the performance of the used robot according to the standard ISO 9283. This standard defines the accuracy of the robot when stopping at a point and when running on a path.

The important value for the investigation is the RP and the RT value, because once the position and the path are calibrated the robot always repeats the position or the path within that radius.

Performance according to ISO 9283

At rated maximum load, maximum offset and 1.6 m/s velocity on the inclined ISO test plane, with all six axes in motion. Values in the table below are the average result of measurements on a small number of robots. The result may differ depending on where in the working range the robot is positioning, velocity, arm configuration, from which direction the position is approached, the load direction of the arm system. Backlashes in gearboxes also affect the result.

The figures for AP, RP, AT and RT are measured according to figure below.



xx080000424

Pos	Description	Pos	Description
A	Programmed position	E	Programmed path
B	Mean position at program execution	D	Actual path at program execution
AP	Mean distance from programmed position	AT	Max deviation from E to average path
RP	Tolerance of position B at repeated positioning	RT	Tolerance of the path at repeated program execution

Description	IRB 2400/10	IRB 2400/16
Pose repeatability, RP (mm)	0.03	0.03
Pose accuracy, AP ⁱ (mm)	0.03	0.03
Linear path repeatability, RT (mm)	0.11	0.15
Linear path accuracy, AT (mm)	0.33	0.41
Pose stabilization time, (PSt) to within 0.4 mm of the position (s)	0.15	0.22

ⁱ AP according to the ISO test above, is the difference between the reached position (position manually modified in the cell) and the average position obtained during program execution

The above values are the range of average test results from a number of robots.

Figure 40: Robot path accuracy according to ISO 9283, Source: ABB product specification IRB 2400 p. 34

RT and RP imply the 6σ spread and accuracy of the robot. What this means for the actual process is explained in the following chapter.

2.5. Process capability

In production every step, every cut represents a process which has a huge amount of influencing factors. In the German speaking area there are the 7M factors very common used to divide the factors into the human, machine, material, management, environment and method. Every factor affects the process and can be a disturbance variable or a control variable as can be seen in Figure 41 below.

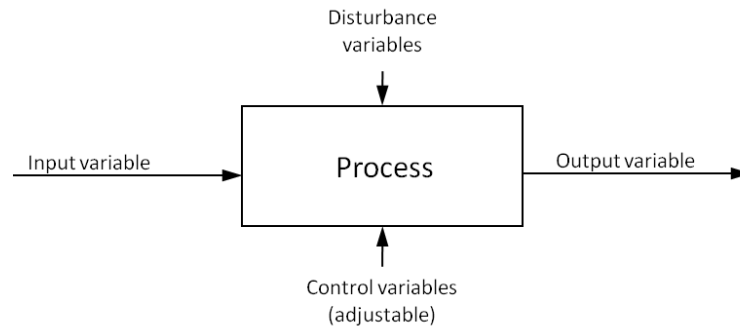


Figure 41: Process in quality control, Source: own illustration

These influencing factors can occur by chance or systematically. Those which **occur by chance** can have different causes like temperature changing's or vibrations and are considered **in the statistical process control**. Most of the time the amount or the value of the derivation is predictable, but the direction of the derivation cannot be foreseen.

Those which have their cause in **systematic methods** like bad adjustments by persons cause a constant derivation from the nominal value and can therefore **not be considered in the statistical process control**.

In this present paper it is tried to determine whether a process is capable of meeting specifications with statistical process control methods. Therefore the process capability c_p is used. c_p is the relationship between the specification spread T and the process spread 6σ .

$$C_p = \frac{T}{6\sigma} > 1 \quad (25)$$

When $c_p = 1$ the production method is with 99.73% capable of the process. That means that T equals 6σ which means that 99.73% of the products are within the required specifications. Technical applications nowadays require a $C_p \geq 1.33$. The automotive industry tends to require even more capability. A $C_p \geq 1.66$ is the standard, which means that 99.997% of the parts are within the border.

Figure 42 illustrates the normal distribution from Gauss which is centred at the arithmetic average \bar{x} . It also shows the standard derivation σ which also represents the turning point of the normal distribution. Between $\bar{x} - \sigma$ and $\bar{x} + \sigma$ are 68.27% of all the products. Furthermore it also represents the tolerance T with the lower specification line and the upper specification line.

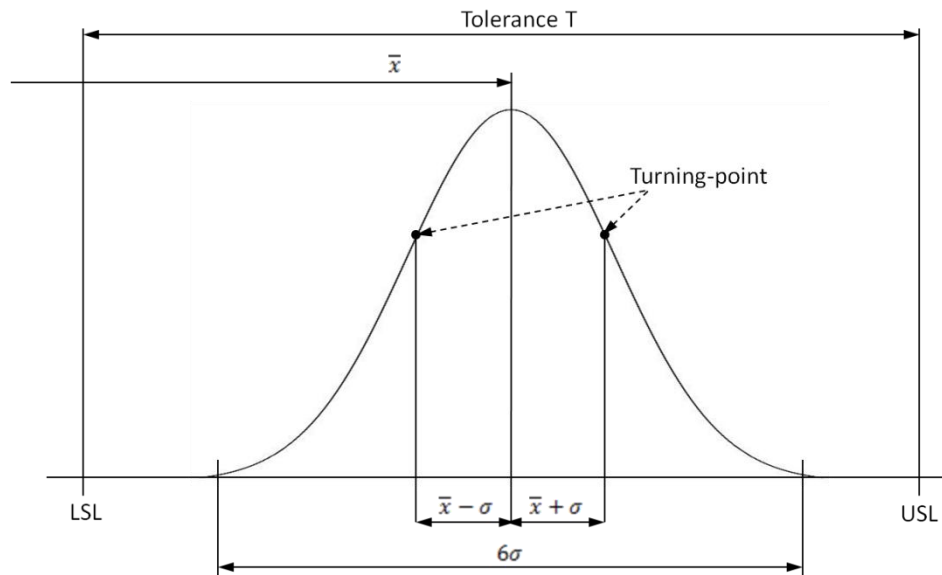


Figure 42: Normal distribution in the center of the tolerance ($C_p > 1.33$), Source: own illustration.

Since C_p is not defining the position of the process within the tolerance T one more index C_{pk} is defined. C_{pk} defines the adjustment of C_p of the non-centered distribution.

$$C_{pk} = \min \left[\frac{USL - \bar{x}}{3\sigma}, \frac{\bar{x} - LSL}{3\sigma} \right] \quad (26)$$

The time-horizon a process is going to be assessed also plays an important factor by defining the process capability. Short term tests can vary a lot from long term ones. Short-term process capability is defined as C_p and C_{pk} and long-term capability is defined as P_p and P_{pk} .

Long term process capability considers all influence variables in the process distribution and is therefore smaller in the value. **Another point of view could be that C_p stands what the process is capable of doing in the future, meanwhile P_p illustrates what has been in the past.**

In order to calculate the process capability out of samples in the following paragraphs necessary theory is described.

Starting by the average of a sample \bar{x} . It is calculated by the following formula and equals the arithmetic average.²⁴

$$\bar{x} = \sum_{i=1}^n \frac{x_i}{n} \quad (27)$$

The variance is an interesting number because it defines the span width or the variability of the sample. It is calculated with the following formula.²⁵

²⁴ Ross, S. M. (2004) p. 17

$$\text{Var}(x) = s^2 = \sum_{i=1}^n \frac{(x_i - \bar{x})^2}{n-1} \quad (28)$$

The standard deviation of the sample s is calculated by the square root of the variance according to the following formula. The standard deviation σ is calculated by considering all samples.²⁶

$$s = \sqrt{s^2} = \sqrt{\sum_{i=1}^n \frac{(x_i - \bar{x})^2}{n-1}} \quad (29)$$

In statistics there are different rules for calculation than in normal mathematics to consider. In the following paragraphs are the most important ones for the present paper explained.

Add to different average values are like in normal mathematics as can be seen in the following formula.

$$\bar{x}_{tot} = \bar{x}_1 + \bar{x}_2 \quad (30)$$

When adding two normal distributions following formula has to be considered.

$$s_{tot} = \sqrt{(s_1)^2 + (s_2)^2} \quad (31)$$

The reason for using formula (31) is the rules for adding the variance as described below.

$$\text{Var}(x_1 + x_2) = \text{Var}(x_1) + \text{Var}(x_2) \quad (32)$$

²⁵ Ross, S. M. (2004) p. 195

²⁶ Ross, S. M. (2004) p. 21

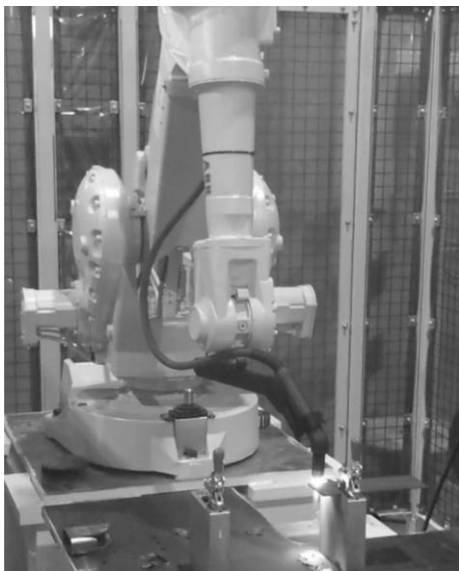
3. Experiments

Now experiments start and conclusions are made. The experiments can basically be divided into the assessment of the cut shape and the effect of the cut on the material. These two chapters are discussed in very detail including a detailed presentation and discussion of the results. Furthermore a chapter is used to describe the implementation of the a robotic plasma system into the process and at last point a benchmark of the robotic plasma and the robotic laser cutting is performed from the quality, the material affection and the financial site.

3.1. Test configuration and Test Cell

The tests performed at Magna CIMS on site included a small robot cell with an ABB robot IRB 2400, two different types of plasma machines of the brand Hypertherm which can be seen in Figure 43 below, a table and security installations. The left hand picture represents the Powermax 105A plasma cutting system mounted on the robot and on the right hand side the high performance 260XD plasma cutting system on the robot.

Powermax 105A



High performance plasma



Figure 43: Test equipment, Source: own illustration

Test approach

To get to the best results the test approach can be divided into three steps in order to find the parameters of influence:

- 1) Cut straight lines on flat plates

The goal of cutting straight lines is to get to characterize the shape of the cut at different speeds, heights and gas pressures. Furthermore with these tests the accuracy of the plasma cut can be assessed.

2) Cut shapes on flat plates

Different shapes and their influence to the plasma vortex should be examined. Furthermore the accuracy of circular cuts can be assessed and the dross formation can be observed.

3) Cut 3D shapes and the benchmark part

3D shapes are the supreme discipline and are performed at last step with the goal of holding the proper cut speed to prevent the formation of dross and to have the proper accuracy.

Test parts and material

Basically three different materials will be tested. The first material is S460MC and it is from a hydro formed tube with a thickness of 3mm. At this material the final cut is made and the study of the heat affected zone is made at this material. For the straight cuts and shape cuts the material 1018 with a thickness of 3 mm is taken. The complete investigation of 1.2 mm thickness plates is done at the hot stamped material Usibor 1500. Table 8 below illustrates the chemical composition.

Table 8: Chemical composition of the tested material, Source: Rautaruukki Corporation (2015), Online Source [06.09.2015].

	Carbon	Mangan	Phosphorus	Sulfur	Silicon	Alu	Nb	V	Ti
S460MC	0.1	1.5	0.025	0.01	0.03	0.015	0.09	0.2	0.15
1018	0.18	0.6-0.9	0.04	0.05	-	-	-	-	-
Usibor 1500	0.22	1.1	0.015	0.015	0.4	0.03			0.04

Measured values

1) Cutting speed or feed rate v_c .

The most important cutting parameter is the cutting speed or feed rate v_c . This value equals the speed of the TCP and can be set at the teach pendant. Besides that also the acceleration and the orientation speed of the TCP can be observed and recorded at the controller.

2) Torch distance h_{torch}

The torch distance is set and controlled by spacer plates.

3) Perpendicularity of the torch

Is controlled by an elbow.

4) Kerf width w_{uk} and w_{lk}

The upper and lower kerf width is measured by an electronic calliper.

5) Perpendicularity u

The perpendicularity is measured by an goniometer and then calculated to the perpendicularity u .

6) TCP

The TCP is set by an ABB feature called “BullsEye” where the tip of the torch is measured exactly with a laser and then the TCP is set with an offset of the tip.

3.2. Cut accuracy and quality

Since cutting of automotive parts is a very dynamic process there are several effects on the cut itself. Here in this chapter it is tried with the assistance of tests to explain these effects, to quantify them for a statement concerning accuracy and alternative solutions.

To provide a better overview Figure 44 illustrates the measurements which are crucial to assess the cut. First of all the plasma torch is guided by the robot and is considered by the measurement Δl_R . By looking at the cut geometry there is the upper kerf radius r_{uk} and the perpendicularity u . Another big parameter of influence to the cut quality is the formation of dross which can be seen on the bottom of the plate.

All of these factors have a certain variation when cutting with different speeds, heights and cutting different shapes.

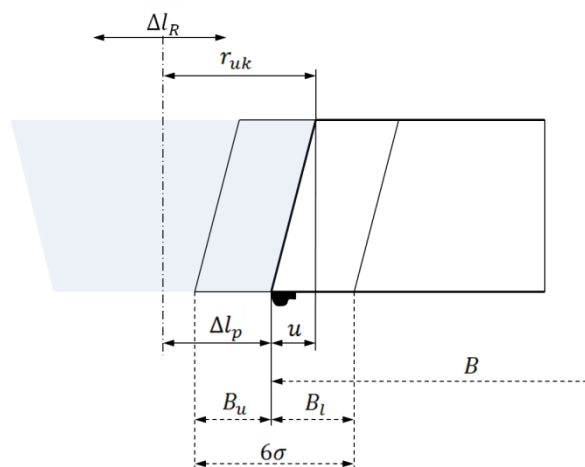


Figure 44: Cut measurements, Source: own illustration

3.2.1. Stabilizing of the plasma vortex – run-in zone

Plasma cutting divides the material by melting it down with a plasma gas flow which at the same moment blows the material out of the cut area. By doing so the plasma as a gas flow has to fight against the rigid material when moving. This resistance is reflected in the dragging of the cut or in other words the plasma gas flow is soft and tends to swing especially when changing direction or velocity. Therefore a slightly swinging of the lower cut can be observed up to five to ten millimeters when changing velocity or direction.

3.2.2. Cut shape influencers

As can be seen in chapter 2.4 Standards of cutting techniques the cut surface quality and tolerance are quantified by the perpendicularity u . That is the horizontal difference between upper- and lower cut edge. According to the standard this perpendicularity refers only to a specific thickness of the material. This is a very general statement because the shape of the cut depends due to our highly dynamic application on various different parameters.

The three most important are cutting speed, torch distance and the shape which needs to be cut. All this parameters affect the cut geometry and at the end the perpendicularity and the size accuracy.

3.2.2.1. Real cut geometry at ideal settings

The picture below, Figure 45, traces the cut geometry of a 3 mm mild steel sheet. It was cut by a PMX 85 System with FineCut consumables and air as a plasma gas. The settings were 55 A, the recommended torch distance of 1.5 mm and a travel speed of 55 mm/s. The cut surface is excellent and there is no dross on the neither the top and bottom side. The cut direction is into the paper, easily recognizable on the good- and bad-side of the cut. That cut is going to be the basis for reference for further derivations and relocations of the cut. Illustrations like Figure 45 are recreated in the 3D-design software SolidWorks according to the measurements.

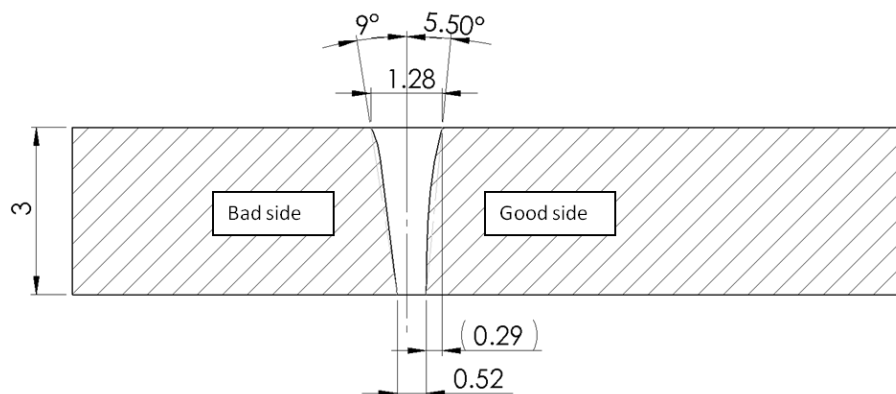
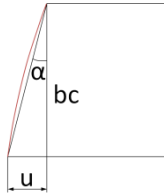


Figure 45: Shape of ideal speed cut with Powermax System and FineCut-Consumables 55A, rebuild in SolidWorks, Source: own illustration

Easily recognizable is that the cut is strongly asymmetric. First of all there is always a good- and a bad-side of the cut as described above. The good-side has a convex and the bad-side a concave cut curve. Furthermore the perpendicularity on the good-side is with 0.29 mm smaller than on the bad-side with 0.42 mm. All thermal cutting processes have that perpendicularity.

The way of determining the measurements

The upper and lower kerf width are measured by an electronic calliper. The perpendicularity u is measured by an analogue angle meter and then calculated to the perpendicularity u by using the formula below. Due to the convex rounding of the cut surface the measurement is quite difficult and that results in a spreading of the values.



$$u = b_c \cdot \tan \left(\alpha_c \cdot \frac{\pi}{180} \right) \quad (33)$$

3.2.2.2. Velocity influence (feed rate)

The velocity factor in cutting with the plasma vortex is significant. As can be seen in the diagram for the kerf width geometry, Figure 46, the upper kerf width is slightly decreasing over the speed spectrum in-between 1.4 mm and 1.2 mm which is due to the lower energy input when travelling faster.

Clearer is the behavior of the lower kerf width. The lower kerf width is decreasing strongly till it is getting very narrow at 65 mm/s.

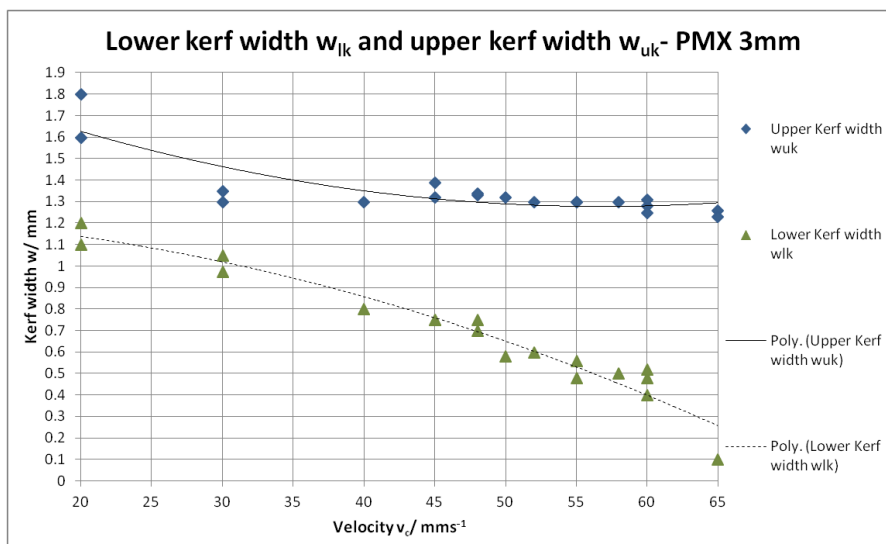


Figure 46: Lower and upper kerf width over speed, Source: own illustration

The important perpendicularity u of the good-side of the cut is shown in Figure 47. It has a big derivation and it slightly increases with higher cutting speed when looking at the interpolated curve. The big distribution is attributed to the plasma gas vortex and the way the samples are measured.

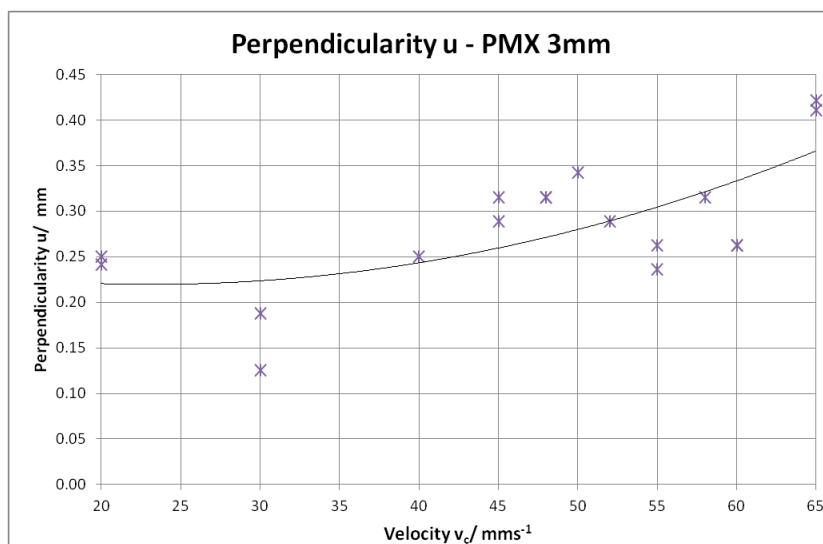


Figure 47: Spread of the perpendicularity u , Source: own illustration.

What are the reasons for this derivation of the cut geometry when changing the path velocity?

There are two effects taking place when changing the velocity. First when increasing the travelling speed the initiated energy does not have enough time to melt as much material as with lower speed. The energy per distance is lower. As a result the upper kerf width decreases and there is less material blown out, as could be seen in the cut geometry Figure 48 right and in the decreasing lower kerf-width in Figure 46. The second effect is the plasma gas vortex. Due to the Magnus-effect (lower static pressure on the good-side because of the higher speed) the vortex gets constantly forced to the good-side of the cut.

Cut geometry compared to the ideal cut geometry

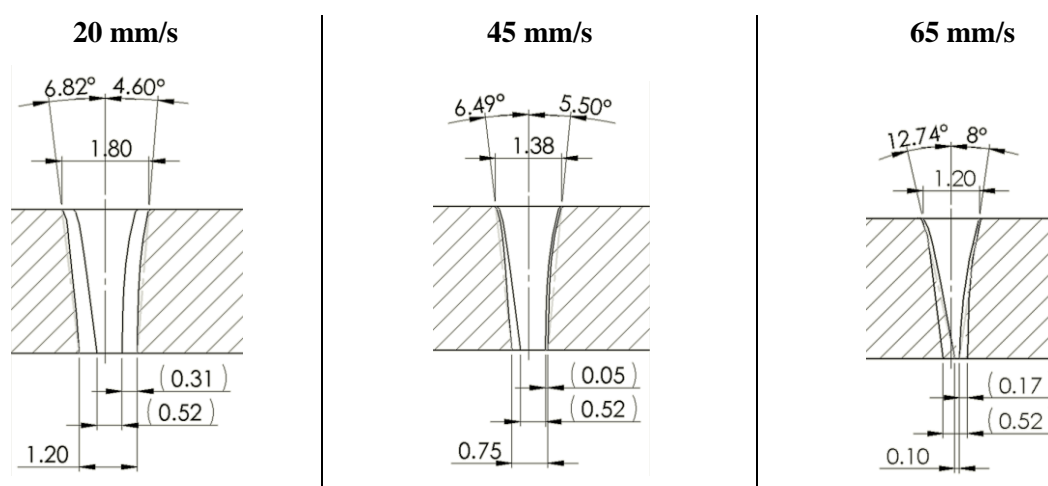


Figure 48: Geometrical influences on cut with different speeds, Source: own illustration.

3.2.2.3. Torch distance influence

As described in the theory part the torch distance has an impact on the cut shape and the dross probability. The torch height h_{torch} is the vertical distance between the part surface and the tip of the plasma torch as can be seen in Figure 49.

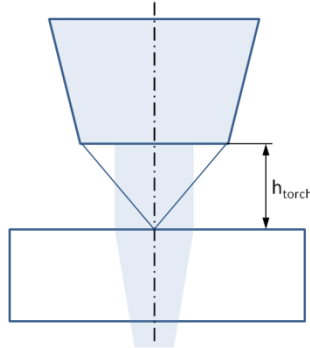


Figure 49: Torch height, Source: own illustration.

Figure 50 below demonstrates how the upper and lower kerf width differ over different speeds and torch heights (one colour equals one height). The recommended torch height is at the used amperage and consumables 1.5 mm and the main focus is in-between 55 and 65 mm/s because of the intention of evaluating where the limit in travel speed is.

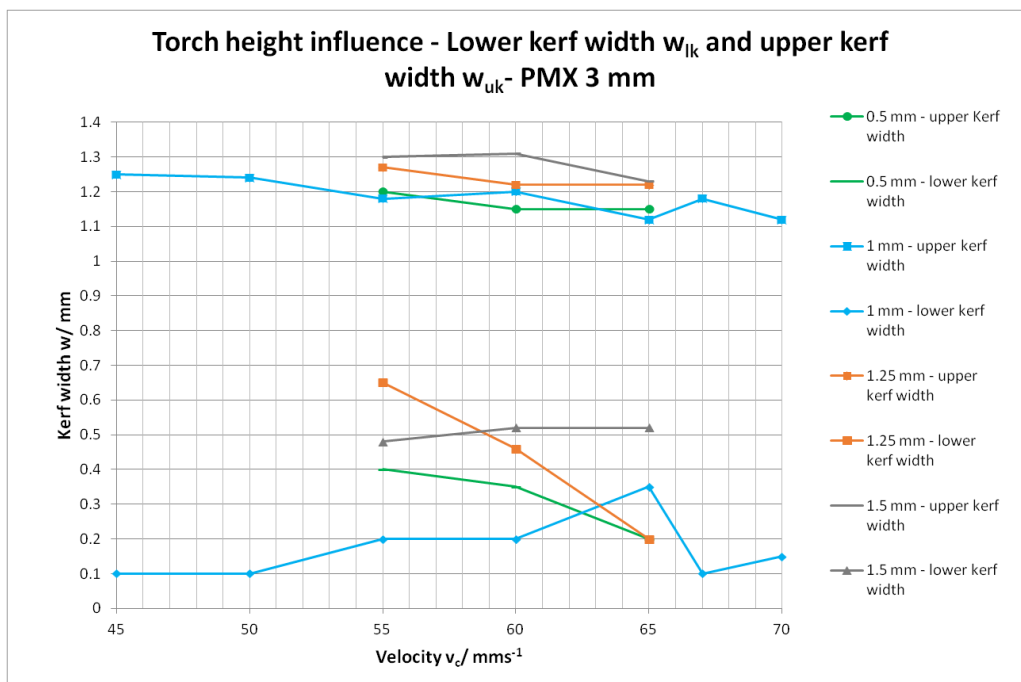


Figure 50: Torch height impact on lower and upper kerf width, Source: own illustration.

As an outcome can be seen that the torch height difference has almost no consequences on the upper kerf width. The upper kerf width remains at almost the same value. On the other hand the lower kerf width increases slightly with higher values of torch height.

Furthermore can be said that by lifting the torch higher than 1.5 mm from the surface the plasma arc get easily turned off during cutting due to the insufficient energy to ionize the gas. Cutting with close distance, closer than 1 mm, affects the consumables due to the immense heat, increases the risk of crashes and destruction of the consumables and the probability for dross.

Following Figure 51 displays the perpendicularity u development of different torch heights over speed. At the ideal cut velocity area between 55 and 60 mm/s there is an interesting trade-off. Cuts with a distance from 0.5 until 1 mm height have a clearly recognizable lower perpendicularity than cuts higher than 1 mm in torch distance. But cutting at this height is not recommendable because of the above described reasons.

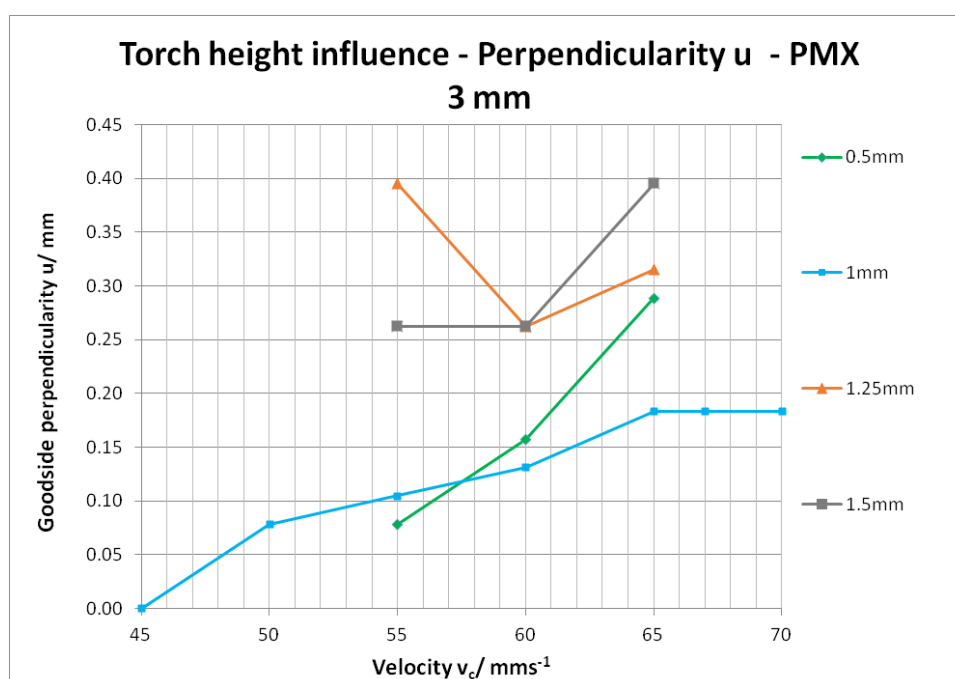


Figure 51: Torch height impact on the cut angle good-side, Source: own illustration.

The geometrical effects visualizes Figure 52 and shows the difference in the perpendicularity by 0.21 mm graphically. The cut in the back is the one with 1.5 mm distance and the one in front with 0.35 mm at the lower kerf width is the one with 0.5 mm torch height.

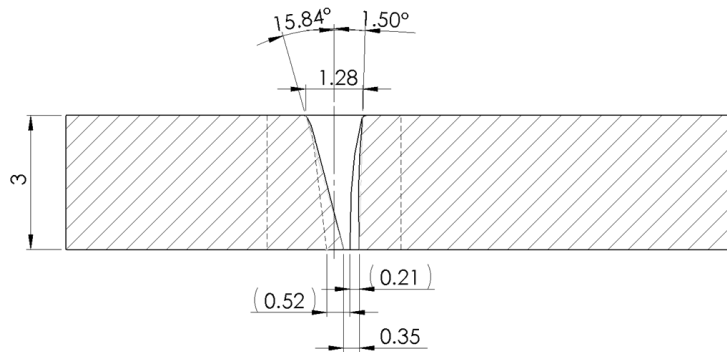


Figure 52: Cut geometry difference of 0,5mm & 1,5mm torch height at 55 mm/s, Source: own illustration.

As a conclusion can be said that the torch height with that type of machine, consumables and material thickness is a big influencer to cut geometry. The gas vortex is unshielded and unsupported and the area of cutting with a constant cross section is short as mentioned in chapter 2.2.3 Plasma arc vortex.

Due to this fact the ideal cut distance value is between 1 and 1.5 mm and this has to be provided in all situations during a cut.

To maintain that torch height special preparations have to be made on the side of the tooling and controlling side. Further information will be provided later.

3.2.3. Cut shape quality

Since the cutting process is an interaction with the robot, the plasma itself and the part with the tooling there are some factors to consider to assess the cut shape quality.

In order to provide a meaningful assessment, it is needed to quantify the accuracies which can be reached by the plasma cutting.

By dividing this assessment into four different areas it can be ensured that an engineer has a founded knowledge about this technology and at the end of the day it can be decided if the robotic plasma cutting is able to hold the required specifications. Therefore also a guideline is developed.

3.2.3.1. Straight cuts

The first and the most important area is the tolerance for straight cuts on flat areas with radius above 100 mm. The speed for the application varies in-between 50 and 60 mm/s. As mentioned to calculate the achievable accuracy 6σ the statistical formulas have to be used with the measured value Δl_p (see Figure 44).

$$\Delta l_p = r_{uk} - u \quad (34)$$

Figure 53 illustrates the important measurement on a cut. It also shows the imaginary Δl_R which is considered by s_{lR} in the calculations.

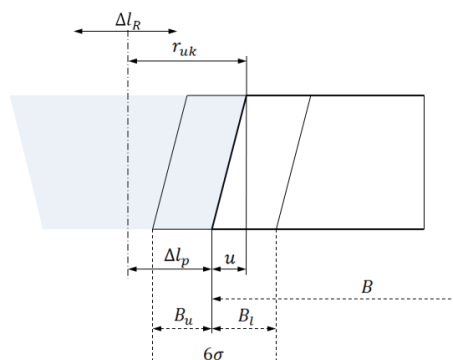


Figure 53: Standard deviation at straight cuts, Source: own illustration.

The achievable standard deviation at linear cuts s_l can be calculated out of the following formula with considering also the robot standard deviation s_{lR} which can be calculated by $RT/3$.²⁷

$$s_l = \sqrt{(s_{lp})^2 + (s_{lR})^2} \quad (35)$$

Table 9 below displays the results s and $6s$ of the cutting system accuracy for the PMX, HPR and a laser cutting system. The cutting velocity is the one ideal for each process.

Table 9: Accuracy for straight cuts, Source: own illustration.

	3 mm				1.2 mm		
	PMX finecut 55 A, 55 mm/s		HPR Bevel 80 A, 100 mm/s	Laser 2.5 kW 200mm/s	PMX finecut 55 A, 100 mm/s		Laser 2.5 kW 300mm/s
	Normal	Bevel cutting	Normal	Normal	Normal	Bevel cutting	Normal
s_{cut} [mm]	0.10	0.10	0.15	0.03	0.04	0.04	0.02
$6s_{cut}$ [mm]	0.57	0.57	0.88	0.15	0.24	0.24	0.11
s [mm]	0.11	0.11	0.16	0.06	0.06	0.06	0.05
$6s$ [mm]	0.65	0.65	0.93	0.34	0.38	0.38	0.32
$T_{straight}$ [mm]	0.86	0.86	1.24	0.45	0.51	0.51	0.43

The laser system is clearly the most accurate solution for both 1.2 and 3 mm thickness when considering s and $6s$. The major influence factor in the derivation is the robot system. The guiding system makes the laser system almost as accurate as the plasma system.

Moreover bevel cutting has the same accuracy when coming down to straight cuts but it has its benefit when looking at the perpendicularity u .

²⁷ ABB product specification IRB 2400 p.34

3.2.3.2. Circular cuts

Circles smaller than 100 mm in radius are in the focus in this chapter. The speed varies between 40 and 60 mm/s at these movements. The following formula illustrates which factors appear when cutting a circle. The circle cut accuracy Δc consists of Δc_p the plasma shape influence, Δc_T for the temperature influence due to the great heat input into the small area, $\Delta c_{lagging}$ for the effect of the lagging behind of the plasma and the related taking of shortcuts as described later and Δc_R describes the robot influence.

$$\Delta c = \Delta c_p + \Delta c_T + \Delta c_{lagging} + \Delta c_R \quad (36)$$

The plasma shape influence consists of the upper kerf radius r_{uk} and the perpendicularity u .

$$\Delta c_p = r_{uk} - u \quad (37)$$

The accuracy of the upper kerf width Δc_u is a good indicator for robot accuracy Δc_R , the widening of the upper kerf Δc_{uk} and the temperature influence Δc_T due to the great heat input into the small area of the plate. Reasons for the great heat input are the small cut radius, the piercing and the slow movement.

$$\Delta c_u = \Delta c_R + r_{uk} + \Delta c_T = \frac{d_{umax} - d_{umin}}{2} \quad (38)$$

All the mentioned formulas above regarding Δc are good for the understanding of what is happening in the cut and which effects are arising but for the assessment important is the shape of the lower cut circle. The following formula shows how this is measured and used for the evaluation. Formula (43) shows how the average diameter is calculated out of the measures.

$$d_m = \frac{d_{lmax} + d_{lmin}}{2} \quad (39)$$

The derivation Δc is calculated by subtracting the average measured diameter from the nominal diameter as can be seen in the following formula.

$$\Delta c = d_m - d_n \quad (40)$$

Figure 54 below displays the ideal and the real cuts of the holes with the robotic plasma cutting. The plasma cut diameter which is the programmed tip of the robot (TCP) and follows its ideal path. An absolute correct path cannot exist in the real world. The picture below also shows the definition of the tolerances and the real cut.

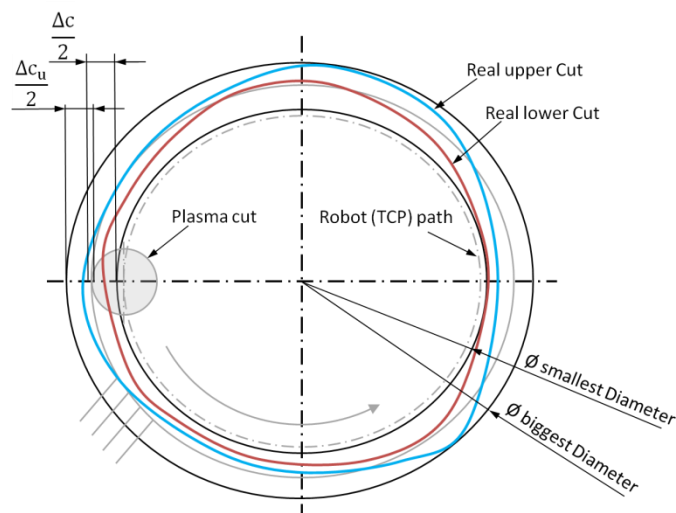


Figure 54: Ideal and Real shape of circular cuts, Source: own illustration.

In the chapter 3.2.2.2 Velocity influence is described that the w_{uk} strongly varies over the speed. The reason for that phenomenon is the higher or lower heat input at a position. For example, if there is more heat input in the material the kerf width expands because of the higher energy in the material. More material gets molded and blown out. The same happens when cutting a hole into the material even though it is cutted at ideal cut speed. Due to the piercing and the running-in path a huge amount of heat is added into the material already. Then the cutting itself on the small area adds additional heat. This variation is considered in Δc_T .

The influence of the **lagging behind** of the plasma during cutting is considered in $\Delta c_{lagging}$. The explanation for that mechanism is that the plasma energy is transported by a flow of gas. This flow of gas first melts the material on the top and then the lower one. By overlapping this with the forward movement of the plasma torch there arises the lagging behind of the cut by an angle of approximately 30 degrees, as can be seen in Figure 55 on the right side. Due to that mechanism the cutting at the lower surface has an offset and leads to the phenomenon that the plasma on the lower surface takes shortcuts. When the robot cuts a corner there always will be a greater radius on the lower side. This phenomenon also takes place when cutting circular shapes and is considered in $\Delta c_{lagging}$. The quality criteria cutting of edges in the following chapter 3.2.3.3 is trying to quantify this issue.

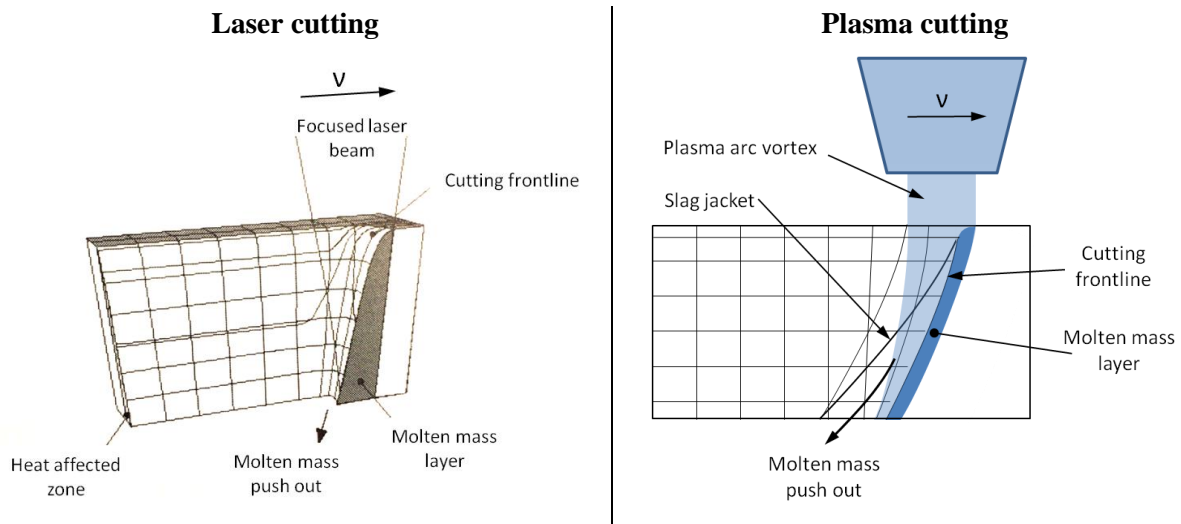


Figure 55: Lagging effect at the laser- and plasma cutting process, Source: left Popraqe (2005) p. 337 (slightly modified), right own illustration

This effect can hardly be avoided with plasma cutting. Reasons for that effect are the low process gas pressure, due to the plasma creation, and the low energy density. Therefore at technologies like oxifuel or plasma cutting where the melting- and the blowing out process are done with the same process gas, this effect cannot be avoided. On the other hand at the laser cutting technology the melting of the material and the blowing out process are separated. As a consequence the pressure of the process gas can be very high and the effect of lagging decreases. In other words the cut with laser is very stiff (low lagging effect) and the plasma cut is soft (high lagging effect).

Furthermore there is another phenomenon when cutting of round holes. The cut itself swings in-between a concave and a convex form as shown in Figure 56 below. This can be tied to the plasma gas vortex, the TCP-movement and the heat input in the material.

Plasma effects of cutting small circular shapes

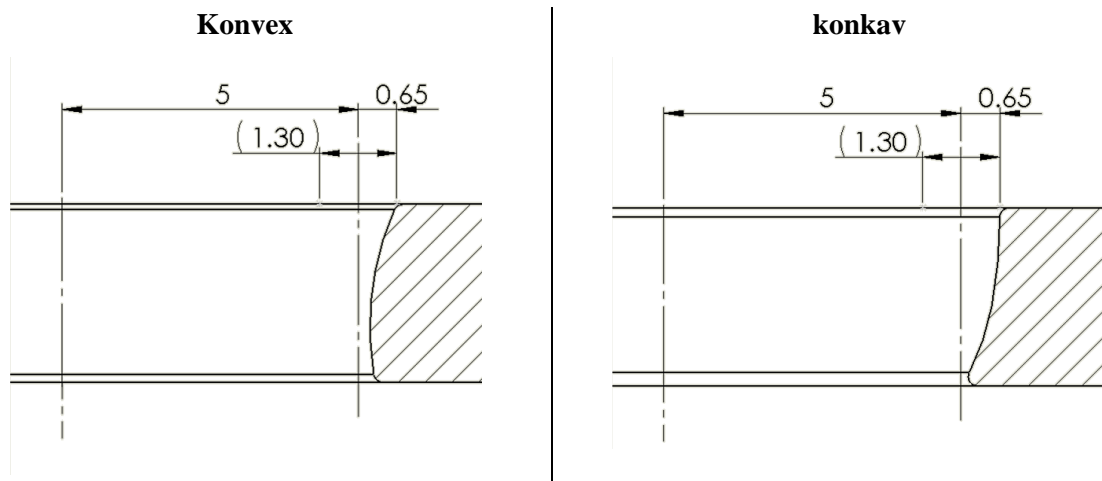


Figure 56: Plasma effects on cutting circular shapes, Source: own illustration.

While observing the samples of the different diameter cut there appears a phenomenon which can be seen in Figure 57. For explaining that phenomenon the complete hole cutting process has to be explained. Starting by the piercing the robot remains the required time (0.5 sec) at the same location and starts then to follow the path into the trajectory of the circle and reaches the final curve on the bottom of the circle. The robot cuts the circle and stops the arc where the surface changes its colour from yellow to blue. This area is interesting because the shape changes from a concave cut at the beginning to a convex cut at the zone where the plasma turns off. This phenomena can be observed at all circular cuts and as well at the rectangular cuts when the new cut is hitting the old one and is a consequence of the strong heat input.

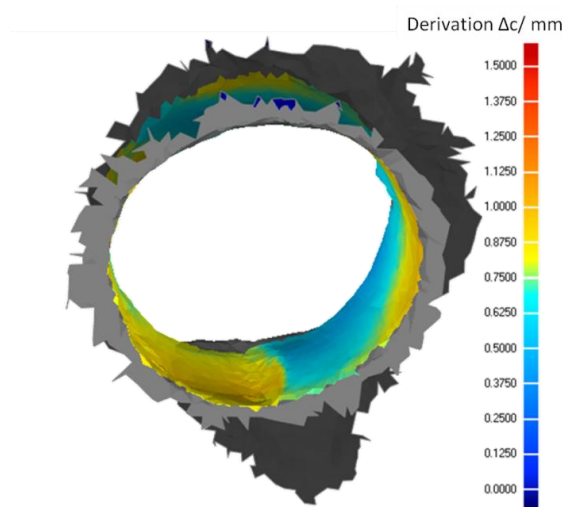


Figure 57: Cut out phenomenon of the plasma at a hole of 5 mm diameter (TCP), Source: own illustration.

With the assistance of the laser scanning system the parts are transformed into the CAD-System and a derivation analysis is performed, as can be seen in Figure 57 above (5 mm circle) and in Figure 58 from below (10 mm circle diameter).

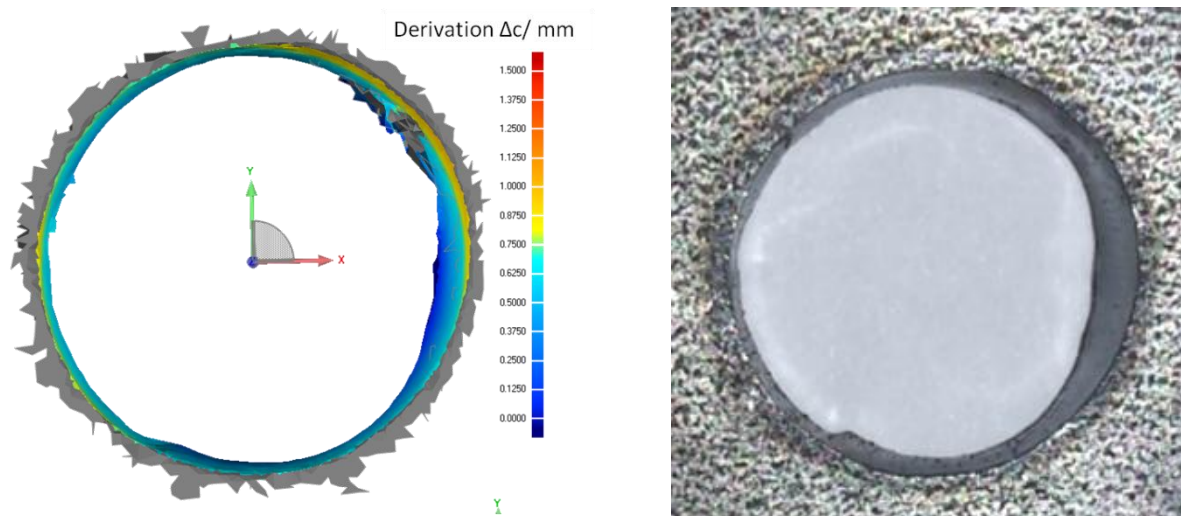


Figure 58: 10mm Circle (TCP) derivation and a picture of the real hole, Source: own illustration.

Furthermore this laser scanning helps by analyzing the shape of the cut surface itself by looking from the outside to the cut sides, as could be seen in Figure 59 and Figure 60. There easily can be spotted how much the cut surfaces differ over the cut path.

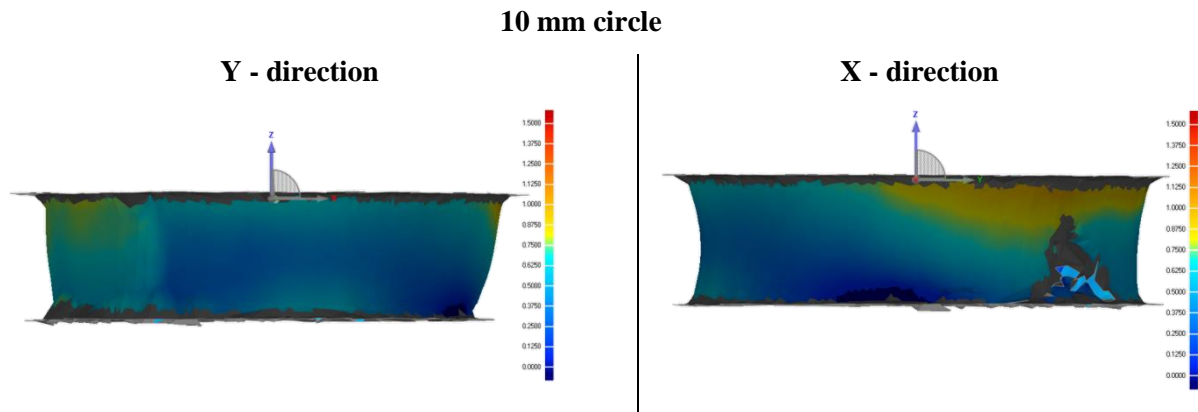


Figure 59: Scan 10 mm Circle (TCP) at 55 mm/s, Source: own illustration.

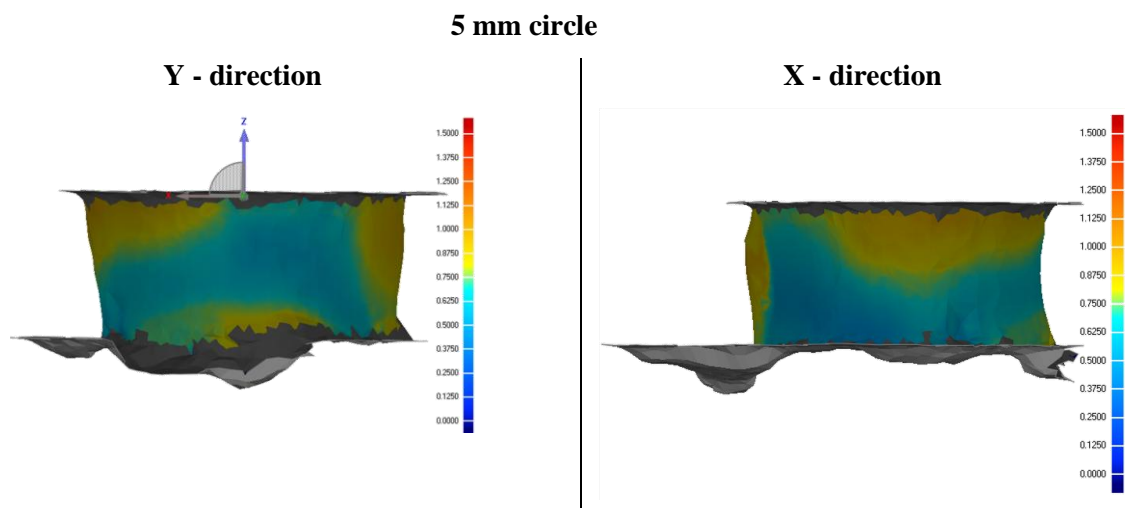


Figure 60: Scan 5 mm Circle (TCP) at 55 mm/s, Source: own illustration.

Looking at the pictures above it can be said that the effect lagging behind is a big influencer in the cut geometry. The gas vortex is unshielded and unsupported and therefore not stiff enough to decrease the angle and provide more accurate cuts.

In the following paragraphs it is tried to quantify the cutting of circular holes. The cutting tests are performed by the powermax finecut plasma system with the standard robot. The mild steel S460MC with 3 mm thickness and the martensitic steel 22MnB5 with 1.2 mm thickness are cut.

Choosing the proper cutting speed is the main issue because due to the heat and dross issues low speeds are not preferable but on the other hand the robot can achieve better results at lower speeds.

Figure 61 illustrates the upper cut derivation Δc_u of a hole with a nominal diameter of 8 mm. It can be seen easily that the robot is more accurate at lower speeds. That fact has to be considered when choosing the optimal speed.

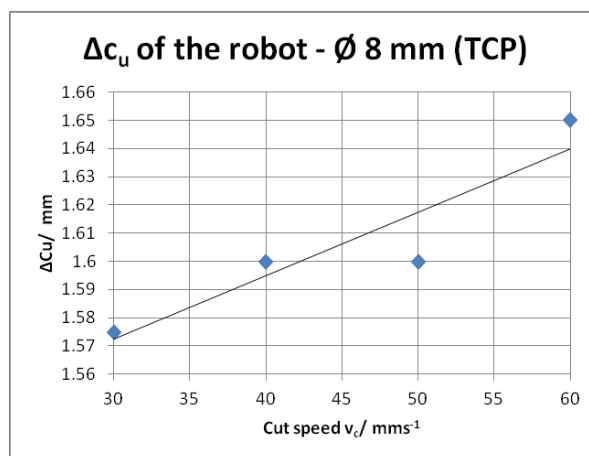


Figure 61: Accuracy at circular movements, Source: own illustration.

Figure 62 shows another effect when cutting with plasma which is worth considering. The overlay zone where the plasma cuts the hole a second time does not reflect the right diameter. As the plasma is an arc which has a pole at the electrode and the other pole is the part it also searches for the material to cut. As an effect the plasma arc cuts the material even more which can be seen at the lower side of the hole. When cutting it has to be ensured.

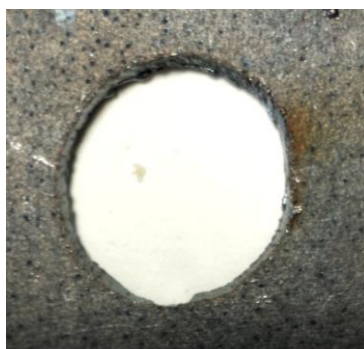


Figure 62: Overlay effect, Source: own illustration.

Figure 63 shows diagrams where the median upper and lower cut diameter d_{mu} and d_{ml} are shown in the ordinate and the cutting speed in the abszisse. The cutted material is the 22MnB5 with a thickness of 1.2 mm. The main outcome of this figure is that the lower cut diameter is approaching the upper cut diameter with decreasing speed. That means the effect lagging behind decreases and the cut gets more perpendicular which also correlates with the results in the straight cuts.

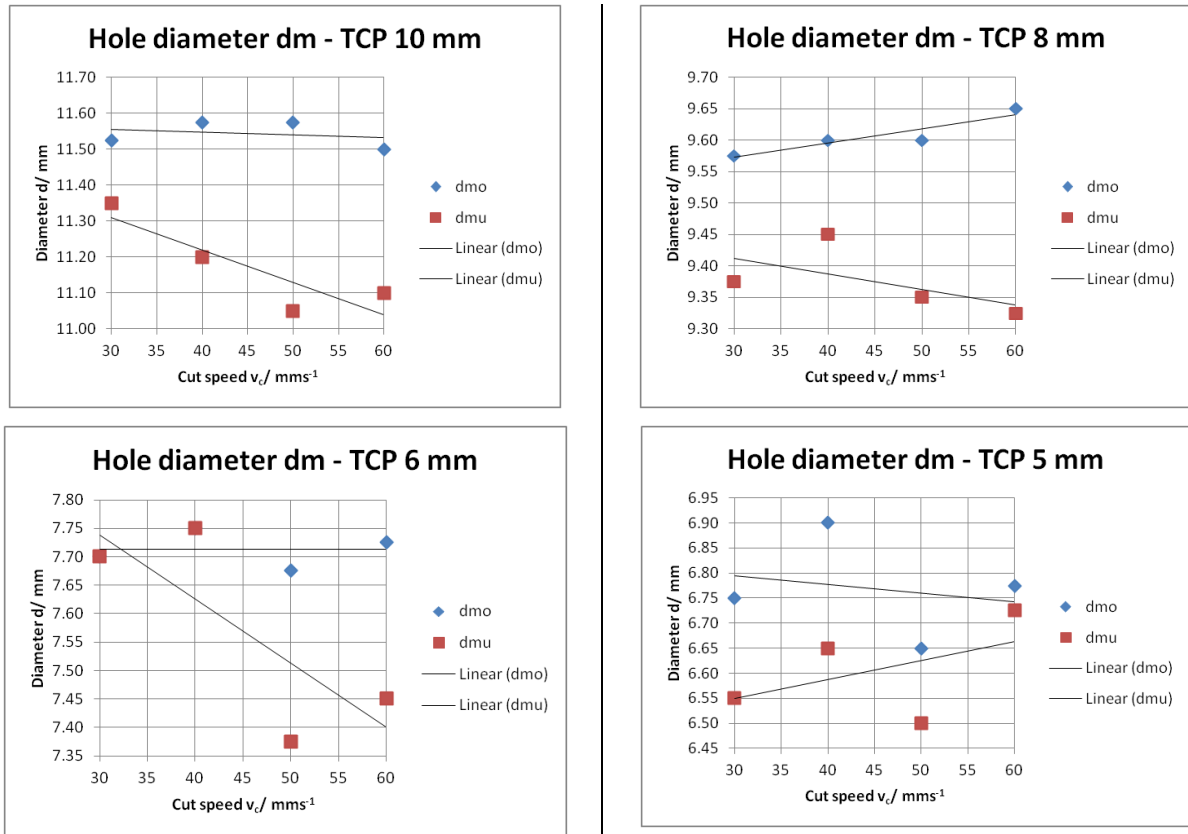


Figure 63: Development of the median cut diameter with speed, Source: own illustration

Figure 63 also outlines that the lower kerf directly response to the upper one and that there are no unexpected phenomena like changing between convex and concave cut shape or something. That means that cutting of thinner shapes is more accurate than thicker ones. In that case the accuracy can be compared to the one of the straight cuts.

On the other hand Figure 64 shows issues with the formation of dross. It seems that the heat input in the material especially at small circles is too high and the formation of dross is supported. This has to be taken into account when deciding. It also illustrates the improvement of the robot accuracy with lower speed.

The Figure 64 below illustrates holes of 11.3, 9.3, 8.3, 7.3, 6.3 and 5.8 mm in diameter.

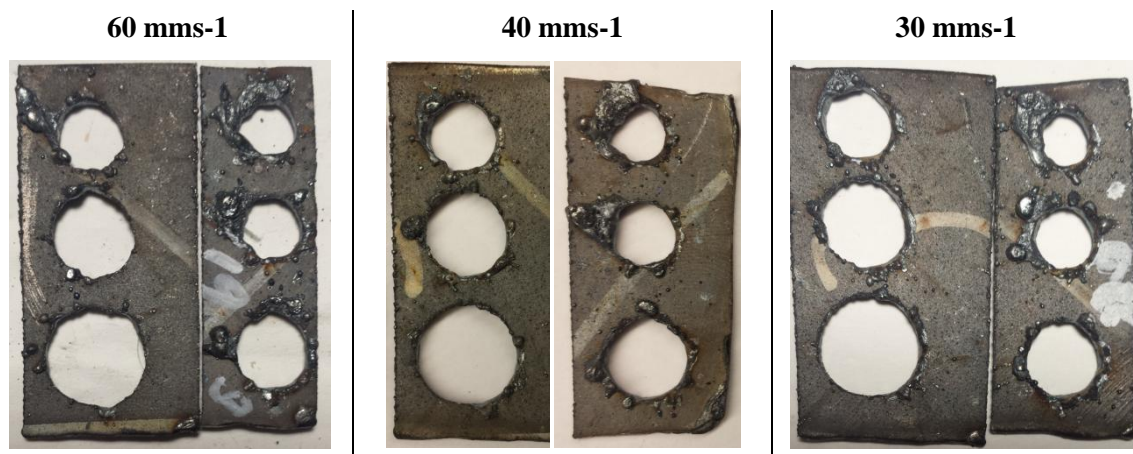


Figure 64: Dross issues with plasma cuts at 1.2 mm thickness, Source: own illustration.

Table 10 illustrates the accuracy of circular cuts at a 3 mm plate of mild steel. It is outstanding that 6σ is very high starting with 0.64 mm at a diameter of 10 mm. That derivation is measured at the bottom cut and includes the lagging of the plasma and the robot inaccuracy. The following formula is a transformation of formula (31) and it is used to calculate the standard derivation of the plasma cut by taking the standard derivation of the lower kerf s_{tot} and subtract the one from the upper kerf s_u .

$$s_{cp} = \sqrt{(s_c)^2 - (s_{CR})^2} \quad (41)$$

Table 10: Accuracy of circular cuts at a plate 3 mm in thickness, Source: own illustration.

PMX finecut 55A, 55 mms-1, 3 mm				
Diameter [mm]	10	8	6	5
d _{mu} [mm]	11.34	9.37	7.30	6.36
d _m [mm]	10.60	8.75	6.78	5.80
s [mm]	0.11	0.12	0.17	0.21
6s [mm]	0.64	0.71	1.02	1.28
s _u [mm]	0.12	0.03	0.15	0.08
6s _u [mm]	0.72	0.20	0.91	0.48
s _p [mm]	-	0.11	0.08	0.20
6s _p [mm]	-	0.68	0.46	1.18
T _{cycle} [mm]	0.85	0.94	1.35	1.70

Based on the assumption that the standard upper derivation s_u considers the robot derivation only and the standard lower derivation s considers everything the derivation of the plasma cut itself is calculated. As a conclusion it can be said, that the derivation of the plasma cut system itself is always lower as the one from the robot. As a consequence the total derivation is mainly defined by the robot.

At thicker materials the formation of dross is more problematic because of more material which is blown out.

Therefore the chosen velocity with 55 mms-1 is proper and the resulting accuracy can be seen in Table 10. Figure 65 below shows a picture of holes photographed from the bottom with 11.3, 9.3, 7.3, 6.3 and 5.8 mm in diameter. This is the best achieved quality regarding to dross and accuracy in the experiments.

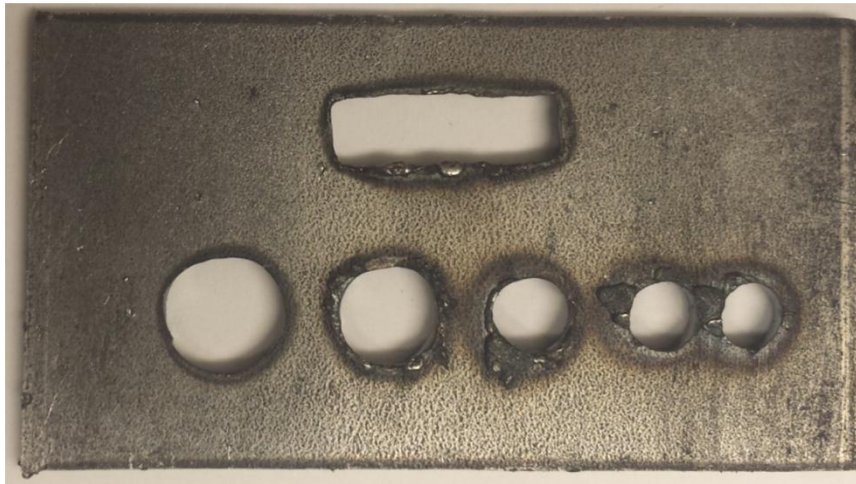


Figure 65: Dross issues with plasma cuts at 3 mm thickness, Source: own illustration.

As a comparison to the laser it can be said that at holes smaller 8 mm the plasma is not able to cut that clean and accurate. Laser has besides the small kerf and the high pressure of the out blowing gas the opportunity to pulse the light and this allows the robot to move at very low speeds and to achieve there the accuracy. The iLC application is to lower the accuracy of the robot by measuring friction, acceleration and time. It has to be said, that at a certain required velocity also this application is not able to maintain the right accuracy and this velocity can be reached with plasma applications easily. A solution for these issues is described in chapter 3.2.5 Adapting of amperage on the flight – command Corner Current below.

Furthermore it has to be expected that at circles up to 100 mm in radius the plasma system has the effects of lagging and the changing in convex and concave. Considerations when choosing the system have to be made.

3.2.3.3. Cutting of edges

The cutting of edges is one of the hardest challenges that all robotic thermal cutting processes face.

In order to produce a cut with a good quality and accuracy the velocity has to be in the cut work area as mentioned at the very beginning. But since the used robots are buckling arm robots and they have to change the direction very fast they tend to vibrations after the edge. This phenomenon is also described in the chapter 2.3.1 Edge movements – Vibrations.

On the other hand there is the plasma process. How is the plasma process reacting on a change of the cutting direction?

With cutting of edges Δe it is tried to quantify this quality criteria and make it comparable to other cutting technologies and different guiding solutions.

The formula below describes the influence factors which affect the cut. It is Δe_p which changes with the cutting speed, $\Delta e_{lagging}$ is a big influencer when the robot moves around the corner and the robot accuracy Δe_R itself.

$$\Delta e = \Delta e_p + \Delta e_{lagging} + \Delta e_R \quad (42)$$

How does the variation in speed affect the shape of the cut or the Δe ? In the deceleration phase, see following Figure 67 on the real upper cut before coming to the corner, it widens up because the bigger heat input and melting down of more material. It has to decelerate from 55 mm/s to approx. 40 mm/s by using the programming of $z0$ in the edge. $Z0$ and the combination of 80 percent of the acceleration resulted in the optimum for programming point to point.

By using the iLC the amount of the velocity remains but the corner radius decreases and the vibrations are less. All in all the movement is more accurate.

One big influencing factor in the accuracy of edges is one more time the effect **of lagging behind** of the plasma. In the figure below (left figure) it can be recognized easily that the plasma takes, due to this effect at edges or changing of directions, the shortcut and generate a conical edge.

A possible solution for cutting of edges can be found in the following chapter bevel method.

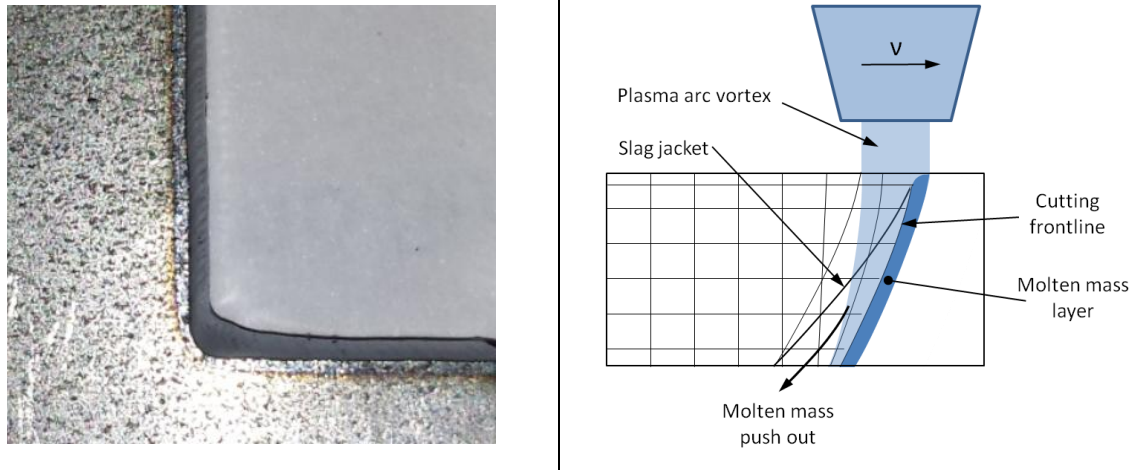


Figure 66: Picture of the cut edge PMX finecut – 55 A, 50 mm/s (left Figure) Source: own illustration; Plasma process with lagging behind (right figure) Source: own illustration.

Figure 67 illustrates Δe and the angle alpha. Δe is measurement between the upper cut in the radius and the related lower cut (red) and should indicate a quality factor regarding the edge cut.

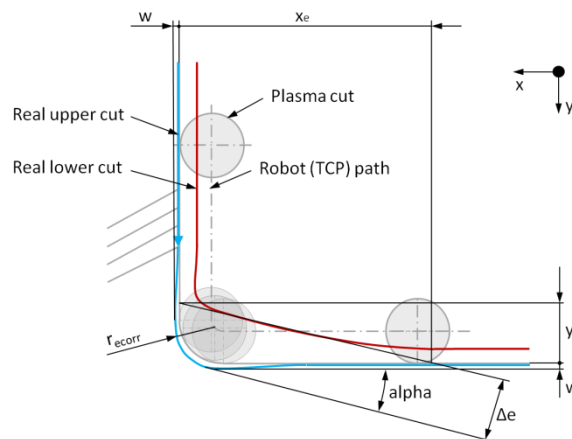


Figure 67: Tolerances at the cutting of edges, Source: own illustration.

The main value in the edge is Δe and can be used to compare the different cutting techniques. The measured values x_e and y_e are used to calculate Δe . These values have to be corrected geometrically by the value w , which is the widening up of the kerf due to the slower cutting speed, to the values x_{e-corr} and y_{e-corr} . With these values the final value Δe is calculated.

Formula (42) helps to understand the influence factors in edge cutting. Δe and alpha are calculated by the following formulas whereby x_e and y_e are measured values. w_{uk} is the upper kerf width at normal speed, w_{uke} is the upper kerf width at the edge and z_0 is the programmed zone of the robot when reaching a corner. Δe results from r_{ecorr} and z_e which can be seen in Figure 68 on the right hand side.

$$\Delta e = r_{ecorr} + z_e \quad (43)$$

r_{ecorr} is the resulting cut radius considering the bigger upper kerf width in the corner w_{uke} and the programmed zone of the robot z_0 .

$$r_{ecorr} = \frac{w_{uke}}{2} + z_0 \quad (44)$$

z_e is the result of the geometrical calculations and trigonometric functions (see Figure 68 right picture).

$$z_e = x_{ecorr} \cdot \sin(\alpha_e) - \frac{r_{ecorr}}{\cos(\alpha_e)} - (r_{ecorr} - r_{ecorr} \cdot \tan(\alpha_e)) \cdot \sin(\alpha_e) \quad (45)$$

The angle of the triangle is calculated according the following formula.

$$\alpha_e = \arctan\left(\frac{y_e}{x_e}\right) \quad (46)$$

The correction of the measured triangle in red to the triangle in green, which can be seen in Figure 68, is calculated as follows.

$$x_{ecorr} = x_e + \frac{w_{uke} - w_{uk}}{2 \cdot \tan(\alpha_e)} \quad (47)$$

Figure 68 represents two graphs whereby the right is an enlargement of the left one and describes the calculation of z_e detailed.

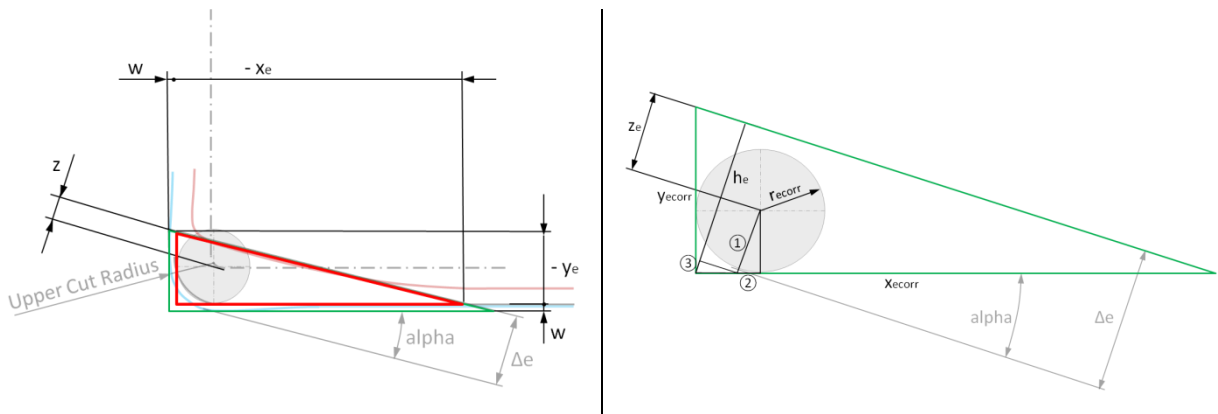


Figure 68: Visual aid for calculation of Δe , Source: own illustration.

Table 11 below displays the calculated results of the Δe for the PMX, the HPR and a laser cutting system. Those values are expected values which have been tested and should give an indication of the quantitative difference between the different processes. There is no derivation considered.

Table 11: Tedge at 3 mm thickness, Source: own illustration.

	3 mm			
	PMX finecut 55 A, 60 mm/s		HPR Bevel 80 A, 60 mm/s	Laser 2.5 kW 200mm/s
	Normal	Bevel cutting	Normal	Normal
W [mm]	0.2	0.2	0.15	0.1
z0 [mm]	0.3	0.3	0.3	0.1
wuke [mm]	1.6	1.8	2	0.16
-xe [mm]	3	2	2	
-ye [mm]	1.5	1	1.5	
-xe corr [mm]	3.52	2.01	2.43	
-ye corr [mm]	1.63	1.00	1.74	
alpha [°]	26.57	26.57	36.87	
Δe (calc) [mm]	1.49	0.89	1.29	0.10
Upper Cut Radius [mm]	1.1	1.2	1.3	0.28

By taking a look at Table 11 it shows that bevel cutting decreases the lagging effect in the edge Δe . That is an useful effect for the geometrical accuracy of the process. Furthermore it also illustrates that the cutting radius is in reality considerably larger comparing to the laser cutting process (plasma w_{uke} is 1.6 to 2 mm and at the laser it is 0.16 mm).

Table 12 displays the achievable tolerances at a plate with 1.2 mm thickness. Here the effect of lagging behind is not that distinctly but it is still recognizable. Also the cutting radius is again a lot bigger than with the laser beam.

Table 12: Tedge at 1.2 mm thickness, Source: own illustration.

	1.2 mm		
	PMX finecut 55A, 60 mm/s		Laser 2.5kW 200mm/s
	Normal	Bevel cutting	Normal
w [mm]	0.2	0.2	0.1
z0 [mm]	0.3	0.3	0.1
wuke [mm]	1.3	1.8	0.16
-xe [mm]	1	1	
-ye [mm]	0.5	0.5	
-xe corr [mm]	1.42	1.01	
-ye corr [mm]	0.61	0.50	
alpha [°]	26.57	26.57	
Δe (calc) [mm]	0.62	0.44	0.10
Upper Cut Radius [mm]	0.95	1.2	0.28

Figure 69 displays an overview of different corner cuts by using a robotic plasma system in reality. There the differences in Δe and upper cut radius can be seen. Furthermore there is also a PMX cut of 1.2 mm thick material displayed.

On the other hand Figure 70 shows a corner cut by a robotic laser solution where no lagging and no corner radius is recognizable besides a widening up of the cut in the corner.

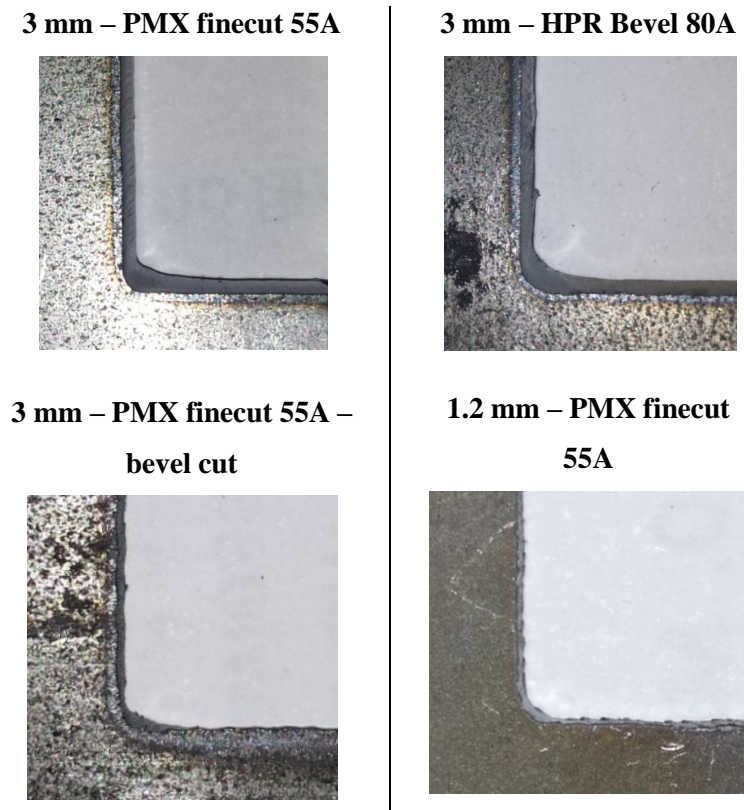


Figure 69: Overview of corner cuts by different robotic plasma cutting technologies, Source: own illustration.

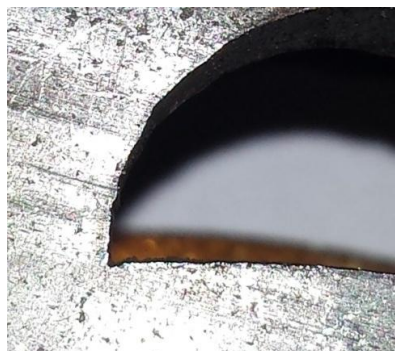


Figure 70: Corner cut by robotic laser cutting system, Source: own illustration.

An outcome of the assessment of circular cuts is the decrease of the effect of lagging behind with decreasing speed. This effect is also valid for the edge cuts. By cutting corners the radius is smaller

than the minimum possible hole radius and also the appearing of dross has to be considered. Therefore the speed has to maintain at the highest possible level.

Bevel method

As described in the chapters before there is an angle on the good-side of the cut. To avoid that angle there is the possibility to compensate that angle by the robot. Figure 71 illustrates that process better. The torch is rotated around the TCP with that angle. The cut direction is normal to the paper. With the help of this mechanism the cut angle on the good-side in theory can be avoided.

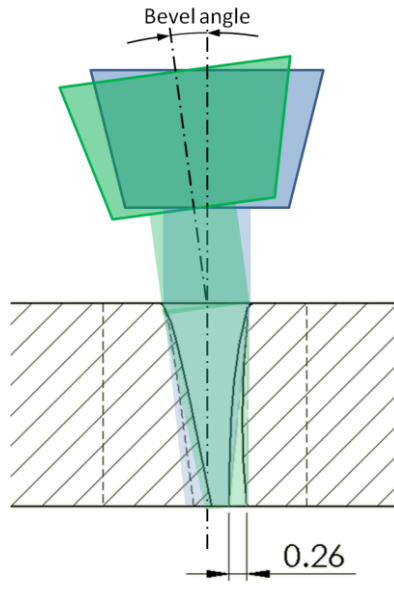


Figure 71: Robotic bevel cutting, Source: own illustration

This mechanism leads also in reality to quite good results as can be seen in Table 13. When rotating the torch up to 5 or 6 degrees the cut angle can be avoided almost completely.

Table 13: Real behavior of the bevel angle, Source: own illustration

Bevel angle	Cut angle good-side	Cut angle bad-side
3°	1.50	14.00
4°	1.50	12.00
5°	0.50	13.50
6°	-0.50	14.50
7°	-2.50	17.00
8°	-4.00	18.50

To realize this bevel angle there are two different ways to program the robot. The first is to program the path point-to-point or the second one is to program it via robotstudio.

What does this mean for our four cutting applications?

- Straight lines can be programmed point-to-point or with robotstudio and are not that much extra effort.
- Circular cuts require much more controlling effort of the robot and are not possible to program point-to-point. It has to be done in robotstudio and requires special attention on acceleration and speeds. Even on flat surfaces it can become as complicated as 3D-cutting. Complete circles or holes smaller than 10 mm in radius are not possible to cut. The critical point here is the lack of software for special movements like wrist movement or other controlling programs which makes the robot move with bevel angle accurate at the required speed.
- Rectangular movements and edges are not so critically. Programming with robotstudio is the easier and faster way as by point-to-point. This is explained in deeper detail here by the use of Figure 72 below. The path of the TCP is the grey dot dashed line which is also the center of the plasma when hitting the surface of the part. The blue circle illustrates the torch normal to the surface. After piercing at this position the torch moves to the path of the rectangle where it already has the bevel angle. After that it moves from corner to corner by changing the bevel angle gradually from point to point. Due to the changing of the angle there is a different speed on the upper and lower surface. But due to the gradually changing of the position this does not affect the cut quality.

Also the geometrical expansion of the plasma due to the impinging with an angle on the surface is minimal (0.002 mm)

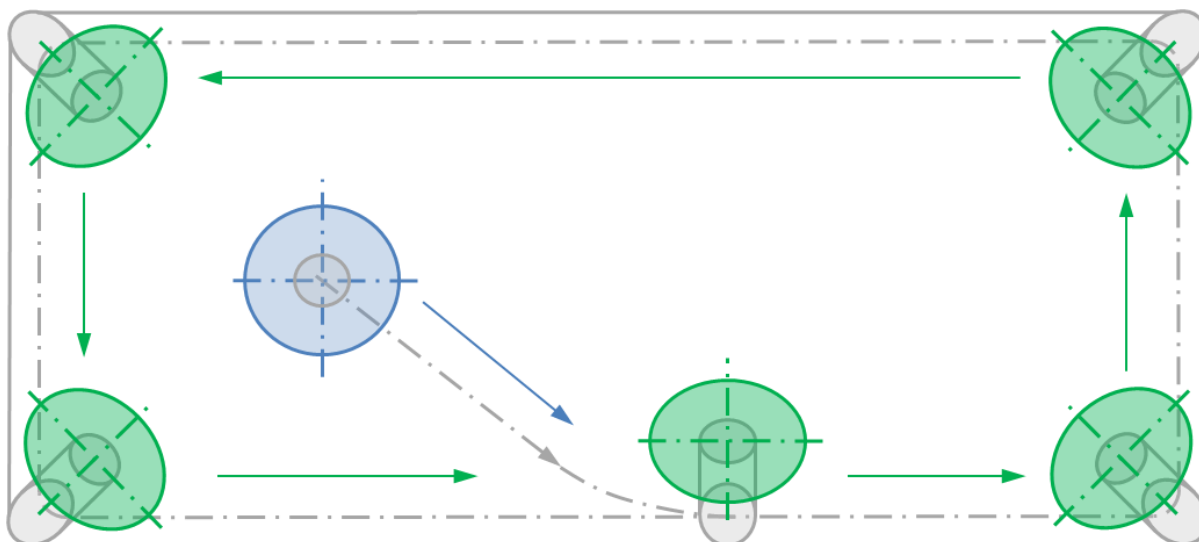


Figure 72: Bevel cutting of rectangle, Source: own illustration

- 3D-Cuts like the one in the following chapter can without exception only be cut by the use of robotstudio.

Robotic bevel cutting is an additional effort for the programmer of the robot but it makes the cut much more accurate. Of course it is also a question of the costs of programming extra hours and the feasibility due to the software readiness.

3.2.3.4. 3D-Cutting

This chapter should explain how the movement affects a cut in 3D by the example of the tube cut. Furthermore it should highlight problems which occur when cutting with plasma in 3D. The formula below provides an overview of the effects which occur while cutting.

$$\Delta 3D = \Delta 3D_p + \Delta 3D_{lagging} - \Delta 3D_{diff} + \Delta 3D_R \quad (48)$$

How does the variation in speed affect the reachable $\Delta 3D_p$? As shown in Figure 73 the speed varies a lot during the cut of the final part. Due to the difficult movements the robot has to slow down during the first segments which can be seen in the real cut on the left side. Tests retrieved that for the benchmark part it is better to limit the velocity at 30 mm/s until the robot ends the difficult area on the top of the part. So the robot has enough time to provide a smooth accurate movement. After the top of the part follows a circular movement on a flat surface. There the robot can cut with a higher speed again.

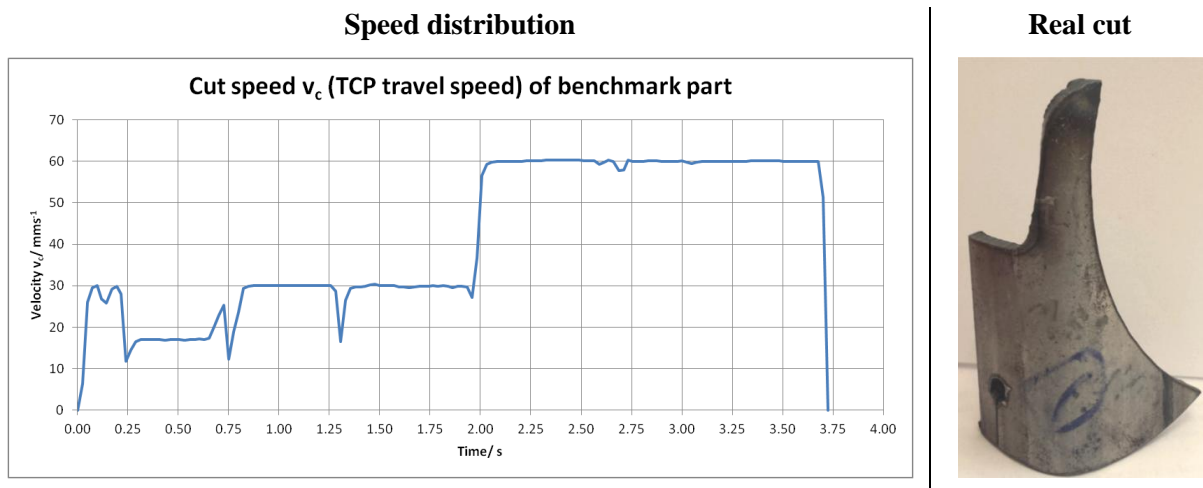


Figure 73: TCP Speed in the final 3D-Cut, Source: own illustration

Due to that slowing down from 60 mm/s to approximately 20 mm/s we have a lot more energy input in the material. As a consequence there is a widening up of the kerf width from 1.28 mm to 1.6 mm on the top surface which affects the w-value as can be seen in Figure 46.

Additional to the slowing down there is another effect that influences the shape of the cut. As can be seen in Figure 74 below there is a speed difference from the upper surface cut, as can be seen in blue,

and the lower surface cut in red. The TCP speed from Figure 73 is the speed from the blue line. As the red line is shorter also the speed is lower. In our case the red line is 25% shorter than the blue one. That means there is always more energy in the lower part of the cut and a widening up of this area is the result. This effect is considered in the factor $\Delta 3D_{diff}$ and can also be seen in the lower first radius on the right lower corner of the cut in Figure 75.

This effect compensates $\Delta 3D_{lagging}$ in our case where there is an overlay of the radial movement and a side-movement.

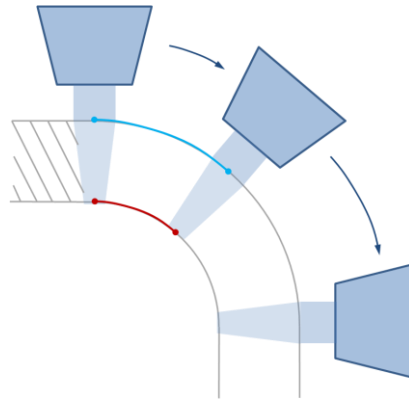


Figure 74: Cutting of a radius in 3D, Source: own illustration

The $\Delta 3D_R$ can be counted as the same as for the last one. But this influencer requires more attention and effort when programming the robot. Additionally we used bevel cutting because we are already programming with robotstudio. So we get the best accuracy out of the cut.

Figure 75 displaces the laser scan of the first part of the 3D-final part cut. There can be seen the derivation of the real surface of the cut.

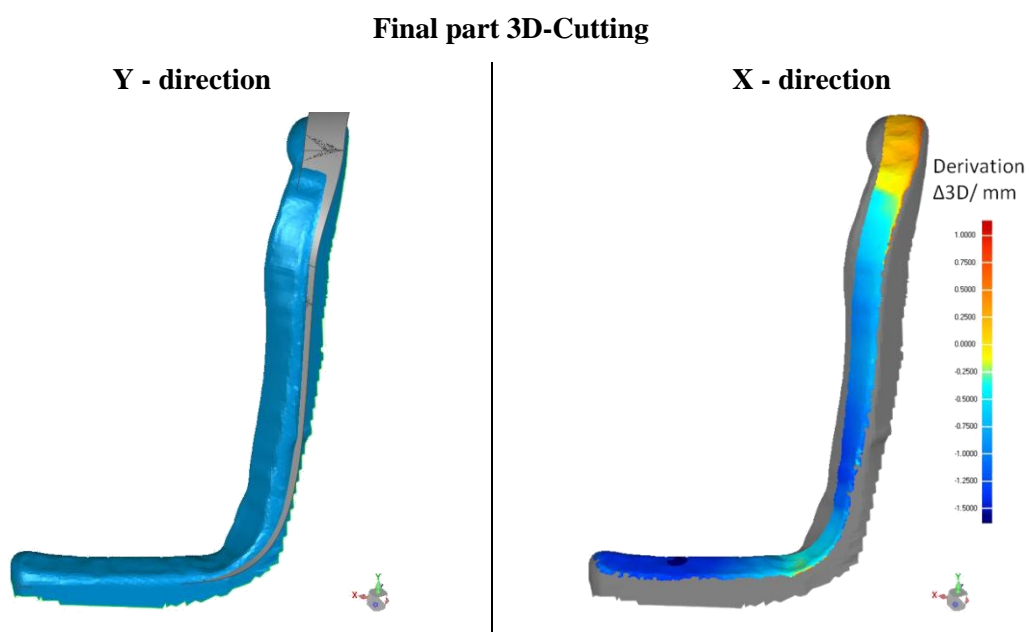


Figure 75: Final part cut derivation, Source: own illustration

3D-movements are several single movements overlaid at the same time. Very often it is the case that a radial movement, like the one explained in Figure 74, is overlaid with a lateral-/side-movement as displayed in Figure 76. Here in this assessment the final part is only cut with the PMX system. It is analysed based on the 3D measurement with the FARO laser system and there are no derivations considered.

For better comparisons the movements are divided into two zones.

1. 60° radial movement (radius outer part 10 mm) and lateral movement 5 mm
2. 10° radial movement (radius outer part 10 mm) and lateral movement 20 mm

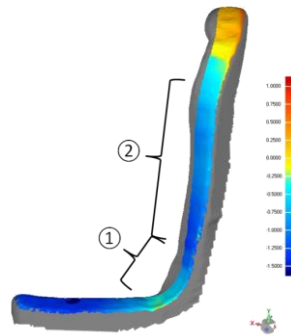


Figure 76: 3D-Cut of the final part, Source: own illustration

The cutting is starting on the left side and approaching zone 1 with the regular 60 mm s^{-1} when entering zone 1 the robot has to slow down and the plasma is doing what described in the last chapters. It expands the kerf and the perpendicularity is decreasing. This effect is overlaid with the lagging behind and as can be seen in Figure 76 the entire radius in zone 1 is shifted by 0.5 mm according the measurements inwards the material. It also can be observed that the robot does not move smoothly. Additionally there is the higher heat input and the hardening in the HAZ increases, see chapter 3.3.2 Influencers on fatigue.

Zone 2 shows a relatively constant cut with low derivation from the claimed surface. This is due to the almost straight movement of the robot without changing the direction and speed. When exiting zone 2 it comes again to high derivations. Here in this zone the same effects happen as described in zone 1.

Furthermore the benchmark part is cut with a bevel angle of 5° which does not improve the accuracy but it declines the perpendicularity u to almost zero where it can be compared to the laser cut.

Figure 77 illustrates the main issue of cutting with plasma such a 3D parts. The dross is formed almost every time in zone 1 and also in the zone after zone 2 where there is a corner and the big radius starts.

A solution for this issue would be the reducing of amperage and a more accurate and at the same time faster movement of the torch. The buckling arm robot is coming to his limit at this application.



Figure 77: Dross issues when cutting the final part, Source: own illustration

The laser as a comparison has besides the missing lagging effects and the small kerf width the function of adaptive energy input what makes the process more accurate. Also the dross formation is less due to the lesser material which has to be blown out.

3.2.4. Cut quality - Dross

The most common cut quality problem of plasma cutting is dross. Many fabrication shops spend much time on reworking by grinding, chipping or sanding part. But what is actually dross, how does it occur and how can it be avoided? That are the main questions which are tried to answer at this point.

The plasma cutting specialist Hypertherm has found a propiate and simple explanation for the see below. Dross is re-solidified oxidized moltem metal that is not fully ejected from the kerf during cutting. Dross may form as a thick bubbly accumulation along the bottom edge of the plate (low speed dross), a small hard bead of uncut material (high speed dross) or a light coating along the top surface of the plate (top spatter).²⁸

The probability of producing dross during cutting is depending on various factors. It starts by the travel speed, the torch to work distance, the amperage and the consumables conditions. Furthermore the type of the material, chemical composition, surface condition and even the temperature are additional influence parameters.

²⁸ Tyler J., Peters J., Liebold S. (2014). Improved plasma cutting of stainless steel, The fabricator. Online source [31.08.2015]

Dross free window

Between the high and low speed dross there is a window where almost no dross occurs.

Finding this window is the key to minimizing secondary operations on plasma cut pieces.

The three most critical influencers in dross formation are cutting speed, torch to work distance and amperage. To adjust these properly there are two methods.

First method is to produce a series of cuts with different speeds and torch heights. The best approach is to go with the proposed height in the manual. Then choose the cleanest cut and investigate on the lag lines. Figure 78 shows three different cuts whereby the cut direction is from right to left. The first cut with the ideal lag lines is the cleanest one. The second one shows a cut where the speed is too high and resulting high speed dross. The last one is cutting at low speed with the low speed dross which can grow and become very large.

The second method is to observe the arc while cutting. The focus of this investigation is to answer the question how the arc exits the bottom of the work-piece. If the plasma gas is air, the arc should be vertical or slightly trailing as it exits the work-piece. The same is happening with nitrogen/hydrogen. By cutting with oxygen as a plasma gas a slightly leading arc is the best. This effects lead to the gas as a influencer to the cut quality described as follows.

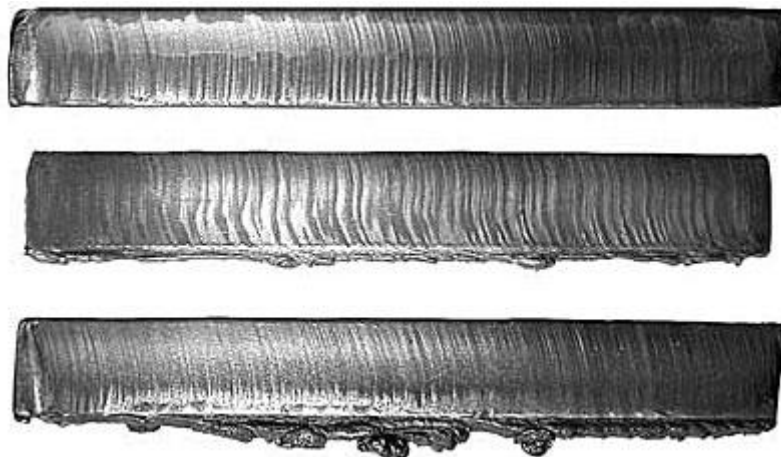


Figure 78: Dross appearance and lag lines of the cut, Source: Hypertherm Inc. (2015), Online Source [30.07.2015].

Plasma gas

The type of plasma gas has an effect on the window of non-dross formation. For instance on carbon steels nitrogen and air plasma gasses have a relatively narrow dross free window, while oxygen as a plasma gas is more indulgent by a wider dross free window. Oxygen is reacting with carbon steel and produces thereby a fine spray of molten metal with a lower surface tension which is easier to blow out from the kerf.

Material

Another big influencer is the type of the material itself. For example the cut of cold rolled steel is much cleaner compared with a hot rolled steel. And the cut also produces less dross on pickled steels than on non-pickled ones.²⁹

Furthermore the thickness of the part is crucial on how big the dross accumulation of dross on the bottom side of the cut is. A part with 3 mm thickness will have a lot more dross than a part with 1 mm in thickness.

As described above plasma cutting has a window where it can work without dross with a good quality. This is quite easy to maintain in straight cuts but when taking a look on shapes like rectangulars, circles or even shapes in 3D there it gets increasingly harder for the robot to guide the plasma torch on the path with accuracy and the proper speed.

Therefore we have the target conflict as described in the introduction.

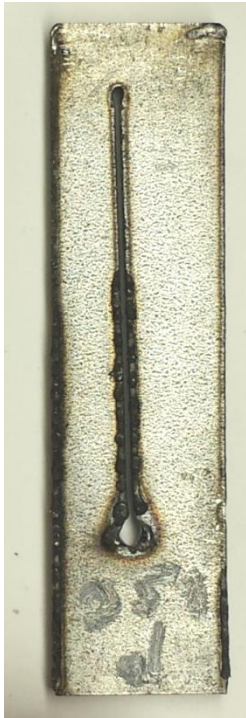
Below more effects are listed which observed in the tests.

3.2.4.1. *Dross dragging along*

When piercing you have to remain at one place for a longer period of time in order to create a hole from which you can start the cut. While remaining at this place you often create some dross around that hole as can be seen in Figure 79 below.

²⁹ Tyler J., Peters J., Liebold S. (2014). Improved plasma cutting of stainless steel, The fabricator. Online source [31.08.2015]

Straight cut with piercing
PMX finecut 55A, 3 mm plate



Rectangular cut with piercing in the middle –
PMX finecut 55A, 5° bevel - 3 mm plate

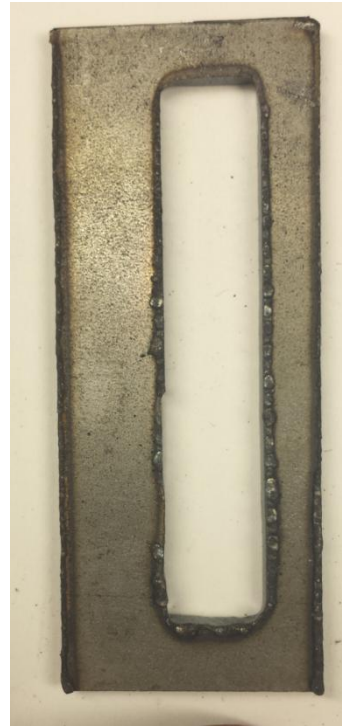


Figure 79: Dross dragging along, Source: own illustration

On the right picture there is a rectangle 60 mm by 10 mm cut by a robotic plasma machine. The piercing is in the middle of the rectangle and then the movement goes to the left side, followed by the top left corner and then cuts the rectangle clockwise. As can be seen in the picture, this effect happened on the first left side until the left top corner. The other dross on the right side is from the effect described in the following chapter.

3.2.4.2. Heat

Dross is more likely to appear when the part is heated up. That means when cutting smaller shapes there is a higher possibility of dross. Figure 80 shows circles of 10 mm, 8 mm, 6 mm, 5 mm and 4.5 mm of diameter. On the top there is a rectangle of 20 by 5 mm. In every shape due to the piercing and cutting a huge energy input into the material as also can be recognized in the bigger heat affected zone of the smaller shapes.

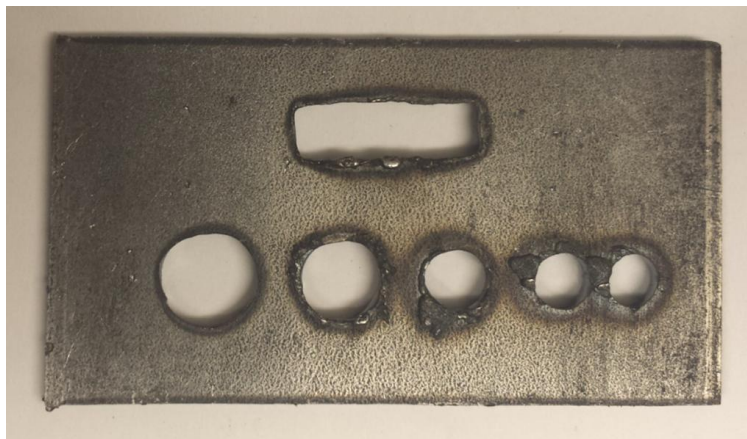


Figure 80: Dross due to heat, Source: own illustration

3.2.4.3. *Dross in a tube*

Another effect which occurs in tubes is shown in Figure 81. The plasma arc is cutting through the metal but since it has rest energy when exiting the kerf it is heated and melted everything up which comes afterwards. Also the material which is blown out is sticking to the other part as can be seen in the picture below.



Figure 81: Dross in a tube, Source: own illustration

3.2.5. Adapting of amperage on the flight – command Corner Current

As described above the plasma is widening up at low velocities. Especially when the cutting shapes likes holes or corners or 3D shapes this effect can affect adversely the achieving of the required tolerances and cut quality.

There are two ways of mastering that issue. First way is to compensate that effect geometrically by programming an offset in the area where low speed is expected. In that way one has to know the

abilities of the robot quite well to assume how and where the robot controller will be slowing down. Besides that it is a more-effort in programming.

The more elegant way to resolve that issue would be by controlling the energy input in the material. The Hypertherm HPR machine has therefore a function called Corner_Current at which the machine reduces the amperage by almost 50%. Figure 82 shows tests with that function. The lower cut shows the cut of straight lines one after another where the robot stopped at each point and activates the Corner_Current command. The speed inbetween that points is 100 mm/s. The line above shows activating the command on the flight. The command is given to the plasma power source at 20 mm after the piercing and the delay distance is 7.5 mm which is equivalent to 75 milliseconds at 100 mm/s.

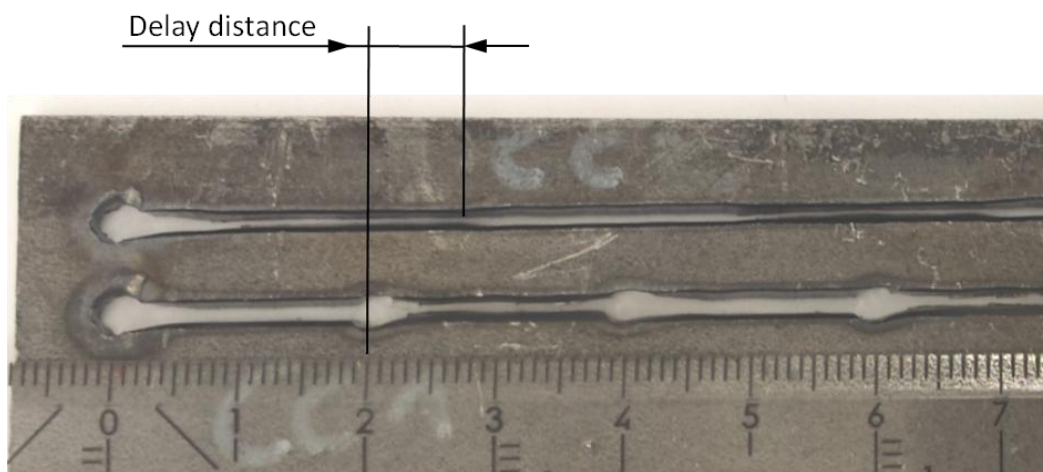


Figure 82: Delay distance 7.5 mm at 100 mm/s, Source: own illustration

Figure 83 below illustrates the cut geometry of normal HPR bevel cutting and the corner current cutting over the speed. Noticeable again is that the widening of the kerf width below 70 mm/s which is highlighted in the area in slightly red. This area is very important when cutting shapes, corners or complex geometries. Especially in that zone the corner current can provide help to get better result in accuracy.

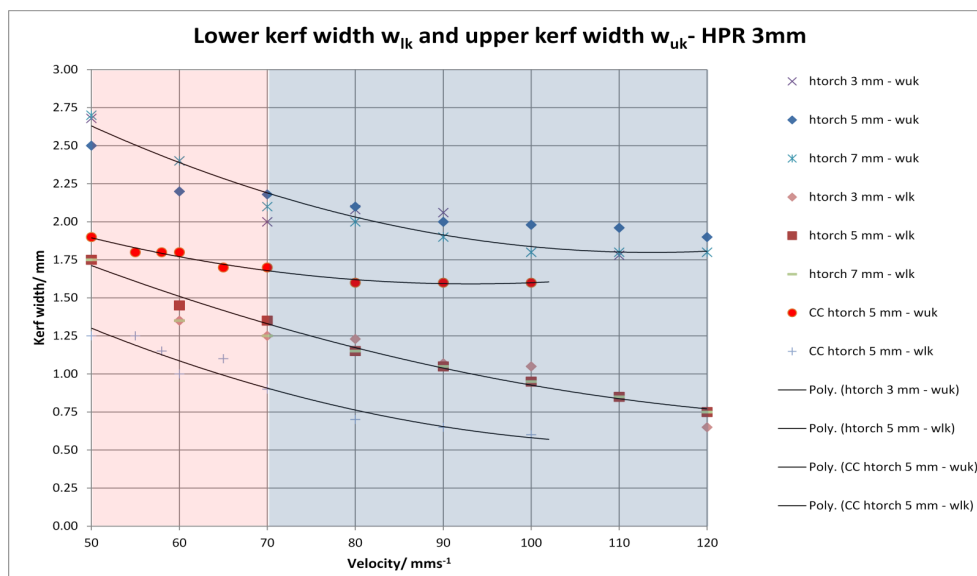


Figure 83: HPR Cut geometry with Corner Current, Source: own illustration

The benefit of accuracy can be seen in Table 14. $w_{upperKerf}$ is halve the amount of cutting without the Corner Current function.

Table 14: Benefit due to Energyreduction on the flight, Source: own illustration

	HPR Bevel 80A, 50-120 mm/s	HPR Bevel 80A from 70-120 mm/s 56A from 40-70 mm/s
w [mm]	0.5	0.25

Figure 84 demonstrates the cutting shapes when cutting with a HPR system and bevel consumables. The left-hand picture illustrates the shape of the cut with 80 A and 80 to 100 mm/s and the right-hand picture illustrates an overlay of the cut shape with the 56 A Bevel cut.

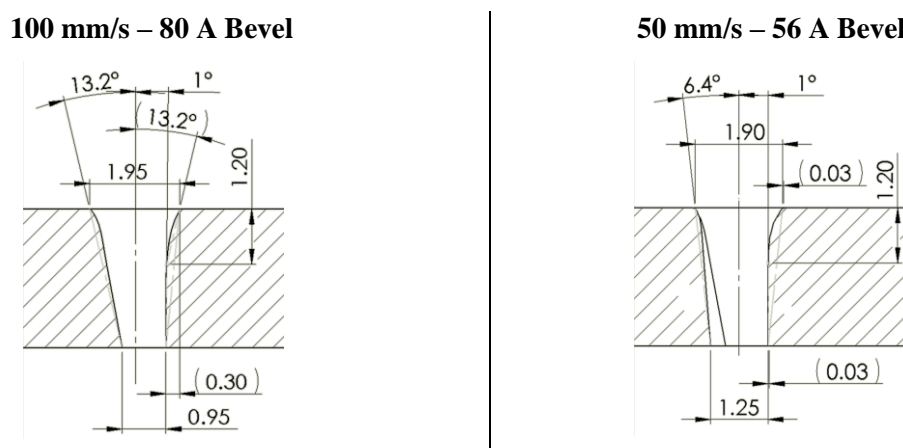


Figure 84: 3 mm HPR 80A bevel cut geometry at different speeds – Plasma Oxygen and Protection Air, Source: own illustration

How can this function be implemented in the programming of the robot cutting system? Since the robot controller cannot really see and steer the plasma machine there are again two possible ways to do this. The first way is to program the activation of the function when the travel speed of the TCP falls below a certain value. This would be the easiest solution if there would not be the issue with the delay time. For instance when cutting a corner the real reduction of the energy would come way to late or in other words, the robot would have passed the corner already when the activation occurs.

The second solution would be to activate the corner current command manually after reviewing the travel speed of the robot by dividing the total cut into zones of normal and bevel cutting.

Solution for the PMX system

Several manufacturers use an analogue input for adapting the amperage at the machine manually. That means the analogue voltage signal correlates to the required cut amperage. If there is an opportunity to set this analogue voltage signal by the robot controller an adaption on the flight can be realized.

3.3. Metallurgical properties as a quality criteria

The zone affected from the thermal cut in the material (HAZ) is crucial for assessments and validation of parts. What causes the changes in the material and how affect these changes the characteristics of the part in their daily usage. These points are tried to describe and test in this chapter.

3.3.1. Plasma gas

At thermal cutting as well as in welding it is important to consider which type of gas is participating in the process because the material is at melting point and it interacts with the surrounded gas. The cutting mechanism can therefore **chemically modify the cut edges** by addition or removal of chemical components.³⁰ There are three possible options for plasma gas when cutting steel with special characteristics as described below.

1) Air

Generally air consists of 21% oxygen, 78% nitrogen and 1% inert gas. Due to the availability of air and the possibility of using a normal compressor in the process it is the most common plasma gas for cutting applications. The problem of air plasma is the nitride contamination which leads to a case hardening in the material which can affect fatigue due to the hardness. Harris, I.D. states: “the amount of nitrogen in the edges also increases with a reduction in the thickness of the steel.”³¹ The nitride contamination can also affect the weldability due to the formation of pores while welding. Furthermore there is according to different manufacturer a formation of an oxide layer on the surface

³⁰ cf. Harris, I. D. (1997) p. 11

³¹ Harris, I. D. (1997) p. 13

of the cut. The topic of weldability has to be considered when implementing the plasma solution and therefore the author refers to the manufacturer of plasma machines.

2) Nitrogen

The use of nitrogen as a plasma gas leads to better quality of the cut surface. As a consequence it also leads to case-hardening and weldability issues. Furthermore it tends to form more dross on the bottom of the cut edge. Nitrogen is preferably used for cutting of aluminium and stainless steel.

3) Oxygen

By cutting with oxygen plasma the effect of nitride contamination can be overcome. This is also the reason for the development of oxygen plasma machines. Furthermore it allows cutting at higher speeds because of the additional thermal energy from the exothermic reaction of oxygen with iron in the steel and the formation of porosity decreases sharply.³²

3.3.2. Influencers on fatigue

As already described in theory in chapter 2.1.3 Material and Heat affected zone the fast **quenching of the heat affected zone can lead to crack-like defects** which are the main cause for fatigue. The present chapter takes a deeper look on that by the use of a light microscope and performs hardness tests of plasma and laser cuts to highlight the differences. Out of these tests conclusions on the hardness and the thickness of the zones which is important information for the assessment of the cut quality are made.

The samples are prepared by grinding, polishing and then etching with a nital (solution of 97% alcohol and 3% nitrid acid) to make the microstructure visible. The light microscope has a magnification up to 1000:1. The hardness tests are performed according Vickers as described in the following paragraphs.

Hardness testing

Depending on the amount of carbon and the amount of martensite in the material the hardness can vary significantly and therefore it is useful to perform hardness tests to provide real values in order to make a statement of the martensitic structure has an influence in the material.

Hardness values represent as Meyers stated in his book “a scale by themselves, allowing the comparison of materials....a comparative test of the resistance of the metal to plastic deformation.”³³ Since the present thesis investigates plasma cutting in respect to laser cutting these tests represents an ideal comparison.

In the investigation a hardness measurement according Vickers is performed. This test uses a pyramid indenter with a square base, made of diamond. The angle between the faces is 136 degrees. The great

³² cf. Harris, I. D. (1997) p. 13

³³ Meyers, M. A., et al. (1984) p. 602

benefit of hardness tests according Vickers is that there is only one indenter used for all hardness classes.

The formula below illustrates how the hardness value is calculated. P represents the load in pond, d is the average length of the diagonals and 2α equals 136 degrees.

$$HV = \frac{2 P_{HV} \sin\left(\frac{\alpha_{HV}}{2}\right)}{d_{HV}^2} = \frac{1.8544 P_{HV}}{d_{HV}^2} \quad (49)$$

Figure 85 below illustrates one test stamp and the square which is laid over the stamp to measure the diagonals. The stamp is in the martensitic structure of the PMX test.

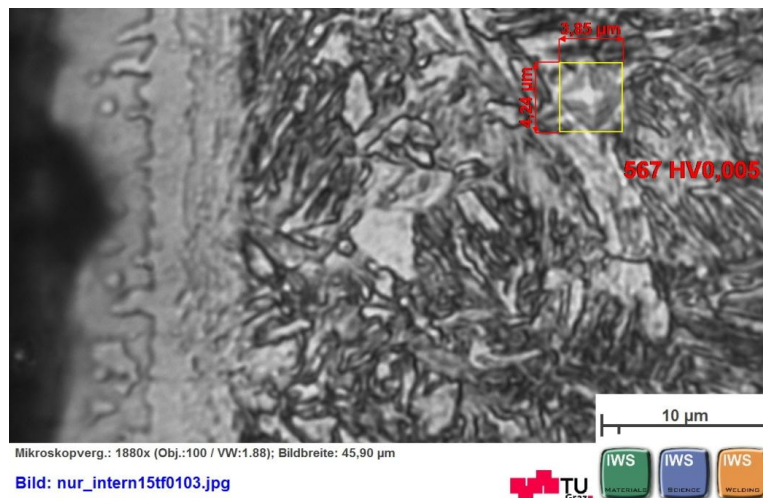


Figure 85: Vickers hardness test

The following paragraphs focuses on two different metallurgical tests of thermal cutting techniques. At first the material S460MC with a thickness of 3 mm and then the hot-stamped material 22Mn5 with 1.2 mm in thickness is tested and compared.

The cut below in Figure 86 shows the cut of the S460MC by the PMX finecut 55 A equipment with air as the plasma gas. The cut is performed by bevel movements of 5° so that the cut is very perpendicular. It illustrates a light microscope picture of the cross section of this part with a 25x optical magnification.



Figure 86: Light microscope picture of the cut cross section

Beginning by the explanation of the different zones Figure 87 below shows a light microscope picture with a 500x optical magnification. By definition the heat affected zone (HAZ) includes zone 1, 2, 3 and 4 and it is crucial at thermal cutting processes. The explanation of the zones according to Harris can be seen below.³⁴

- 0) The original ferrite pearlite base steel
- 1) A ferrite pearlite heat tempered zone
- 2) A partially transformed layer of martensite bainite and ferrite
- 3) A layer of martensite with peak hardness
- 4) A thin layer of resolidified molten material

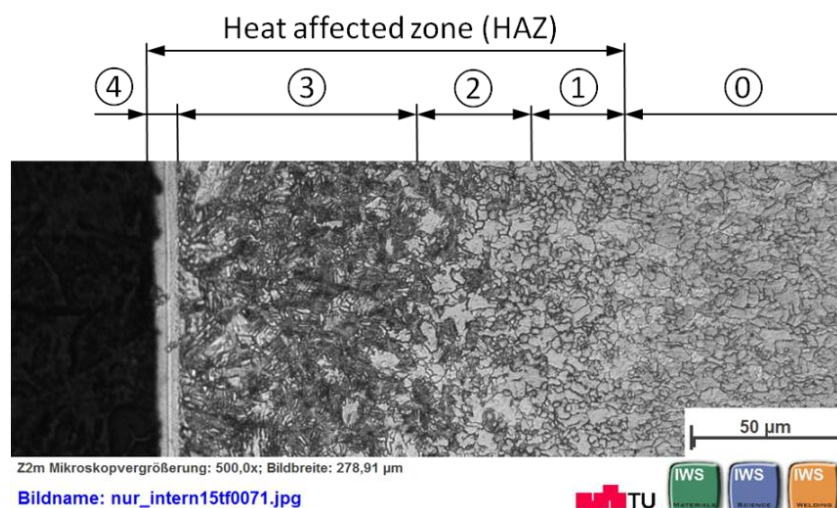


Figure 87: Heat affected zone, S460MC – PMX 55 A – 60 mms⁻¹, Source: own illustration.

Figure 88 below illustrates the micro structure of a HPR plasma system with oxygen as a plasma gas. Compared to the air plasma gas it can be seen that the heat affected zone is slightly smaller but there also is this thin layer of resolidified molten material at the cut surface. This layer is thinner and

³⁴ cf. Harris, I. D. (1997) p. 12

appears more consistent without any notches. If the layer is structurally connected to the martensitic layer cannot be seen clearly.

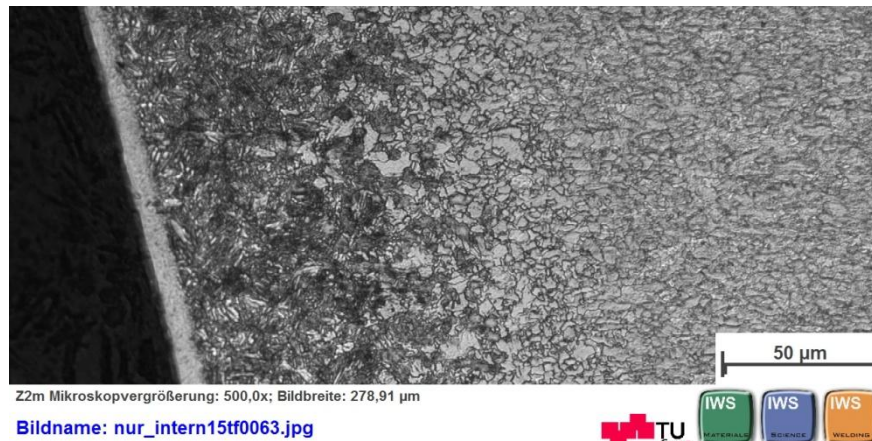


Figure 88: Heat affected zone, S460MC – HPR 80 A – 100 mms-1, Source: own illustration.

Figure 89 below shows the micro structure of a laser cut with nitrogen as a process gas. Compared to the two plasma cuts the heat affected zone is smaller and a difference in the structure can also be noticed. The effects of this differences can be analysed by hardness tests.

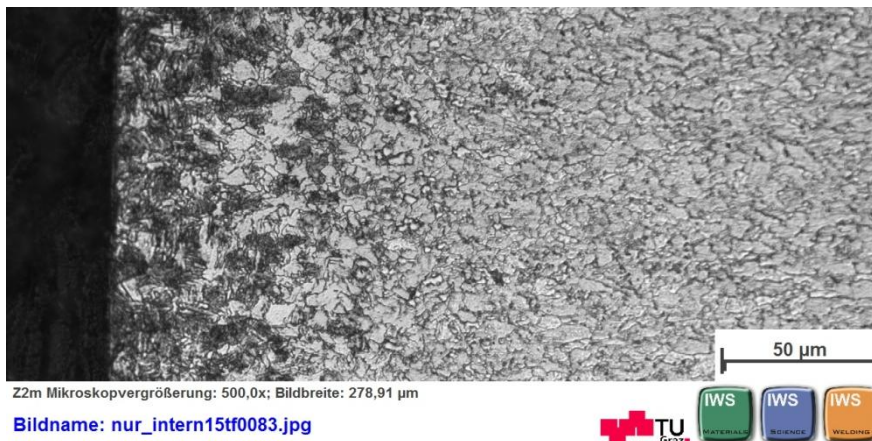


Figure 89: Heat affected zone, S460MC – Laser 2 kW – 150 mms-1, Source: own illustration.

A comparison over the different thicknesses of the heat affected zones and the resolidified zone is displayed in Figure 90.

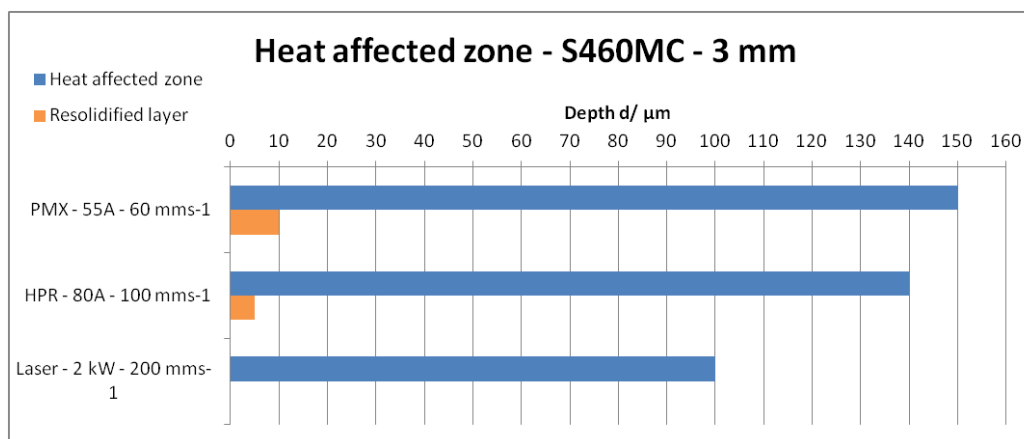


Figure 90: Different depth of the heat affected zone, Source: own illustration

Figure 91 provides an overview of the hardness peaks with the different cutting techniques. It appears that the thin layer of resolidified molten material, displayed by the orange boxes, certainly contains a higher rate of carbon because the hardness increases very strong in this zone. In that zone it comes to the carburization of surface due to the preferential removal of iron when cutting with oxygen.³⁵ The green boxes illustrate the peak hardness of the martensite structure and the red dotted line the average hardness of the base material with 284 HV0.005.

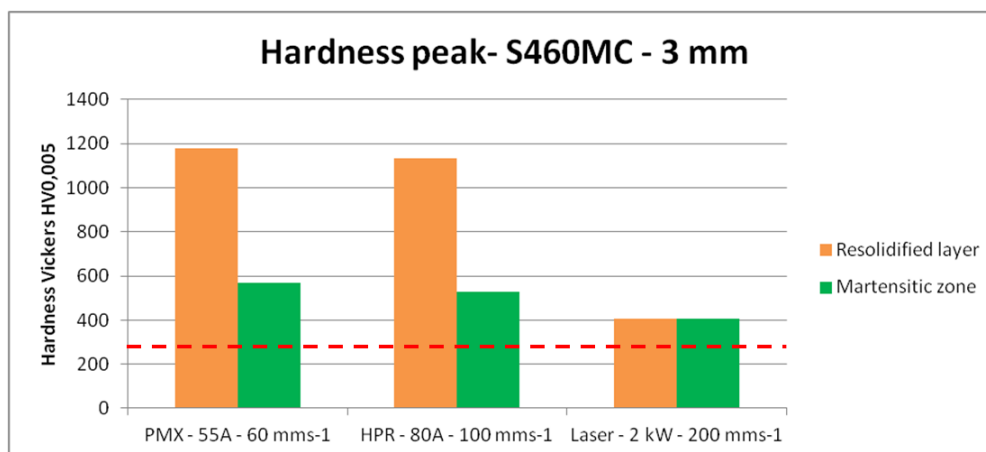


Figure 91: Hardness peak at the S460MC material, 3 mm, Source: own illustration.

As a conclusion for the S460MC material it can be said that both plasma systems have a clearly higher hardness peak in the resolidified layer as well as in the martensitic structure than the laser. Furthermore there is an increase in the hardness of the heat affected zone. This can affect the fatigue of the material depending on the state of the stress. In case tests as agreed with the customer have to be performed.

³⁵ cf. Harris, I. D. (1997) p. 11

The second investigated material is the hot-stamped 22MnB5 with a thickness 1.2 mm of the B-Pillar. Unfortunately no martensitic structure can be seen in the base material in Figure 92. Instead a very fine-grain ferritic and perlitic structure is noticeable.

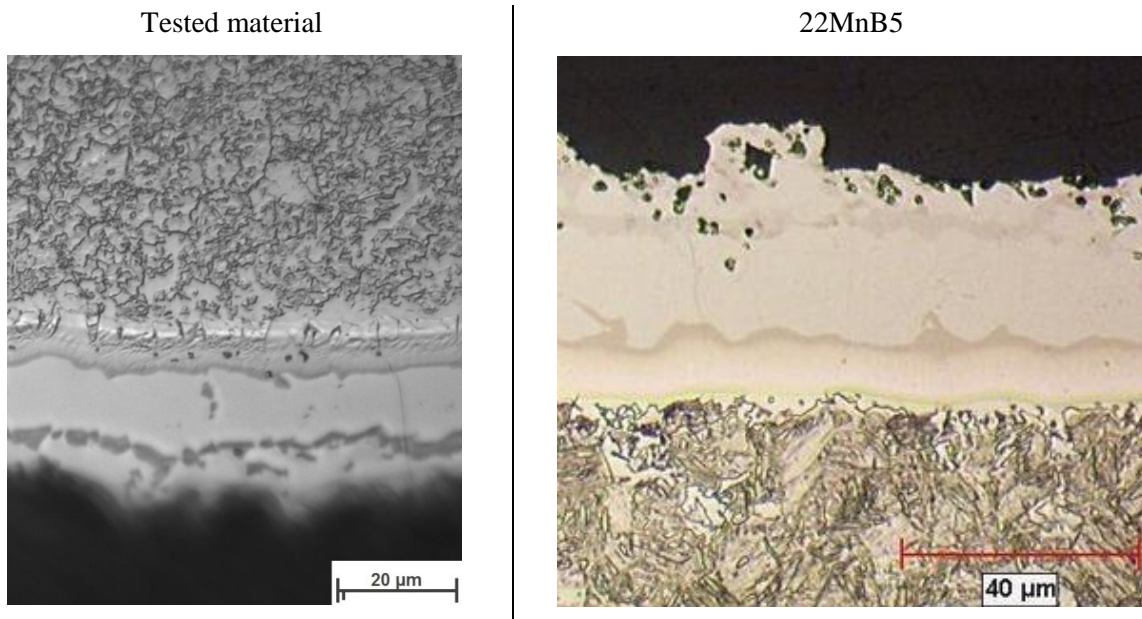


Figure 92: Tested material versus supposed material, Source: own illustration.

The tested hardness of the base material is 193 HV10. Figure 93 illustrates a TTT-Diagram for the 22MnB5 and by looking at the hardness and the correlating cooling curve the micro structure of the material should contain 60% ferrite, 15% pearlite and 25% bainite.

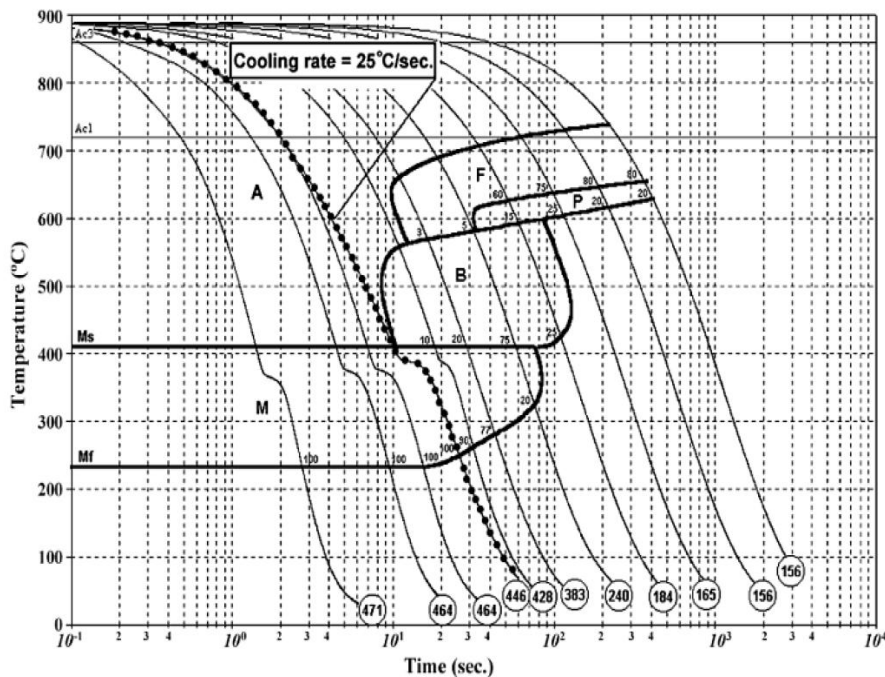


Figure 93: TTT-Diagram of 22MnB5, Source: Naderi M. et al. (2007) p. 446.

Reasons for the different structure are issues at the production of the B-pillar. The exact reason is not stated in this thesis but the part is taken as another research material for the plasma application because there are several reasons for it like the thickness, coating, chemical consistence etc.

Figure 94 below shows the cut of the 22MnB5 by the PMX finecut 55A equipment with air as the plasma gas. The resolidified layer is very thin compared to the one described above in Figure 87. The size of the heat affected zone is similar with $140\ \mu\text{m}$.



Figure 94: Heat affected zone, 22MnB5 – PMX 55 A – 100 mms-1, Source: own illustration

Figure 95 below illustrates the laser cut with nitrogen as a process gas. A thin layer of resolidified material can be noticed as with the plasma process and the size of the heat affected zone is similar to the one from the plasma process with $130\ \mu\text{m}$.



Figure 95: Heat affected zone, 22MnB5 – Laser 2 kW – 200 mms-1, Source: own illustration

Figure 96 illustrates the an overview of the hardness peaks in the heat affected zone at the 22MnB5 material. Both the plasma cut and the laser cut show almost the same hardness. The red dot dashed line reflects the average hardness of the base material with 275 HV0.005.

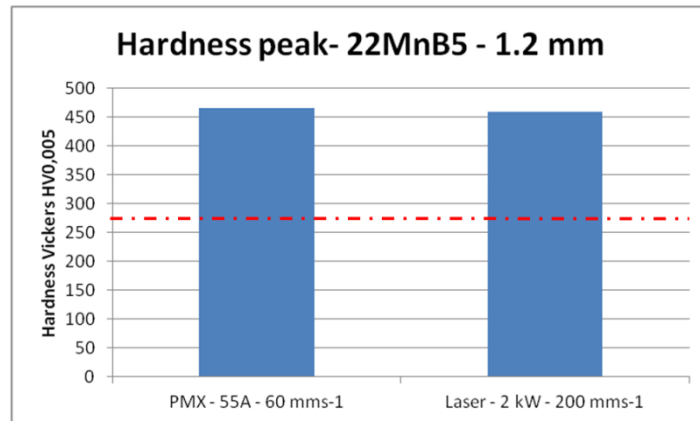


Figure 96: Hardness peak at the 22MnB5 material, 1.2 mm, Source: own illustration

As a conclusion can be said that there is almost no difference between the laser and the plasma cut. Furthermore the peak hardness is not that much higher than the peak at the thicker material. Depending on the state of the stress further investigation on fatigue have to be performed.

According to Harris the thickness of the layers of the different structures varies with steel chemistry, heat input and travel speed. Harris illustrates in Figure 97 the relationship between micro hardness, the microstructure and the residual stress of a plasma gas cut material. When getting closer to the surface the hardness is increasing rapidly. Furthermore the residual stress is displayed and it can be seen that the formation of martensite limits the tensile residual stresses at the cut surface and creates a region of compressive residual stress. This can be beneficial for the cut surface.

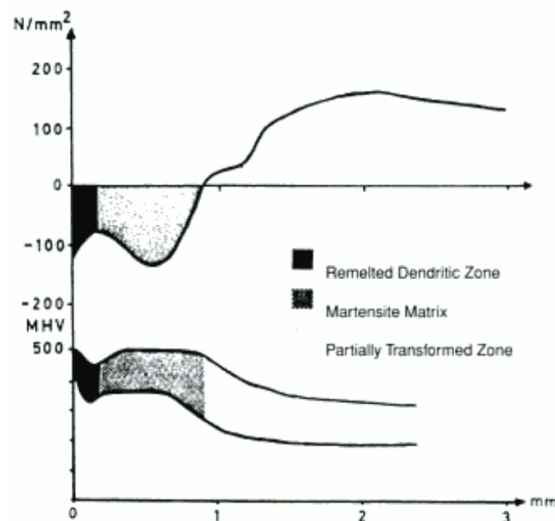


Figure 97: Relationship between microhardness, microstructure and residual stress at a plasma gas cut surface in ST 52-3 steel, Source: Harris, I. D. (1997) p. 12.

3.4. Implementation of robotic plasma cutting

This chapter provides solutions and approaches how the implementation of plasma cutting in the production process can be done and highlights what is necessary to consider.

3.4.1. Torch height control

As described in 3.2.2.3 Torch distance influence the torch distance has an influence into the cut shape and at the end to the accuracy. Furthermore the arc is created between the positive charged part and the negative charged electrode and therefore the maintenance of the proper torch distance is important. If the torch is too low the torch can be damaged due to the heat and if the torch is too high the arc can be turned off due to the insufficient energy to ionize the gas. Especially at cutting with low amperages this is the case. Since the parts have derivations, the robot has derivations and the tooling or the way the part is placed in the tooling has derivations it is a challenge to maintain the torch height from part to part. The basic issue is displayed in Figure 98.

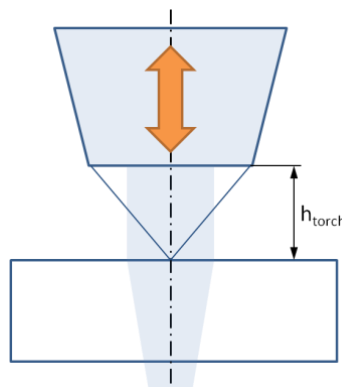


Figure 98: Torch height control, Source: own illustration

Laser systems are facing the same challenge and therefore cutting system manufacturer invented the torch height control. At laser systems a capacitive sensor is measuring the distance to the part and a separate axis with a motor is constantly adapting this distance on the flight and separately from the guiding system. By the fact that it works separately it is optimized only for that function and works very rapidly.

Since the plasma system has a little window in the torch height there are three different options to maintain the process torch height:

1) Accurate and stiff tooling

Depending on the part stiffness, shape and the deviations when arriving to the cutting process the tooling has to be designed that it can absorb that derivations or force the part to be always at the same

position. By doing so the robotic cutting process can be made without a torch height control. This can preferably be done by thinner material thicknesses and accurate pre-production steps, like hot-stamping.

2) Robot torch height control

Most of the plasma machines are able to measure the real voltage which is transferred over the arc. This voltage corresponds to the distance immediately and has a linear behaviour. Each difference in voltage correlates to a difference in distance. Furthermore is it an indicator for the usage of the consumables or rather the electrode. As can be seen in Figure 99 the hafnium electrode from where the plasma arc starts is getting used from state 1 to state 2. That means that the torch by keeping the same voltage (blue line) is getting closer to the part. By sensing the height of the torch and the voltage the usage of the electrode can be determined. The height of the torch can be determined via the touch sensing of the robot.

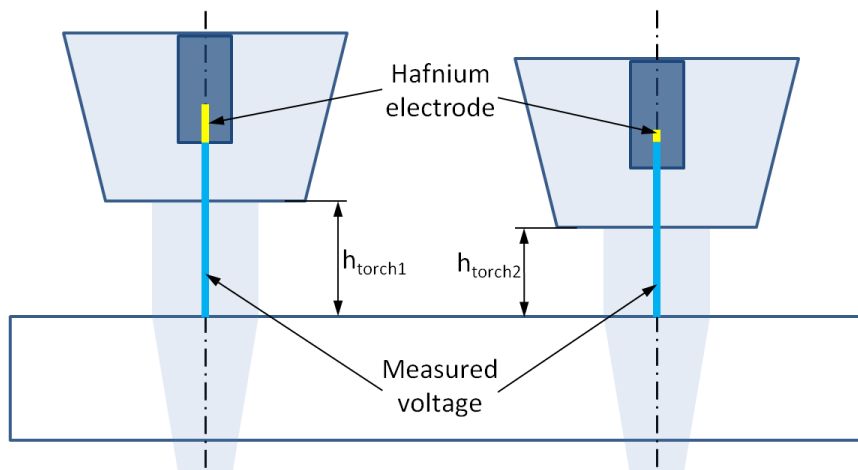


Figure 99: Arc voltage for sensing the torch height, Source: own illustration

For the robot torch height control the robot has to apply two functions. The torch sensing to determine the actual height and the adaption of the vertical axes or rather the torch height control on the fly. A big advantage of this solution is that no further axis plus control is needed. This leads to a very light tool. Disadvantageous is the delay time which devotes due to the adaption of all the axes of the robot. According to the manufacturer ABB there is a time delay of 0.02 to 0.06 seconds which equals by cutting with 60 mms^{-1} to approximately 3 mm of distance delay.

3) Separate torch height control similar to the laser system

The separate torch height control uses the transferred arc voltage which can be measured by the plasma machine as an input parameter similar to the robot torch height control. The difference is that there is the need to implement another axis plus motor and control at the robot tool which adapts the height of the torch on the flight. It is similar to the solution of the laser and has the big advantage of the rapid adaption with almost no delay time.

Figure 100 below illustrates the two different options of torch height control.

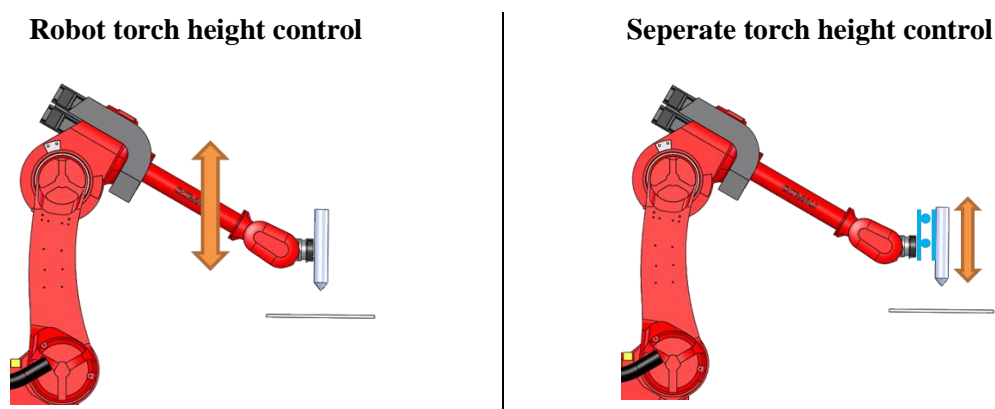


Figure 100: Different types of torch height control, Source: own illustration

The last two solutions require further investigations or adaptations to make the control able to fulfil the function. For example when the plasma travels over a hole the torch height sensing will cause a tilting of the torch in order to maintain the right height. This can lead to crashes with the part. These adaptations have to be made part specific.

3.4.2. Tool changer

The consumables which create and guide the plasma arc out of the orifice of the torch wear out. According to manufacturer information the consumables have a lifetime of approximately 2 hours cutting time and every change of these consumables takes about 3 to 5 minutes of production time. That sounds not that much but the cost of idling are immensely high.

Therefore considering a tool changer where the robot changes the whole torch and can cut further with almost no time loss adds a big benefit to the system.

3.4.3. Robot position

The following Table 15 illustrates the cutting of a rectangle with the plasma PMX system and the usage of the bevel method with an angle of 5 degrees. It can easily be seen that the robot movement at position 0m in the short side of the rectangle slower is than the robot in the position one meter higher.

Table 15: Robot position - TCP speed, Source: own illustration

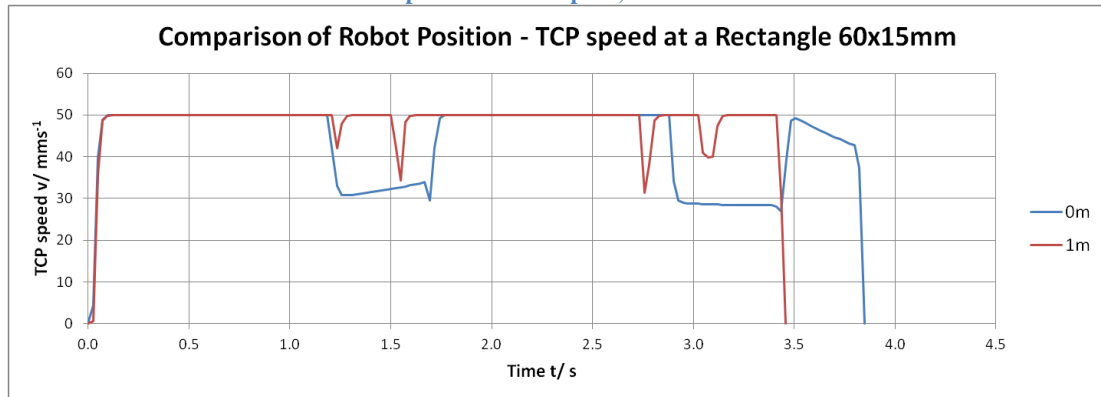


Figure 101 illustrate the different robot position. According to the bevel method, already explained in chapter 3.2.3.3 Cutting of edges the robot compensates the perpendicularity u and lowers the edge influence of the lagging behind.

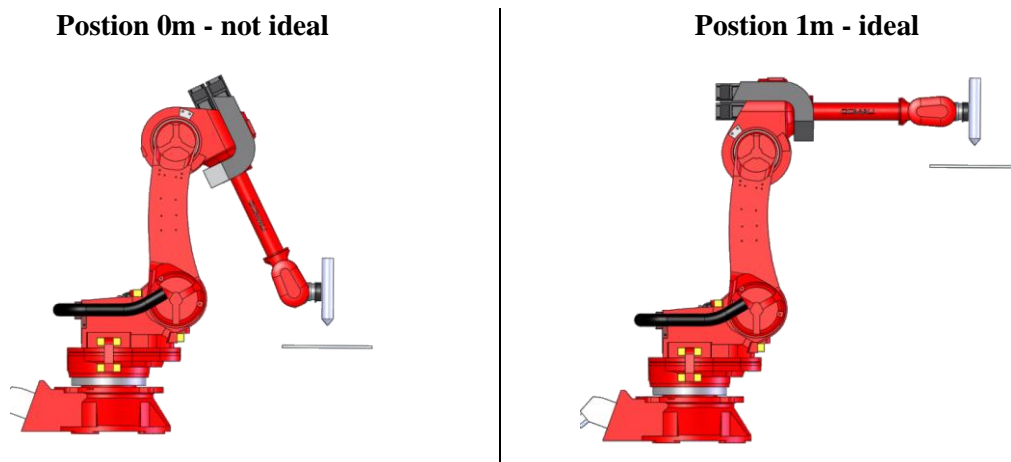


Figure 101: Robot position, Source: own illustration

3.4.4. Plasma integration into the programming infrastructure of the robot

For a better handling of the plasma system the complete integration into the robot programming should be achieved. Furthermore the adaption of the power input should also be the goal. The application corner current at the HPR system is one solution. For the PMX system there are no solutions available. According to the manufacturer miller their machines have an analogue I/O where the amperage can be set. By setting the amperage there a adaption of the energy input on the flight can be achieved. Both of that solutions require further tests and investigations.

3.5. Benchmark robotic plasma cutting against robotic laser cutting

In this chapter a founded benchmark of robotic plasma cutting and robotic laser cutting is evolved. The benchmark is performed from three different perspectives which are the cut quality, metallurgical properties and the costs.

3.5.1. Cut shape quality

The cut shape quality is assessed for the three different cutting technologies in the following Table 16 by dividing the assessment into the cut shape, the cut quality and the implementation. It has to be said that by cutting with plasma different equipment combination like consumables, shielded- unshielded or gases can be used, which can be seen in the manual for the cutting solutions. For this investigation the manufacturer recommended combination is used.

Table 16: Cut shape quality benchmark, Source: own illustration

	Mat. thickn. bc/ mm	PMX finecut 55A	HPR Bevel 80A	Laser 2.5 kW
Shape				
Straight lines achievable tolerances	1.2	0.51	ns.	0.43
	3	0.86	1.24	0.45
Hole cut	1.2	> d=10 mm dross-free > d=8 mm possibility of dross	ns.	> 5 mm dross-free
	3	> d=10 mm dross-free > d=8 mm possibility of dross	ns.	> 5 mm dross-free
Corners		high lagging effects	medium lagging effects	low lagging effects
Cut Speed v_c / mms-1	1.2	100	180	300
	3	55	100	200
Cut width w_{uk} / mm		1.3	1.8	0.16
Perpendicularity u / mm	1.2	0.24	ns.	0.18
	3	0.27	0.42	0.12
Adaptable energy-input		no	partly	yes
Quality				
Risk of dross formation	1.2	medium - little spatters	ns.	low
	3	high	medium	low
Risk of rework	1.2	medium	ns.	low
	3	high	medium	low

Implementation				
Torch height control required	1.2	special considerations - see chapter	no	no
	3	special considerations - see chapter	no	no
Torch geometry / accessibility		good	bad	good
Machine complexity		low	medium	high
Special maintenance training required		no	no	yes

Beginning by the achievable tolerance the laser is the most accurate solution but especially when cutting thinner thicknesses the powermax solution is getting more accurate too. As already mentioned in chapter 3.2.3.1 Straight cuts the laser cutting itself is very accurate. The reason what makes the laser that inaccurate is the robot system. From the physical and mechanical side the plasma system fits better to the robot than the laser system.

Plasma has clearly disadvantages when cutting of holes. Due to the higher heat input, the wider kerf and the lagging effect first of all the accuracy is not as good as the laser and the possibility of dross is also higher. Therefore holes smaller than 8 mm can hardly be cut. Furthermore the corner are also not as good as with the laser technology due to the high lagging effect. By using bevel cutting this effect gets better.

Due to the high energy density of the laser the cutting speed is clearly higher than with the plasma solutions. This also has to be considered when designing a production line. Eventually more equipment has to be considered when using the plasma technology.

As already described the cut shape itself by means of the cut width and the perpendicularity also differ a lot. Laser also sets the standards here.

Furthermore the possibility to adapt the energy-input is completely implemented in the laser solution. The HPR plasma has the opportunity to set the corner-current which means a halving of the amperage. This can be used for specific zones when cutting in 3D. For the powermax system there are no solutions on the market and therefore also not part of the investigation. Further information see in chapter 3.2.5 Adapting of amperage on the flight – command Corner Current.

The plasma solution has problems with the formation of dross. When cutting at the right speed the possibility of dross formation is very low. But when cutting out of the dross free window the possibility is increasing. What also can be observed is if there is dross formation the amount or the

volume of dross is clearly higher than the dross of laser. This is due to the higher amount of material blown out of the kerf. Due to that reasons also the risk of rework is increasing.

Regarding the implementation of the solutions there are several factors to consider. The first is the torch height control. Especially at low current plasma cutting, lower than 55 Amperage, the influence on the shape is high. Therefore the special considerations for plasma cutting have to be made as can be in 3.4.1 Torch height control. The laser solution has already a torch height control implemented in the laser head.

Furthermore the torch geometry is very important to consider. Especially at the HPR plasma system the main body of the torch is very wide in diameter and with low current consumables also the head is very flat. This results in low accessibility when cutting three dimensional shapes.

Generally can be said that the complexity of the machine and the maintenance is at plasma the lowest. Therefore also no special trained workers are required.

3.5.2. Metallurgical properties

How does the heat affected zone influence the cutting technology? This question is tried to answer in the following paragraphs. Table 17 illustrate a brief overview of the influencing factors and the results.

Table 17: Cut metallurgical properties benchmark, Source: own illustration.

	Material thickn. bc [mm]	PMX finecut 55A	HPR Bevel 80A	Laser 2.5 kW
HAZ thickness [μm]	1.2	140	ns.	130
	3	150	140	100
Hardness [HV0.005]	1.2	465	ns.	460
	3	570	530	405
Resolidified zone [-, HV0.005]	1.2	no	ns.	no
	3	yes, 1180	yes, 1134	no
Adaptable energy-input [-]		no	no	yes
Risk of fatigue [-]	1.2	medium	ns.	medium
	3	medium-high	medium-high	low
Process gas [type]		Air	Oxygen-Air	Nitrogen

The plasma solutions have a bigger heat affected zone than the laser one. This can be attributed to the higher energy input. Especially when cutting thicker material this effect is increasing. Due to the high

energy input and the fast heat transfer or cooling afterwards at all solutions the formation of martensitic structure in the heat affected zone can be observed. Martensite affiliates a higher hardness than the basic material. It can be observed that there is a correlation between the thicknesses of the heat affected zone and the hardness. For example the HAZ of the plasma and the laser at the 1.2 mm cuts are almost similar, so do also the hardness. On the other hand the HAZ is clearly higher at the plasma solutions at 3 mm cuts and therefore also the hardness is higher. **Concluding can be said that if there is a thicker heat affected zone the martensitic concentration is higher and therefore also the hardness.**

Cutting the thicker material (3 mm) also results in the formation of a resolidified layer of the molten material at the plasma solutions. At thinner material 1.2 mm the formation of the zone cannot be seen. In which extent this layer effects the creation of cracks has to be tested. An important factor here could be the bonding of the resolidified material to the basic material.

The more energy is added into the material the bigger is the heat affected zone in the material. Tests of the 3D-part also retrieved that fact. As mentioned above this leads to a higher martensitic concentration and at the end to a higher hardness. Therefore the adaption of the energy (current) input at plasma solutions has beside the good geometric effects also good effects regarding the creation of martensite, the hardness and at the end for fatigue.

If this adaption is not possible considerations regarding the design of the parts have to be made. The key here is to get stress peaks out of zones where it is not possible to cut with the proper speed.

The considerations can be:

- Plasma conform design of the part (bigger radius in corners)
- Early stage involvement of the production team into the design process

Doubts regarding the plasma cut ability of the 22MnB5 material are can be rejected. The doubts were that the coating on the surface of the material is only low electric conductive and therefore cutting with plasma is not possible. Since the plasma systems are starting with a high frequency voltage and the plasma is temperature is that high it is no problem to create a closed loop of electricity through the part and cutting can be performed.

3.5.3.Costs

Part of this benchmark is also the consideration of the cost perspective. As already mentioned in the introduction the benchmark is performed between the robotic solution of plasma- and laser cutting. Since for the guiding device the same robot can be used the robot is not part in the cost benchmark.

Furthermore the difference in equipment between these two technologies is considered.

With the scope a cost comparison regarding the investment costs and the operative costs is performed in the following chapters.

3.5.3.1. *Investment costs*

Investment costs are the costs to purchase a machine or good to create values. In our case these are the cutting equipment and the peripheral equipment which facilitate the cutting process.

Table 18 illustrates the costs of a plasma powermax system. The power source is considered in position 1. For the integration into the production line also a tool changer with two torches and brackets is considered. All prices are based on quotation of the supplier which is in the present case Hypertherm Inc.

Table 18: Cost overview plasma powermax PMX system, Source: own illustration

Pos.	Pc.	Plasma PMX equipment	[\$/pc.]	[\$]
1	1	Powermax 105 plus cables and fixtures	5,500.00	5,500.00
2	2	Mechanized torch and cable (estimated)	900.00	1,800.00
3	2	Bracket (estimated)	1,000.00	2,000.00
4	1	Fencing (estimated)	1,000.00	1,000.00
		Investment costs		10,300.00

Table 19 below illustrates the costs of the high performance plasma system. There is also a tool changer considered. Furthermore an additional console for the control of the gas is considered.

Table 19: Cost overview plasma high performance HPR system, Source: own illustration

Pos.	#	Plasma HPR equipment	[\$/pc.]	[\$]
1	1	High performance plasma HPR 130XP plus cables and fixtures	30,000.00	30,000.00
2	2	Torch (estimated)	3,000.00	6,000.00
3	1	Console for Control of Gases	1,000.00	1,000.00
4	2	Bracket (estimated)	500.00	1,000.00
5	1	Fencing (estimated)	1,000.00	1,000.00
		Investment costs		39,000.00

Table 20 below illustrates the cost of a laser system. This system consists of the power source in position 2, the chiller in position 3, the fibre cables in position 4 and on top of the robot there is the laser head in position 1. Moreover for the laser solution an enclosure with a roll-up door is considered in position 6 and 5.

Table 20: Cost overview laser cut system, Source: own illustration

Pos.	#	Laser equipment	[\$/pc.]	[\$]
1	1	Laser Head – Laser Mech	50,612.00	50,612.00
2	1	Trumpf 4kW Laser	343,990.00	343,990.00
3	1	Chiller for Trumpf laser	27,000.00	27,000.00
4	1	ROBOT TRANSFER Easom 10.7m	52,175.00	52,175.00
5	1	Roll Up Door	9,500.00	9,500.00
6	1	Enclosure Laser 15' x 18' x 13'	96,620.00	96,620.00
		Investment costs		579,897.00

As can be seen in the tables above there are big differences in costs of the solution. While the laser cutting system is the most accurate one so it is also by far the most expensive one. Technology has its price.

3.5.3.2. Operative costs

Operative costs are the costs which relate to the operation of a process. Which goods are consumed to run the process and how much do they cost? This is the main question here. The calculation period is one year. General assumptions for the calculation can be seen in Table 21 below.

Table 21: General assumptions for operative costs, Source: own illustration

Working days	6	[pc.]
Working weeks	48	[pc.]
Working days per year	288	[pc.]
Shifts per day	3	[pc.]
Working hours per day	24	[h]
Cut time - efficiency	0.6	[-]

The operative costs to run a cutting process can be divided into the consumables like nozzles etc., the needed process gas and the electrical energy consumed.

Consumables

The quantity of needed consumables is based on real consumptions and manufacturer information. Table 22 below illustrates the comparison of the consumables and the costs per year of the different cutting technologies.

Table 22: Operative costs of consumables, Source: own illustration

Plasma PMX consumables				
Items per week		Costs per item	Costs per week	Costs per year
[#]		[\$]	[\$/w]	[\$/a]
32.73	Electrode	9.10	297.82	14,295.27
32.73	Nozzle	6.65	217.64	10,446.55
1.64	Shield	17.45	28.55	1,370.62
0.33	Retaining Cap	32.45	10.62	509.76
0.65	Swirl Ring	20.55	13.45	645.64
	Consumables cost per year			27,267.84
Plasma HPR consumables				
0.24	Shield cap	84.05	20.17	968.26
1.20	Shield Bevel	17.58	21.10	1,012.61
0.24	Nozzle retaining cap	168.10	40.34	1,936.51
24.00	Nozzle	27.06	649.44	31,173.12
0.48	Swirl ring	24.24	11.64	558.49
24.00	Electrode	23.73	569.52	27,336.96
0.48	Water tube	12.10	5.81	278.78
	Consumables cost per year			63,264.73
Laser consumables				
0.08	Mirrors	400.00	30.00	1,440.00
4.00	Nozzle	6.65	26.60	1,276.80
0.03	Fibre cable	1,000.00	30.00	1,440.00
0.06	Optics	400.00	24.00	1,152.00
	Consumables cost per year			5,308.80

It can be seen that the costs of the consumables are higher than the one from the laser cutting. With plasma cutting the nozzle and the electrode are exposed to the arc and therefore wear out quicker. The average cutting time at the plasma systems are therefore 2.2 hours at the PMX-system and 3 hours at the HPR-system. To avoid downtime of the production, one change of the consumables at the plasma systems need up to three minutes, a tool changer is proposed and calculated above in the investment costs.

Process gas

There are several gases which can be used for cutting as described in chapter 3.3.1 Plasma gas. To provide these gases there are two different ways which are considered in the calculation. Nitrogen and oxygen are bought from external companies in big cylinders and air is usually prepared internally by

compressors. The power necessary to compress the air is calculated by the formula below. The compression is adiabatic and free of friction.

$$P_v = p_i \dot{V} \cdot \left(\frac{\kappa}{\kappa - 1}\right) \cdot \left(\frac{p_2}{p_i}\right)^{\frac{\kappa-1}{\kappa}} \cdot \frac{1}{\eta_c} \quad (50)$$

The compressor efficiency η_c equals 0.7, the isentropic exponent of air equals 1.4 and the environmental air pressure p_1 equals 1 bar. The consumption of the nitrogen consumption is calculated by formula for an ideal gas flow through a nozzle as can be seen below. A_d stands for the outflow area, μ for the outflow number and is depending on the design of the nozzle, Ψ is the outflow function as calculated below, p_a for the pressure before the nozzle, p_i the environmental pressure and ρ_a the density of air at environmental state.

$$\dot{V} = A_d \cdot \mu \cdot \Psi\left(\frac{p_a}{p_i}, \kappa\right) \cdot \sqrt{2 \cdot p_i \cdot \rho_i} \cdot \frac{1}{\rho_a} \quad (51)$$

The outflow function Ψ is depending on the pressure quotient $\frac{p_a}{p_i}$ (in the formula below considered as x) and the critical pressure ratio $\left(\frac{2}{\kappa+1}\right)^{\frac{\kappa}{\kappa-1}}$.

$$\Psi(x, \kappa) = \begin{cases} \sqrt{\frac{\kappa}{\kappa - 1} \cdot x^{1/\kappa} \cdot (x^{1/\kappa} - x)} & \left(\frac{2}{\kappa + 1}\right)^{\frac{\kappa}{\kappa-1}} < x < 1 \\ \left(\frac{2}{\kappa + 1}\right)^{\frac{\kappa}{\kappa-1}} \cdot \sqrt{\frac{\kappa}{\kappa + 1}} & x \leq \left(\frac{2}{\kappa + 1}\right)^{\frac{\kappa}{\kappa-1}} \end{cases} \quad (52)$$

In the present case $\frac{p_a}{p_i}$ is always smaller than $\left(\frac{2}{\kappa+1}\right)^{\frac{\kappa}{\kappa-1}}$ and therefore the second formula is considered as the outflow function Ψ .

Further consideration to calculate the operative costs of the process gas are illustrated in Table 23 below.

Table 23: Considerations to calculate the gas costs, Source: own illustration

1 el. kWh	0.2	[\$]
O2	1.52	[\$/m ³]
N2	2.2	[\$/m ³]

Table 24 below illustrate the consumption and the costs for the process gas for each technology per year.

Table 24: Operative costs of process gas, Source: own illustration

Plasma PMX process gas		
Compressed air p2	6.00	[bar]
Consumption	8,000.00	[l/h]
	0.00	[m ³ /s]
Power to compress Air	1.85	[kW]
Energy per day	44.49	[kWh]
Energy per year	12,814.16	[kWh]
Costs per year compressed Air	2,562.83	[\$/a]

Plasma HPR process gasses		
Oxygen pressure	8.00	[bar]
Consumption	2,016.00	[l/h]
	2.02	[m ³ /h]
Consumption per day	48.38	[m ³ /d]
Consumption per year	13,934.59	[m ³ /a]
Costs per year O2	21,163.69	[\$/a]
Compressed air p2	8.00	[bar]
Consumption	1,344.00	[l/h]
	0.00	[m ³ /s]
Energy to compress Air	0.34	[kW]
Energy per day	8.12	[kWh]
Energy per year	2,337.20	[kWh]
Costs per year compressed Air	467.44	[\$/a]

Laser process gas		
Nitrogen pressure	19.00	[bar]
Consumption	8,500.00	[l/h]
	8.50	[m ³ /h]
Consumption per day	204.00	[m ³ /d]
Consumption per year	58,752.00	[m ³ /a]
Costs per year N2	129,254.40	[\$/a]

Due to the higher working pressure and the higher price per cubic meter nitrogen the costs for the process gas at laser cutting is tremendously higher than the one from the plasma solutions.

Electrical energy

The electrical power consumption is calculated according to manufacturers' information. According to their information the electrical power can be calculated according to following formula which considers the three electrical phases.

$$P_{el} = U \cdot I \cdot \sqrt{3} \quad (53)$$

The power factor PF has to be considered when using alternating current AC. The power factor can be calculated with the following formula.

$$PF = |\cos \varphi| \quad (54)$$

The real electrical power consumed can be calculated by the formula below.

$$P_r = \frac{P_{el}}{PF} \quad (55)$$

The real energy consumption results from the power multiplied by the time it is consumed. These calculations are done for all three processes and compared in the following Table 25.

Table 25: Operative costs of electrical energy, Source: own illustration

Plasma PMX electrical energy		
el. Power	19.00	[kVA]
Real power	22.95	[kW]
Energy per day	550.72	[kWh]
Energy per year	158,608.70	[kWh]
Costs for electrical energy	31,721.74	[\$/a]

Plasma HPR electrical energy		
el. Power	51.60	[kVA]
Real power	62.32	[kW]
Energy per day	1,495.65	[kWh]
Energy per year	430,747.83	[kWh]
Costs for electrical energy	86,149.57	[\$/a]

Laser electrical energy		
el. Power Chiller	20.78	[kVA]
Real power Chiller	25.10	[kW]
el. Power power source	12.47	[kVA]
Real power power source	15.06	[kW]
Real power total	40.16	[kW]
Energy per day	963.92	[kWh]
Energy per year	277,610.09	[kWh]
Costs for electrical energy	55,522.02	[\$/a]

Due to the high efficiency of the laser power source the electrical energy consumption is the lowest although the power source needs a chiller to cool the power source.

Figure 102 illustrates a comparison of the investment and the operative costs of the different solutions. Extraordinary is the high investment which has to be made when using laser equipment. Both plasma solutions have very low investment costs. At this point it should be noted that at the plasma solutions tool changers are considered but no equipment for implementing the torch height control or special toolings. By looking at the operative costs the high process gas costs of the laser is outstanding due to the high pressure to push the gas out of the kerf. Besides that the consumables and the electricity costs are very low at the laser compared to the plasma. The other way around is the case of the high performance plasma with high operating costs due to the higher electricity and consumables costs. The powermax system is the cheapest solution also in terms of the operative costs.

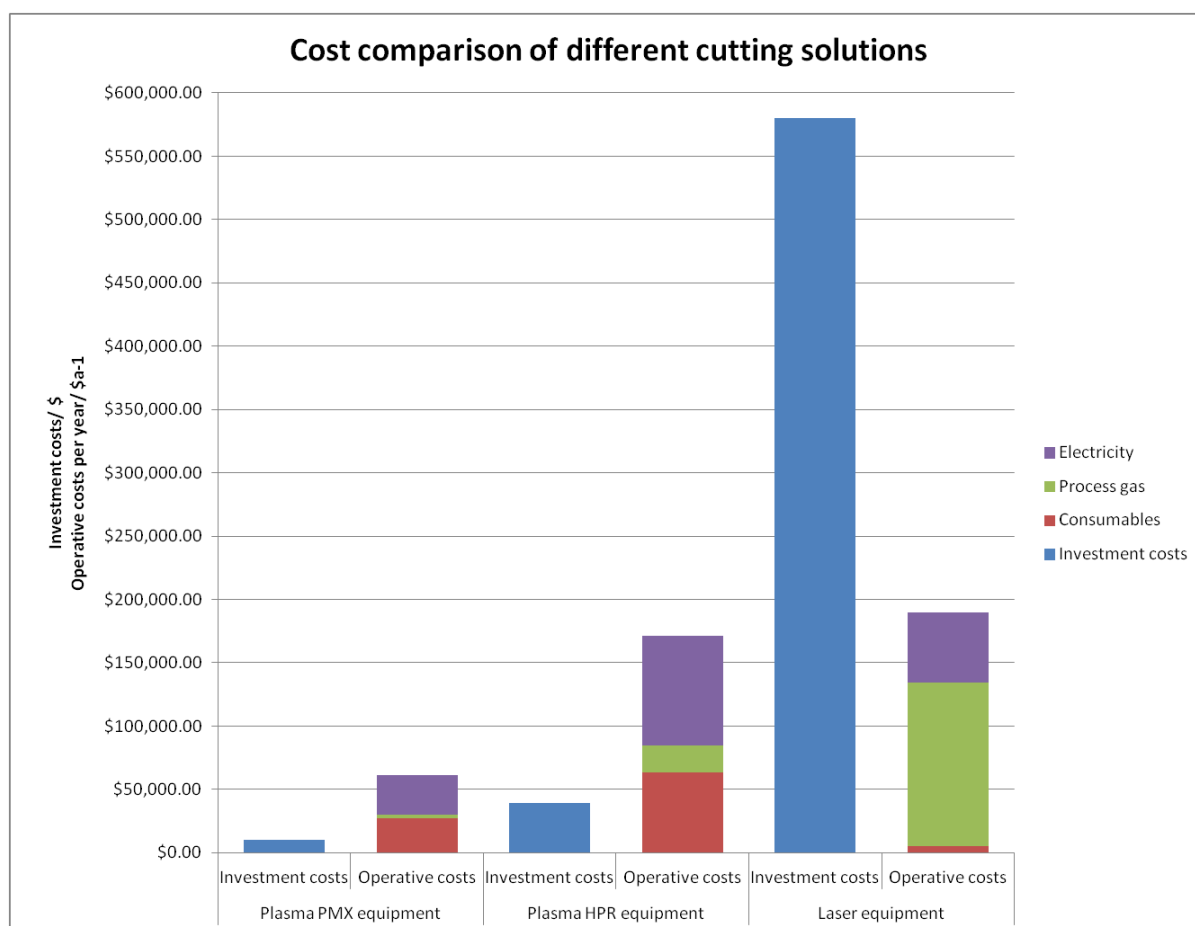


Figure 102: Comparison of the investment- and the operative costs of the different solutions, Source: own illustration

4. Conclusion

In the present chapter it is tried to formulate conclusions of all gathered information of the analysis of plasma cutting technology. Furthermore a guideline is developed to enhance the decision making process and at last a prospect is given.

When assessing the quality of plasma cutting it can be divided into two different areas. First there is the accuracy and secondly the dross probability. The cut accuracy is increasing by decreasing material thickness because the “softness” of the plasma flow and the resulting lagging effect of the plasma is decreasing. Sure the accuracy of the laser system is unachievable but when looking at the integral system with the robot the plasma cutting system fits better to the robot as a guiding system than the laser does. Especially when cutting thinner materials as the B-Pillar. The main restriction here is the cutting of holes. A possible solution for that issue is the adaption of the power input which is discussed in the prospect.

The dross probability at plasma cuts is very low when cutting straight cuts where the speed can be hold. When cutting shapes when the torch is moving slow or when the arc returns to another cut, 3D curves or simple when the temperature in the material is increasing the dross probability increases. Furthermore at plasma cuts more material is blown out of the kerf which leads to more pollutant as resolidified metal especially at the tube cuts where the resolidified metal cannot carried away. Precautionary measures have to be made.

The influence of the plasma cut on the HAZ and the metallurgical effects are also part of the present analysis. As an outcome it can be said that at both, laser and plasma cuts, hardening of the border material occur. When cutting thinner material there is almost no difference in the peak hardness and the size of the heat affected zone between the two cutting technologies. Cutting thicker materials with three millimetres thickness produces a very hard resolidified layer with the plasma technology. Also the size of the HAZ is bigger. The impact of these metallurgical changes on fatigue has to be tested especially when cutting at slower speed which leads to an even bigger HAZ. As a prime example there is the final part 3D cut where easily can be seen that the HAZ has a further expansion.

The cost factor is the big advantage of the plasma solution. As discussed there are very low investment costs of both solutions and the operative costs are by using a Powermax system unbeatable and at the high performance solution comparable to the laser.

All in all the robotic plasma solution stands out because of its simplicity, flexibility and cost effectiveness. It can be seen as a good and cheap alternative for cuts which do not require the accuracy

of a laser cut. Especially cutting of thinner materials with continuous straight cuts all the strengths of the plasma system are gathering together. Robotic plasma cutting has some troubles with shapes and cutting returning cuts but with the described hints it can be trimmed to good results.

4.1. Guideline for decision process Plasma or Laser cutting

Choosing the right system and considering the entire influencing factors is a real challenge when planning a cutting system. In the present chapter it is tried to prepare a guideline with the gathered information of this investigation in order to simplify the decision making process when implementing a cutting system in future.

Figure 103 illustrates the developed guideline which can be divided in different layers. It starts by the thickness of the material, followed by the accessibility, the restrictions and achievable accuracy, the speed and the costs. The cutting technologies which can be selected are the ones which are part of the investigation the high performance plasma, the powermax plasma and the laser cutting technology.

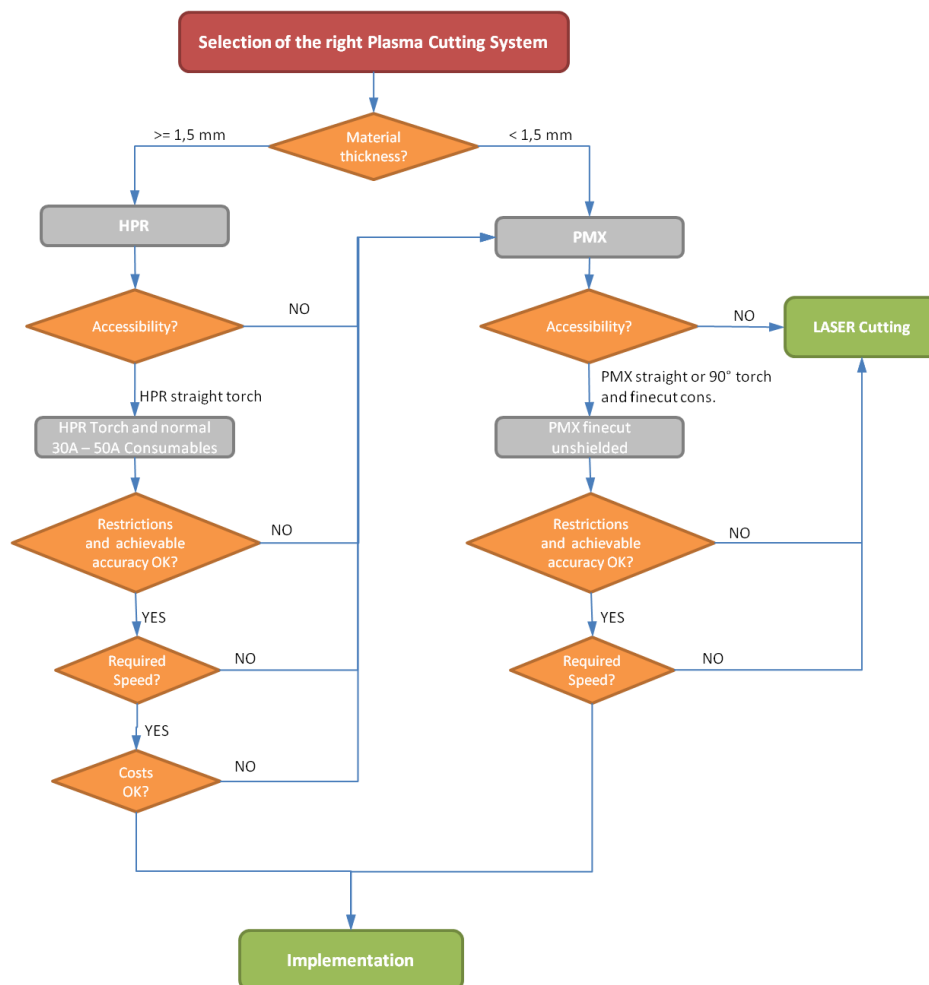


Figure 103: Guideline for cutting solution, Source: own illustration.

The first decision is about the thickness of the material which needs to be cut. As already known cutting thicker material leads to several effects like the lagging behind, the bigger HAZ with the hard resolidified material and to a higher possibility of dross formation. Therefore the high performance machine is the better solution for thicker material and moreover it has the function corner_current where the amperage can be adapted when moving slower at difficult shapes. The tested high performance cuts were with the 80 A bevel consumables which are too strong for that thickness and not representative for a good cut. The consumables which should be used for a material with three millimetres thickness are the one for 50 A.

The next point is the accessibility of the torch. Depending on the shape of the part and the cut path it is often the case that the torch just cannot follow the required path especially with the HPR torch and the normal 50 A consumables. The design of the powermax system is smaller and therefore beneficial in that case.

The restrictions and achievable accuracy also have to be considered and valued. Useful information therefore is in the performed benchmark in chapter 3.5.1 Cut shape quality. Regarding the performance of the HPR system with normal 50 A consumables further tests have to be performed.

Another big influencing factor is the cutting speed. This is often linked with the next factor the costs. How fast can the machine cut? What is the required cycle time? How many machines are needed to get to the result? Is there a need for more reworking? How much labour is needed? These questions have to be answered and helpful information can be found in chapter 3.5 Benchmark robotic plasma cutting against robotic laser cutting.

At the end there is the implementation of the solution. Information therefore can be found in chapter 3.4 Implementation of robotic plasma cutting where several further considerations have to be made when implementing a plasma solution.

4.2. Prospect

The present paper addresses the effects of the plasma cutting technology and performs a benchmark to the state of the art laser technology by taking a deep look on the quality and accuracy of the cut, the impact in the heat affected zone and a cost comparison. Furthermore several solutions to enhance the technology are developed and it is shown how the technology can be implemented into the production

line. To pass and share the maximum amount of information for the daily business in a company at last a guideline is developed.

Depending on the application there still needs designing and testing work to be done. The most important ones are the current adaption and the development of a tool changer. The advantage of current adaption is besides the better geometrical accuracy at difficult paths and holes also the controlling of the hardness in the material. It has to be said that the hardness is increasing when cutting with low speed and high energy input. This can lead to product validation issues due to the unexpected fatigue of the part. For a good user based solution also the implementation of the plasma machine into the framework of the robot has to be enhanced.

The development of a tool changer is a must for line production. The downtime costs of a manufacturing line are high and in times of high competition this is not efficient.

Furthermore the maintenance of the torch height is an issue which needs a closer look. There are three possible solutions as described in chapter 3.4.1 Torch height control. When implementing a plasma solution these point has to be considered.

The tested material in the present paper is the S460MC and the 22MnB5 with a thickness of 3 and 1.2 mm. For other materials or thicknesses further tests have to be performed. The same has to be said for the tested equipment.

References

Literature

Baum, L. Und Fischer H. (1976): Der Schutzgasschweisser Teil I: WIG-Schweissen / Plasmaschweissen, 2nd ed., München

Beyer L. (2004), Genauigkeitssteigerung von Industrierobotern, Dissertation
Hamburg

Bhadeshia, H. K. D. H. (2007): The Nature, Mechanism and Properties of Strong Bainite, International Steel Science, The Iron and Steel Institute of Japan

Bramfitt, B. L., et al. (2002): Metallographer's Guide: Practice and Procedures for Irons and Steels, ASM international, Materials Park Ohio

Gerstmann, U. (1991): Roboter Genauigkeit, Der Getriebeeinfluß auf die Arbeits und Positionsgenauigkeit, VDI-Verlag GmbH, Düsseldorf

Harris, I. D. (1997): Plasma Arc Cutting of Bridge Steels, Issue 384, Washington: Transportation Research Board

Neger, T. (2013): Experimentelle Plasmaphysik, Literature for the lecture LV-Nr. 511.123 at the Technical University of Graz

Herwig, H., et al. (2006): Wärmeübertragung, Physikalische Grundlagen, illustrierte Beispiele, Übungsaufgaben mit Musterlösungen, Vieweg & Sohn Verlag, Wiesbaden

Hesse, S. et al. (2010): Taschenbuch Robotik, Montage, Handhabung, Fachbuchverlag Leipzig im Carl Hanser Verlag, Leipzig

Kou S. (2003), Welding Metallurgy Second Edition, New Jersey: John Wiley & Sons, Inc.

Klocke, F. (2007): Fertigungsverfahren – Abtragen, Generieren und Lasermaterialbearbeitung 4th ed., University of Aachen

Meyers, M. A., et al. (1984): Mechanical Metallurgy, Principles and Applications, Prentice Hall Inc., New Jersey

Naderi M., Saeed-Akbari A., Bleck W. (2007), The effects of non-isothermal deformation on martensitic transformation in 22MnB5 steel, Mat.Sci.&Eng. A485, 445-455.

Poprawe, R. (2005): Lasertechnik für die Fertigung, Grundlagen, Perspektiven und Beispiele für den innovativen Ingenieur, Springer-Verlag, Berlin Heidelberg

Pollack, H. W. (1988): Materials Science and Metallurgy, 4th edition, Reston Pub Co, Prentice-Hall

Radaj, D. (1995): Ermüdungsfestigkeit, Grundlagen für Leichtbau, Maschinen- und Stahlbau, Springer-Verlag, Berlin Heidelberg

Radaj, D. (2002): Eigenspannungen und Verzug beim Schweißen, Rechen- und Meßverfahren, DVS-Verlag, Düsseldorf

Radaj, D. (1992): Heat effects of welding, Temperature field, Residual stress, Distortion, Springer-Verlag, Berlin Heidelberg

Ross, S. M. (2004): Statistik für Ingenieure und Naturwissenschaftler, 3rd edition, Spektrum Akademischer Verlag – Elsevier, München

Schijve, J. (2009): Fatigue of structures and materials, 2nd edition, Springer-Verlag, Berlin Heidelberg

European committee for standardisation (CEN) (1998): Manipulating industrial robots – Performance criteria and related test methods – German version (ISO 9283:1998)

European committee for standardisation (CEN) (2002): Thermal cutting – Classification of thermal cuts – Geometrical product specification and quality tolerances – German version (ISO 9013:2002)

Österreichisches Normungsinstitut (ON) (1990): Thermisches Schneiden – Plasmaschneiden, Verfahrensgrundlagen, Begriffsbestimmungen, Güte, Maßtoleranzen (ÖNORM M 7857, DIN 2310 – Teil 4)

Österreichisches Normungsinstitut (ON) (1991): Thermisches Schneiden – Laserstrahlschneiden von metallischen Werkstoffen, Verfahrensgrundlagen, Begriffsbestimmungen, Güte, Maßtoleranzen (ÖNORM M 7858, DIN 2310 – Teil 5)

Deutsches Institut für Normung e. V. (DIN) (2000): Test code for machine tools (DIN ISO 210 – Part 1-6)

ABB AB (2014): Product specification IRB 2400, Revision E, ABB Sweden, Västerås

Online sources

TRUMPF GmbH + Co. KG. (2015). URL: <http://www.trumpf-laser.com/en/solutions/industry-solutions/automotive-production/body-in-white.html>

Hypertherm Inc. (2015). URL: <http://www.hypertherm.com>

Hypertherm Inc. (2015). URL:

http://www.hypertherm.com/en/Torches_and_consumables/Centricut_consumables/Centricut_plasma/Articles/article_PlasmaCutQualityProblems-Dross.jsp

Tyler J., Peters J., Liebold S. (2014). URL:

<http://www.thefabricator.com/article/plasmacutting/improved-plasma-cutting-of-stainless-steel>

Chegg Inc. (2015). URL: <http://www.chegg.com/homework-help/questions-and-answers/thin-pieces-1080-eutectoid-steel-heat-treated-following-ways-use-ttt-diagram-knowledge-pre-q7529785> (cit. on

Laboratory for scientific visual analysis, Virginia (2015), URL: <http://www.sv.vt.edu>

Rautaruukki Corporation, Helsinki (2015), URL: <http://www.ruukki.com/Steel/Cold-rolled-steels/Hardenable-steels/Boron-steel-22MnB5>

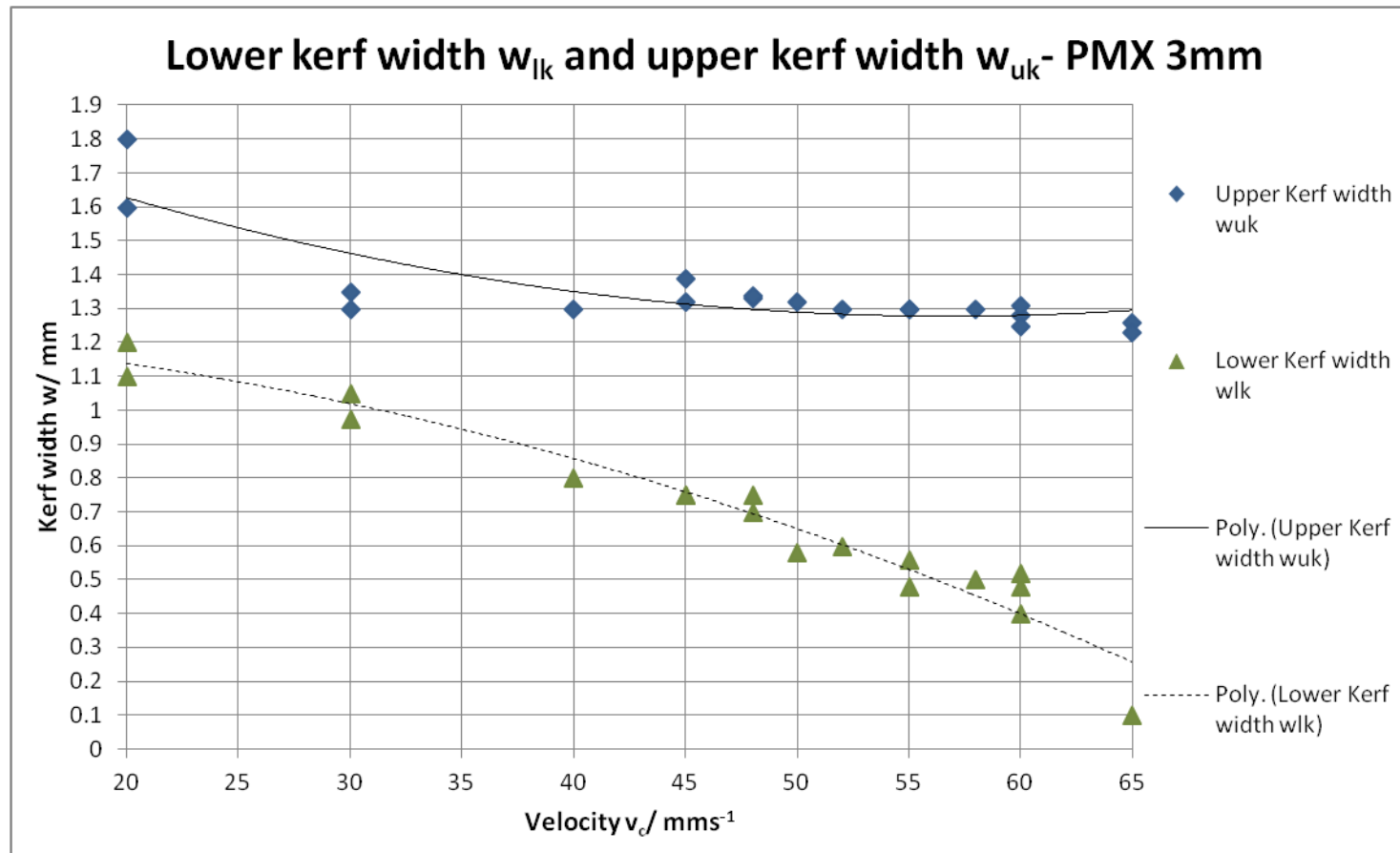
Oriental motor, U.S.A Corp (2015), URL: <http://www.orientalmotor.com/products/stepper-motors/stepper-motor-only-HG-g geared.html>

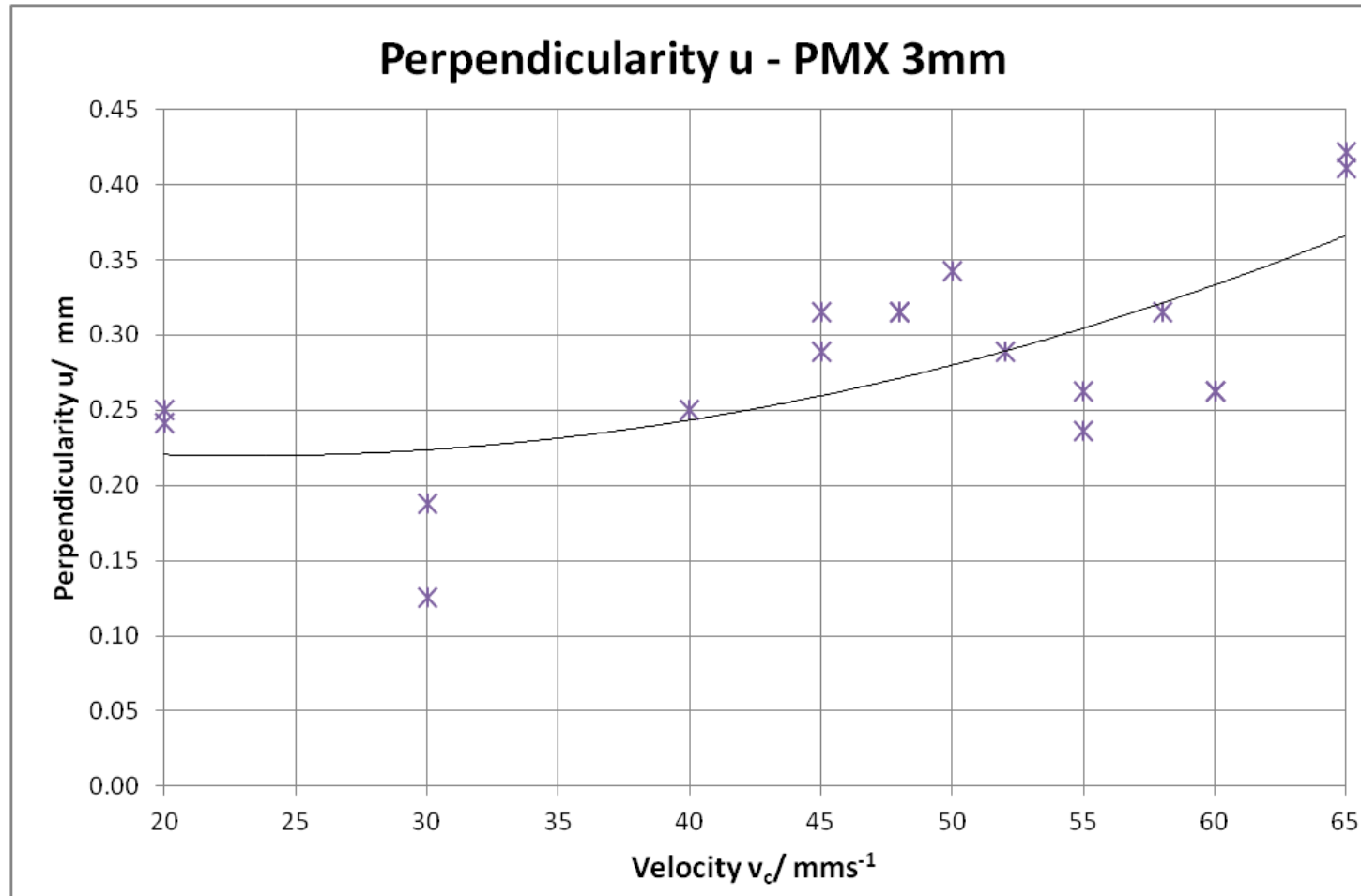
IDA Control Automation Robotics, Panagiotis M. Pikiş and Co (2015), URL:
<http://www.idacontrol.com/>

CAE Simulation & Solutions Maschinenbau Ingenieurdienstleistungen GmbH, Vienna (2015), URL:
<http://www.cae-sim-sol.com/en/limit-stress-evaluation/finite-life-fatigue-strength>

Appendix

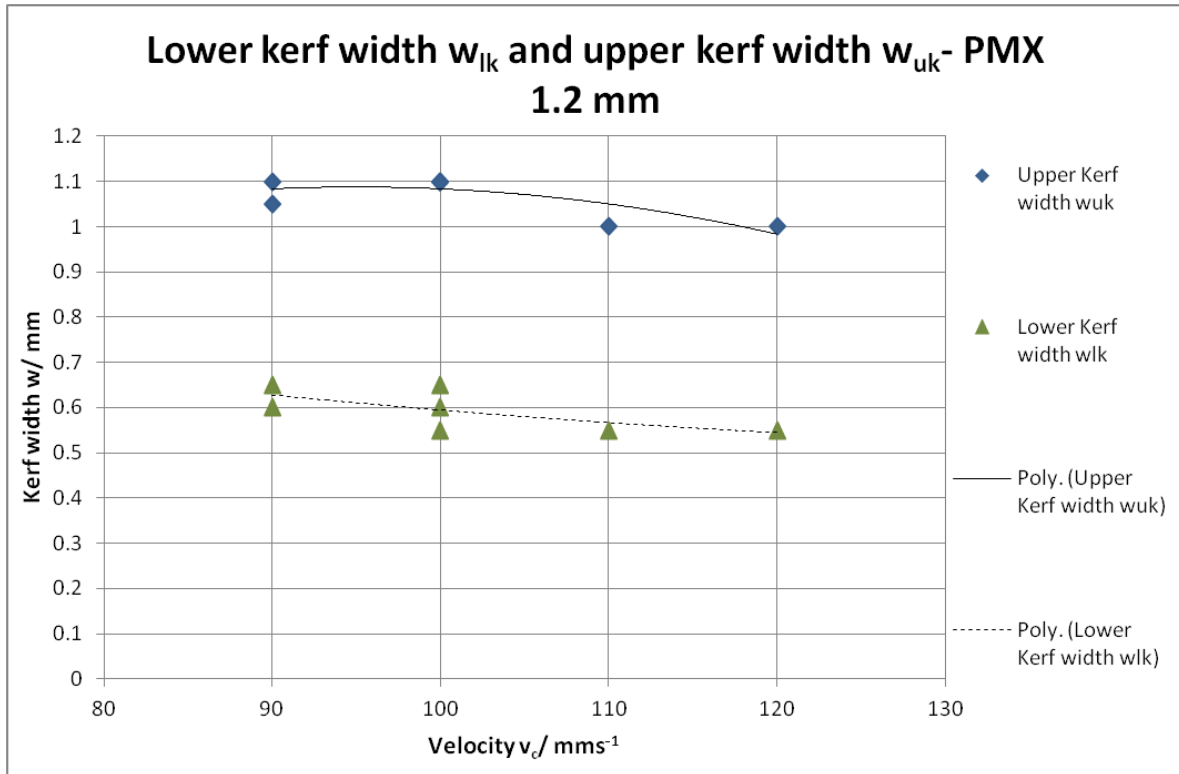
A.1 Powermax system 3 mm thickness – AISI 1018 – kerf

Lower kerf w_{lk} and upper kerf w_{uk} width

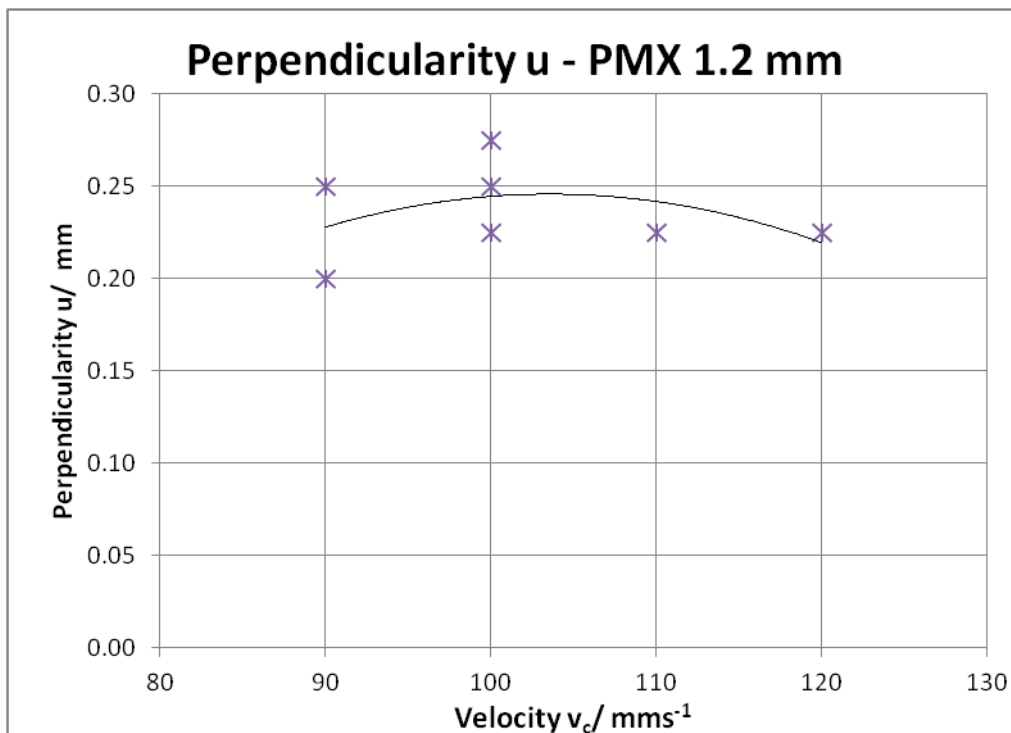
A.2 Powermax system 3 mm thickness – AISI 1018 – Perpendicularity u

A.3 Powermax system 3 mm thickness – AISI 1018 – kerf

Lower kerf w_{lk} and upper kerf w_{uk} width

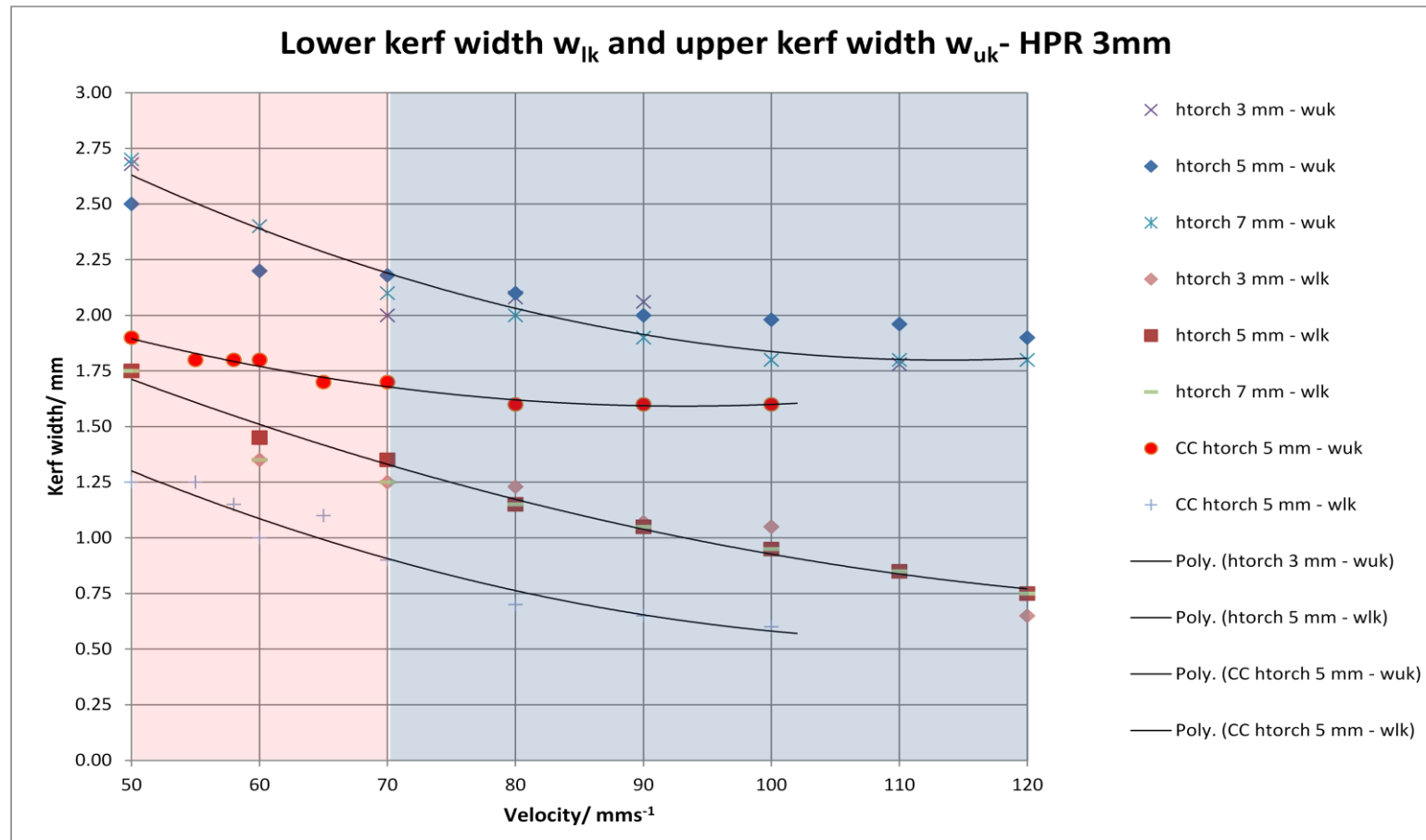


A.4 Powermax system 3 mm thickness – AISI 1018 – Perpendicularity u



B.1 High performance system 3 mm thickness – AISI 1018 – kerf

Lower kerf w_{lk} and upper kerf w_{uk} width



B.2 High performance system 3 mm thickness – AISI 1018 – Perpendicularity u

